การวิเคราะห์แบบความโค้งมากของโครงสร้างที่มีพฤติกรรมแบบยืดหยุ่นและไม่มีการยืดหดตาม
แนวแกนด้วยวิธีการรวมสติฟเนสแบบตรง

นายพีรศักดิ์ ตั้งเนาวรัตน์

วิทยานิพนธ์นี้เป็นส่วนหนึ่งของการศึกษาตามหลักสูตรปริญญาวิศวกรรมศาสตรมหาบัณฑิต
สาขาวิชาวิศวกรรมโยธา     ภาควิชาวิศวกรรมโยธา
คณะวิศวกรรมศาสตร์  จุฬาลงกรณ์มหาวิทยาลัย
ปีการศึกษา  2551

# LARGE CURVATURE ANALYSIS OF LINEAR ELASTIC, INEXTENSIBLE STRUCTURES BY A DIRECT STIFFNESS METHOD
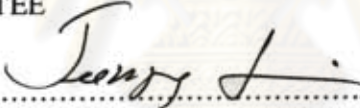
Mr.Peerasak Tangnovarad

A Thesis Submitted in Partial Fulfillment of the Requirements
for the Degree of Master of Engineering Program in Civil Engineering
Department of Civil Engineering
Faculty of Engineering
Chulalongkorn University
Academic Year 2008
Copyright of Chulalongkorn University

Thesis Title            LARGE CURVATURE ANALYSIS OF LINEAR ELASTIC, INEXTENSIBLE STRUCTURES BY A DIRECT STIFFNESS METHOD

By            Mr.Peerasak Tangnovarad

Field of Study            Civil Engineering
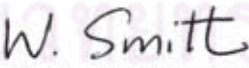
Advisor            Jaroon Rungamornrat, Ph.D.

---

Accepted by the Faculty of Engineering, Chulalongkorn University in Partial Fulfillment of the Requirements for the Master's Degree
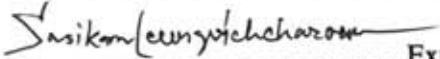
.................................................... Dean of the Faculty of Engineering

( Associate Professor Boonsom Lerdhirunwong, Dr.Ing. )

THESIS COMMITTEE

.................................................... Chairman

( Associate Professor Teerapong Senjuntichai, Ph.D.)

.................................................... Advisor

( Jaroon Rungamornrat, Ph.D.)

.................................................... Examiner

( Assistant Professor Watanachai Smittakorn, Ph.D. )

.................................................... External Examiner

( Assistant Professor Sasikorn Leungvichcharoen, D.Eng. )

iv

พีรศักดิ์ ตั้งเนาวรัตน์ : การวิเคราะห์แบบความโค้งมากของโครงสร้างที่มีพฤติกรรมแบบยืดหยุ่นและไม่มี
การยืดหดตามแนวแกนด้วยวิธีการรวมสติฟเนสแบบตรง.(LARGE CURVATURE ANALYSIS
OF LINEAR ELASTIC, INEXTENSIBLE STRUCTURES BY A DIRECT
STIFFNESS METHOD) อ.ที่ปรึกษาวิทยานิพนธ์หลัก : ดร.จรูญ รุ่งอมรรัตน์, 97 หน้า.

การศึกษานี้นำเสนอระเบียบวิธีการอย่างง่ายสำหรับวิเคราะห์โครงสร้างยืดหยุ่นเชิงเส้น            ไม่ยืดหดตาม
แนวแกน และเกิดความโค้งและการหมุนมาก โดยใช้วิธีรวมสติฟเนสแบบตรงร่วมกับการแก้ปัญหาไร้เชิงเส้นด้วย
วิธีนิวตันราฟสัน         โดยเมตริกสติฟเนสสัมผัสของชิ้นส่วนถูกพัฒนามาจากสมการกำกับเชิงอนุพันธ์ไร้เชิงเส้น
โดยตรงซึ่งเป็นวิธีที่คล้ายคลึงกับการแก้ปัญหาอีลาสติกาแบบดั้งเดิม      ข้อจำกัดของความยาวของชิ้นส่วนที่เกิด
จากสมมุติฐานไม่ยืดหดตามแนวแกนถูกรวมอยู่ในเมตริกสติฟเนสสัมผัสของชิ้นส่วนโดยตรงทำให้ขนาดของ
เมตริกเพิ่มขึ้นหนึ่งมิติ ซึ่งเมตริกสติฟเนสสัมผัสของชิ้นส่วนที่ได้นั้นจะอยู่ในรูปแม่นตรงและมีความสมมาตรโดยที่
แต่ละสมาชิกเขียนอยู่ในรูปแบบปริพันธ์เชิงวงรีหรือปริพันธ์ที่คล้ายกัน  ข้อดีของการใช้เมตริกสติฟเนสสัมผัสแบบ
แม่นตรงในวิธีรวมสติฟเนสแบบตรงคือผลเฉลยที่ได้จากการวิเคราะห์จะเป็นผลเฉลยแบบแม่นตรงโดยไม่
จำเป็นต้องทำการแบ่งชิ้นส่วนโครงสร้างออกเป็นชิ้นส่วนย่อยๆ   ดังนั้นวิธีการที่พัฒนาขึ้นสามารถใช้เป็นผลเฉลย
อ้างอิงสำหรับเปรียบเทียบกับผลเฉลยที่ได้จากวิธีอื่นๆ        ความถูกต้องและประสิทธิภาพของระเบียบวิธีการที่
พัฒนาขึ้นนำเสนอโดยทำการวิเคราะห์คานและโครงข้อแข็งจำนวนมากพร้อมทั้งแสดงและอภิปรายผลที่ได้
ประกอบ

ภาควิชา ........วิศวกรรมโยธา........ ลายมือชื่อนิสิต ............................................

สาขาวิชา ........วิศวกรรมโยธา........ ลายมือชื่ออ.ที่ปรึกษาวิทยานิพนธ์หลัก ..................

ปีการศึกษา ............2551............

## 4970486821 : MAJOR   CIVIL ENGINEERING

KEYWORDS: TANGENT STIFFNESS MATRIX / LARGE CURVATURE / INEXTENSIBILITY / ELASTICA / DIRECT STIFFNESS METHOD.

PEERASAK TANGNOVARAD : LARGE CURVATURE ANALYSIS OF LINEAR ELASTIC, INEXTENSIBLE STRUCTURES BY A DIRECT STIFFNESS METHOD. ADVISOR: JAROON RUNGAMORNRAT, Ph.D., 97 pp.

This study proposes a simple technique that has a capability of analysis of linearly elastic, inextensible beam and frame structure undergoing large curvature and rotation. The technique utilizes a standard direct stiffness strategy along with a standard nonlinear solver based on Newtow-Ralphson iteration. The element tangent stiffness matrix is derived directly from the governing nonlinear differential equations; in particular, a standard procedure analogous to that used to construct solutions for classical elastica problems is employed as a basis of the development. The length constraint equation arising form the beam inextensibility is additionally incorporated to the element tangent stiffness matrix in a straightforward fashion and, as a result, increasing the dimension of the matrix by one. The derived element tangent stiffness matrix is exact and essentially symmetric, and its final expression is given in a concise and explicit form in terms of elliptic integrals and other integrals of the same kind. A key advantage of exploiting exact element tangent stiffness matrices in the direct stiffness method is that an exact solution can directly be obtained without any refinement on the size of elements. In this sense, it additionally provides a means for generating results that can be used as benchmark solutions for a comparison purpose. To demonstrate the capability and robustness of the current technique, extensive analysis of beam and frame structures are preformed and results are then reported and discussed.

Department: .....Civil Engineering....... Student 's Signature:.........................

Field of Study: ..Civil Engineering....... Advisor 's Signature:...........................

Academic Year:...........2008................

# ACKNOWLEDGEMENTS

# CONTENTS

# LIST OF TABLES

ศูนย์วิทยทรัพยากร
จุฬาลงกรณ์มหาวิทยาลัย

# LIST OF FIGURES

# LIST OF ABBREVIATIONS

E      - Youngs elastic modulus

I      - moment of inertia

$\kappa$      - curvature (rate of changing angle)

$\varepsilon$      - strain (elongation per undeformed length)

$f_x$      - internal axial force

$f_y$      - internal shear force

m      - normalized internal bending moment

$f_{xi}$      - horizontal applied load at node i

$f_{yi}$      - vertical applied load at node i

$m_i$      - normalized applied bending moment at node i

L      - length

v      - vertical displacement

u      - horizontal displacement

$\hat{f}_x$      - normalized internal axial force

$\hat{f}_y$      - normalized internal shear force

$\hat{m}$      - normalized internal bending moment

$\vartheta$      - moment-dependence function

$\hat{f}_{xi}$      - normalized horizontal applied load at node i

$\hat{f}_{yi}$      - normalized vertical applied load at node i

$\hat{m}_i$      - normalized applied bending moment at node i

$\xi$      - normalized length

$\theta^*$      - rotation at specific point

$\hat{v}^*$      - normalized vertical displacement at specific point

$\hat{u}^*$      - normalized horizontal displacement at specific point

$\hat{d}$      - normalized projected lenght

$\mathcal{R}$      - residual function

$\theta_i$      - rotation at node i

$\theta_z$      - rotation at inflection point

$\hat{v}_i$      - normalized horizontal displacement of node i

$\hat{u}_i$ — normalized horizontal displacement of node i

$\mathbf{f}_{(s)}$ — force vector of simply-supported beam

$\mathbf{u}_{(s)}$ — displacement vector of simply-supported beam

$\mathbf{g}$ — tangent stiffness matrix of simply-supported beam

$\mathbf{f}$ — force vector of local coordinate system

$\mathbf{u}$ — displacement vector of local coordinate system

$\mathbf{f}^*$ — force vector of deformed member coordinate system

$\mathbf{u}^*$ — displacement vector of deformed member coordinate system

$\mathbf{R}$ — transformation matrix (deformed member to local coordinate)

$\overline{\mathbf{R}}$ — transformation matrix (deformed member to local coordinate) (special case)

$\mathbf{k}_\ell$ — local element tangent stiffness matrix

$\mathbf{k}_g$ — global element tangent stiffness matrix

$\mathbf{Q}$ — transformation matrix (local to global coordinate)

$\overline{\mathbf{Q}}$ — transformation matrix (local to global coordinate) (special case)

$\mathbf{P}$ — force vector of entire structure

$\mathbf{U}$ — displacement vector of entire structure

$\mathbf{K}_t$ — tangent stiffness matrix of entire structure

# CHAPTER I

## INTRODUCTION

### 1.1 General

It is well-known that a small-deformation analysis of flexure-dominating structures (e.g. beams and rigid frames) based primarily on linear kinematics, linear constitutive relation and fully decoupled axial-bending interaction (e.g. [1-2]) can lead to results that are of insufficient accuracy, especially when the displacement, rotation and curvature of the structure are large and the axial-bending interaction becomes significant. A well-known case is the P-delta effect phenomena; presence of the compressive force within the member generally yields the bending moment higher than that obtained from linear analysis.

To clearly demonstrate such coupling effect, let consider a simple case associated with a simply-supported beam subjected to a transverse load Q at the mid span and an axial load P at the right end as indicated in Figure 1.1. A linear structural analysis, when applied to solve this particular problem, provides no information about the influence of the axial load P on the bending moment induced at any cross section; in particular, results from the analysis indicate that the maximum bending moment occurring at the mid span is independent of P and is equal to QL/4. However, it is
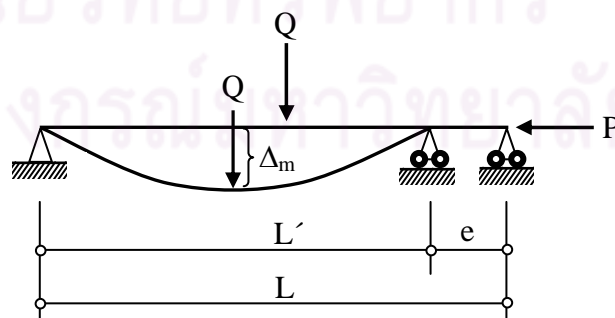


Figure 1.1 Schematic of simply supported beam subjected to transverse load Q and
axial load P

evident that as the member deflects under the action of the transverse load Q, the horizontally projected length of the member becomes L´ < L and the axial load P produces an extra bending moment $P\Delta_m$ at the mid span of the beam in addition to that caused by the load Q where $\Delta_m$ denotes the downward deflection at the mid span. As a consequence, the actual maximum bending moment at the mid span becomes QL´/4 + $P\Delta_m$ if P is in compression and QL´/4 – $P\Delta_m$ if P is in tension. As the axial load P (in compression) becomes large in comparison with the buckling load of the beam, the deflection $\Delta_m$ can be substantial and the shortening e becomes significant. This renders the maximum bending moment predicted by the linear analysis significantly deviates from the actual value.

Another limitation of the linear analysis is that it provides very limited information on the stability of the structure (e.g. bifurcation loads and identification of stability status of structures) and as well as the behavior beyond a point of bifurcation (i.e. post-buckling behavior). To clearly demonstrate such limitation, let consider a perfectly straight cantilever column of constant flexural rigidity EI and length L and subjected to an axial load P as shown schematically in Figure 1.2(a). The linear analysis, when applied to this particular problem, simply yields a trivial solution that the column remains in a straight configuration for any value of the load P; i.e. the relation between the load P and the lateral deflection at the tip of the column, denoted
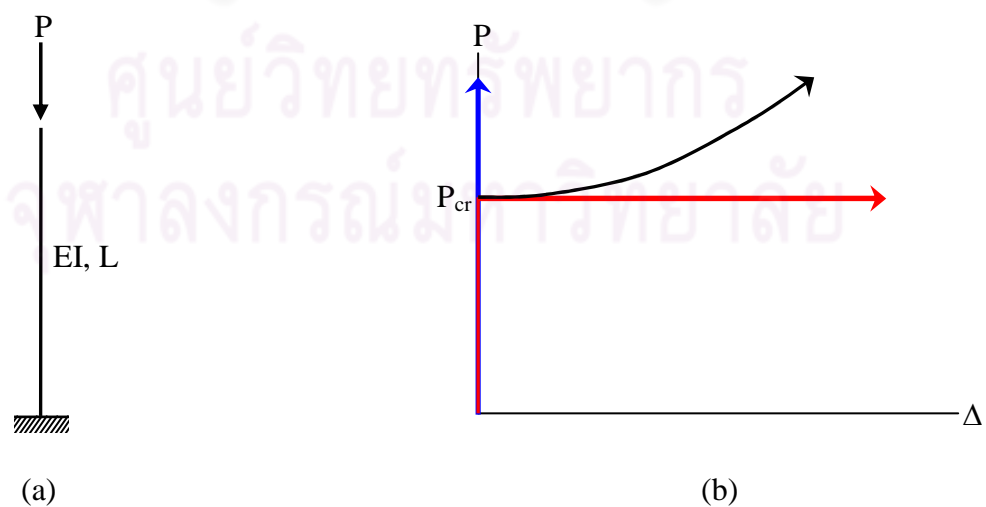


Figure 1.2 (a) Schematic of perfectly straight cantilever column subjected to axial load P and (b) relation between load P and tip deflection $\Delta$.

by Δ, is indicated by the blue line shown in Figure 1.2(b). A better solution can be obtained if the second order analysis (Timoshenko and Gere, 1972; Sampaio and Hundhausen, 1998) is employed; results from this analysis are indicated by the red line shown in Figure 1.2(b). While the second order analysis can predict the bifurcation or buckling load of the column ($P_{cr} = \pi^2 EI/4L^2$), the behavior beyond the bifurcation point cannot be predicted (the tip deflection beyond the bifurcation point is still indeterminate) according to the limitation posed by a linear kinematics assumption. If an exact kinematics (i.e. an exact relation among the curvature, rotation and deflection) is employed as in the case of the large curvature analysis, the post-buckling behavior of the column can now be captured as indicated by the dark line in Figure 1.2(b).

The limitation of the linearized-kinematics-based analysis becomes more apparent when applied to very slender or very flexible structures where change of their configuration is sensitive to load applications. For instance, a moment-resisting cable, shown in Figure 1.3, can undergo very large displacement and rotation under service loads. For this particular situation, a simple analysis based on the linear kinematics and enforcement of static equilibrium in the undeformed configuration is insufficient and cannot predict behavior of such a complex structure in an acceptable level of accuracy.
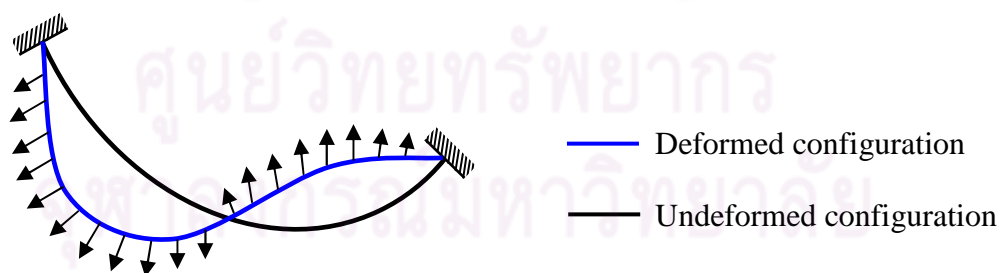


Figure 1.3 Schematic of the deformed and undeformed configurations of a moment-resisting cable under service loads.

Besides mathematical curiosity and computational challenge, necessity to incorporate proper nonlinear kinematics in the mathematical model is obligatory and

arises naturally in numerous practical applications as described above, e.g. analysis and design of structural components where the axial-bending interaction is crucial, analysis of very slender and flexible structures such as bending resisting cables and beams of a large span and high flexibility where the displacement and rotation can be substantial, the determination of the bifurcation load of axial-dominated structural systems and their post-buckling behavior, etc. Due to complexity of the boundary value problem posed by the governing nonlinear kinematics, works concerning large curvature analysis of flexure-dominating structures are still relatively less extensive than those based on linear analysis and this motivates the current investigation.

## 1.2 Background and Review

Linear structural analysis has widely been used in the analysis and design procedure of flexure-dominating structures (e.g. beams and rigid frames) as a result of its simplicity, sufficient accuracy of analysis results for various practical situations, and its vast availability in a form of commercial packages. The key assumptions that are central to this analysis technique include that (1) static equilibrium of the structure is enforced only on its undeformed configuration, (2) the constituting material is linearly elastic, and (3) the linearized kinematics relating the deformation and displacement is pertained (Gallagher and Ziemian, 2000; West, 2002). As a consequence of these assumptions, the corresponding mathematical model is significantly simplified and renders an ease in the construction of its solution; in particular, the response of such a mathematical model is a linear function of external applied loads. Beside its simplicity, the model offers no answer to various questions of practical importance for instance, the critical load and stability status of the structure, the post-buckling behavior, change of stiffness of the structure due to change of its geometry, etc. Note further that in analysis of various structural problems (e.g. modeling of very slender and flexible structures or structures with load-dependent stiffness) the constitutive model based upon linear elasticity is still sufficient and applicable for a wide range of applied loads; however, the major source of error from linear analysis is due to the presence of geometric nonlinearity. This type of nonlinearity becomes more apparent when the change of configuration of the

structure from the original state is significant and, as a result, the assumptions (1) and (3) described above constitute no longer the good approximation of real behavior of the structure. This therefore necessitates an integration of the geometric nonlinearity into a process of mathematical modeling or structural idealization.

One simple approach that has extensively been used to model geometric nonlinearity is known as the second order analysis (Krawinkler and Seneviratna, 1998; Li, 2001; Silvestre and Camotim, 2007). The influence of the geometric nonlinearity was incorporated into the mathematical model by forming static equilibrium equations based upon geometry of the structure in a deformed state. Treatment of geometric nonlinearity in this manner renders the model capable of exploring certain characteristics of the structure such as the critical or bifurcation load and its stability status (Timoshenko and Gere, 1972; Sampaio and Hundhausen, 1998) and the influence of the axial load on the bending moment and the stiffness of the entire structure (Krawinkler and Seneviratna, 1998; Silvestre and Camotim, 2007). While the technique provides an answer to several questions as the linear analysis cannot, the second order analysis still possesses several limitations due to its underline assumptions. For instance, it provides no information on behavior of the structure beyond points of bifurcation (i.e. post buckling behavior) and provides results of insufficient accuracy when the displacement and rotation of the structure are relatively large and the discrepancy between the deformed and undeformed configurations is obvious. The key restriction results from the use of a linearized kinematics, i.e. the curvature of the member is assumed to be small and it is related linearly to the displacement and rotation.

To further broaden the range of modeling capability concerning geometric nonlinearity, a more sophisticated mathematical model incorporating exact kinematics was introduced and the associated problem was known as the "elastica" problem. In addition to equilibrium equations being set up in the deformed configuration, the model uses exact relationship among the curvature, the displacement, and the rotation. A first set of studies of elastica problems can be traced back to the late eighteen century according to the work of Euler (1774) and Lagrange (1770-1773); in those original works, the calculus of variation and the analytical integration via

representation of solutions in terms of a series were utilized with the primary objective to find an exact elastic curve (the deflected shape) of the beam undergoing large deflections. Later, Kirchoff (1859) addressed an analogy between a problem of finding elastica of a perfectly straight cantilever column subjected to an axial load beyond the value of its buckling load and a problem of oscillations of a pendulum. With such analogy, a closed-form solution of the elastic curve can be constructed using a so-called, elliptic integral method. Since then, a series of investigations concerning the elastica problem has continuously been conducted (see Timoshenko, 1953 for extensive historical discussion).

The large curvature analysis based on the exact kinematics has, nowadays, gained significant attention and, extensively, been used to investigate various aspects of post-buckling behavior of structures. This is owing to a significant progress on the computer-aid tools and existing powerful numerical techniques allowing the treatment of more complex boundary value problems. Here, we summarize certain relevant works aiming not only to present the series of historical breakthrough but also to demonstrate the current gap of knowledge and the original aspect of this current investigation.

The first set of works summarized below is associated with the study of a single member subjected to various end conditions and applied loads. Wang (1997) employed, instead of the classical elliptic integral method, the numerical method based upon the perturbation technique to investigate the post-buckling behavior of a prismatic, cantilever column subjected to a point load at the tip. The post-buckling behavior of the same column under the combined action between a uniformly distributed load on the entire member and a concentrated load at the tip was later examined by Lee (2001). In his analysis, the numerical integration procedure based on Butcher's fifth-order Runge-Kutta method was utilized to construct the numerical solutions. Phungpaingam and Chucheepsakul (2002) employed the elliptic integral technique and the shooting method to analyze a simply supported beam of variable arc-length and subjected to an inclined follower force at any location within the member. Vaz and Silva (2003) generalized the work of Wang (1997) by replacing the clamped end of the column by a rotational spring. In their investigation, they

employed a two-parameter shooting method to explore both the buckling and post-buckling behavior of the column. Results from their study revealed that the rotational constraint at the end of the column significantly influences the post-buckling configuration. Madhusudan et al. (2003) extended the work of Lee (2001) to explore the influence of nonuniform cross section on the post-buckling behavior of the cantilever column. The problem is cast within the context of dynamic formulation and the resulting nonlinear equations are solved by a fourth-order Runge-Kutta scheme. Wang et al. (2006) reexamined a cantilever beam subjected only to a point force at the end. In their work, they employed a homotopy analytical method to construct an explicit solution of the rotation and displacement at the free end. Shavartman (2007) investigated a cantilever beam with the clamped end replaced by a rotational spring and subjected to a follower force at the tip. In the analysis, the proper change of variables was applied to convert the two-point boundary value problem to the initial value problem. It was suggested from this study that results can be obtained in a more efficient manner than that by the numerical shooting method and fourth order Runge-Kutta method. Recently, Benjaree et al. (2008) exploited the shooting method along with the adomain decomposition to further perform large curvature analysis of a cantilever beam under more complex loading conditions and containing an inflection point.

Note that all works described above are restricted primarily to structures consisting of only a single member. Based on extensive literature review, work focusing on the large curvature analysis of structures consisting of multiple members is still limited. For instance, Dado et al. (2004) investigated the post-buckling behavior of a cantilever column consisting of two segments of different properties connecting by a rotational spring. In their work, the following three different methods were used: a semi-analytical method based upon the governing equations cast in terms of elliptic integral and being solved by Newton-Raphson technique, the numerical integration technique, and the large displacement finite element analysis using NASTRAN. Result from their study revealed that the semi-analytical has proved to be computationally efficient and accurate in comparison with the other two. Suwansheewasiri and Chucheepsakul (2004) used an elliptic integral method to

investigate the buckling and post-buckling behavior of a two-member, inextensible frame structure of a particular configuration; both the symmetric and non-symmetric post-buckling shapes of the structure were investigated. Most recently, Hu et al. (2007) employed the differential quadrature element method (DQEM) to perform the large deformation analysis of the frame structures containing discontinuity conditions. Note that while the proposed method seems to be computationally efficient, quite general, and applicable to large displacement analysis of structures with general configurations, the method itself is an approximate scheme and the discretization of the problem must be properly treated in order to obtain converged numerical results. To the best knowledge of the investigator, a systematic technique based upon the simple direct stiffness method furnishing by exact element tangent stiffness matrices is not available, and the current investigation is proposed to close this gap of knowledge.

## 1.3 Research Objective

The proposed investigation aims to develop a systematic, efficient and accurate technique that is capable of performing large curvature analysis of flexure-dominating structures (e.g. beams and frame) of arbitrary configurations and under various loading conditions. The primary objective is to employ such the developed technique to explore the behavior and various aspects of beams and frames when the exact kinematics is taken into consideration.

## 1.4 Research Scopes

Structures focused on the proposed investigation are two-dimensional and consist of a collection of straight and prismatic members. Each individual member is made of a homogeneous, isotropic, linearly elastic material. Both shear and axial deformations (extensibility) are negligible and can be discarded without loss. The development is restricted to the case that external loads are applied only at joints or defined node. The numerical technique proposed is to be implemented into an in-house, computer program using FORTRAN90.

**1.5 Research Methodology**

A computational technique proposed is based upon a semi-analytical approach. A classical elliptic integral technique is employed to derive a complete set of differential equations governing each individual member. This set of equations is to be solved first for a member of simple boundary conditions, e.g. the simply-supported beam, to obtain useful basic solutions. Such results are then used along with the coordinate transformation and direct and indirect differentiations to form the exact element tangent stiffness matrix for a two-dimensional member. A direct stiffness method is proposed to assemble the element tangent stiffness equations into the tangent stiffness equations for the entire structure. The resulting system of nonlinear algebraic equations is to be solved by Newton-Raphson technique.

**1.6 Research Significance**

The current investigation proposes a systematic and robust technique that is well-suited for large curvature analysis of two-dimensional, flexure-dominating structures. The attractive features of the proposed techniques are that it is based primarily upon a simple direct stiffness strategy which therefore allows the treatment of structures of general geometry and consisting of multiple members, and that the exact element tangent stiffness matrix for each element is exploited which therefore allows the analytical solution (within the round off and solution errors) to be obtained without mesh refinement.

An additional contribution of the proposed investigation is that the developed technique, after performing careful verification, can be used to generate the benchmark solutions such a general nodal displacement or deformed configuration for various structures; these reference solutions are useful for verification of any new developed numerical techniques.

# CHAPTER II

## BASIC EQUATIONS

This chapter briefly summarizes key assumptions that are pertinent to the current development and the integration of three basic equations, i.e. static equilibrium, kinematics and constitutive relation, to form a set of differential equations governing behavior of an individual flexure-dominating member.

### 2.1 Assumptions

Basic assumptions employed in the development of a mathematical model and the derivation of a set of key governing differential equations for a flexure-dominating member are summarized as follow:

 (1) The member is perfectly straight and prismatic;

 (2) The constituting material is isotropic, linearly elastic and homogeneous across the member;

 (3) The displacement, rotation and curvature are related through exact kinematics;

 (4) Static equilibrium is enforced in the deformed configuration;

 (5) Loads acting within the member are absent;

 (6) The member is inextensible;

 (7) The cross section remains plane before and after undergoing deformation; and

 (8) Shear deformation is negligible.

### 2.2 Basic Equations

Let consider a perfectly straight, prismatic member of length L and moment of inertia I and made of an elastic material of Young's modulus E. Both undeformed and deformed configurations of the member are shown schematically in Figure 2.1(a). The undeformed configuration of the member occupies a straight line defined by $x \in [0, L]$

and y = 0 and, resulting from loads acting at both ends, it moves to a new, deformed configuration. In particular, the material point (x, 0) in the undeformed configuration displaces to the same material point (x + u, v) in the deformed configuration where u = u(x) and v = v(x) denote the x-component and the y-component of the displacement of the material point (x, 0), respectively. Let $f_x = f_x(x)$, $f_y = f_y(x)$ and $m = m(x)$ denote a resultant internal force in x-direction, a resultant internal force in y-direction, and a resultant bending moment about the z-axis (the axis pointing outward of the paper), respectively.
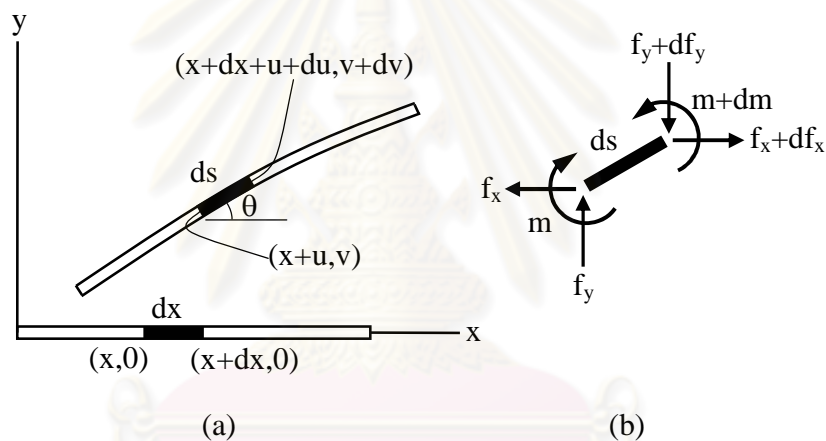


Figure 2.1 (a) Schematic of deformed and undeformed configurations and (b) free body diagram of infinitesimal element ds

Let dx and ds be the same infinitesimal material elements in the undeformed configuration and in the deformed configuration, respectively. In particular, dx is a straight element connecting a point (x, 0) to a point (x + dx, 0), and ds is a curve element connecting a point (x + u, v) to a point (x + dx + u + du, v + dv) as shown in Figure 2.1(a). From geometric consideration of the element ds along with the assumption (6) (i.e. ds = dx), components of the displacement u and v can readily be related to the rotation at any point of the member, denoted by θ, by

$$\sin\theta = \frac{dv}{dx} \ , \tag{2.1}$$

$$\cos\theta = 1 + \frac{du}{dx} \ . \tag{2.2}$$

By enforcing static equilibrium of the infinitesimal element ds in the deformed configuration (see Figure 2.1(b) for the free body diagram of the element ds) and then using the geometric relations (2.1) and (2.2), it leads to three differential equilibrium equations

$$\frac{df_x}{dx} = 0 \ , \tag{2.3}$$

$$\frac{df_y}{dx} = 0 \ , \tag{2.4}$$

$$\frac{dm}{dx} = f_x \sin\theta + f_y \cos\theta \ . \tag{2.5}$$

Clearly, the first two equilibrium equations (2.3) and (2.4) simply imply that the internal resultant forces $f_x$ and $f_y$ are constant throughout the member and they can fully be obtained if the end forces are known.

Upon exploiting the assumptions (6), (7) and (8), the value of normal strain ($\varepsilon$) varies linearly as a function of the distance z from the neutral axis. The explicit expression is given by

$$\varepsilon = -z\kappa \tag{2.6}$$

where $\kappa$ is the curvature of the cross section and the minus sign simply emphasizes that the positive curvature produces a compressive normal strain at any point above the

neutral axis (z > 0). Combining the strain-curvature relation (2.6) and the assumption (2) and then computing the moment resultant across the section leads to a well-known, linear moment-curvature relationship

$$m = EI\kappa \; .$$
(2.7)

Upon using the definition of the curvature along with the inextensible assumption (i.e. ds = dx), it leads to an exact kinematic relation

$$\kappa = \frac{d\theta}{ds} = \frac{d\theta}{dx} \quad .$$
(2.8)

Combining (2.5), (2.7) and (2.8) yields an alternative form of the moment equilibrium equation

$$\frac{d^2\theta}{d\xi^2} = \hat{f}_x \sin\theta + \hat{f}_y \cos\theta$$
(2.9)

where non-dimensional parameters are defined by $\xi = x/L$, $\hat{f}_x = f_x L^2 / EI$ and $\hat{f}_y = f_y L^2 / EI$. To suit the direct integration of the differential equation (2.9), a term on the left hand side of (2.9) is first re-expressed as

$$\frac{d^2\theta}{d\xi^2} = \frac{d}{d\xi}\left(\frac{d\theta}{d\xi}\right) = \frac{d\theta}{d\xi}\frac{d}{d\theta}\left(\frac{d\theta}{d\xi}\right) = \frac{1}{2}\frac{d}{d\theta}\left(\frac{d\theta}{d\xi}\right)^2$$
(2.10)

With use of the relation (2.10), the equilibrium equation (2.9) can directly be integrated to obtain

$$\left(\frac{d\theta}{d\xi}\right)^2 = C - 2\hat{f}_x \cos\theta + 2\hat{f}_y \sin\theta$$
(2.11)

where a constant C, arising form the integration process, can be determined from boundary conditions. It is worth noting that, from the moment-curvature relationship (2.7), the normalized curvature $d\theta/d\xi$ possesses an identical sign as that of the bending moment. As a consequence, only one of the two solutions of $d\theta/d\xi$ obtained from (2.11) is physically admissible and such a choice depends primarily on the sign of the bending moment. The unique solution can be expressed in a concise form as

$$\frac{d\xi}{d\theta} = \frac{\vartheta(\hat{m})}{\sqrt{C - 2\hat{f}_x\cos\theta + 2\hat{f}_y\sin\theta}} \qquad (2.12)$$

where $\vartheta(\hat{m})$ is a moment-dependence function defined by

$$\vartheta(\hat{m}) = \begin{cases} 1 & , \quad \hat{m} > 0 \\ -1 & , \quad \hat{m} < 0 \end{cases} \qquad (2.13)$$

with $\hat{m} = mL/EI$ denoting the normalized bending moment. Combining (2.12) and the geometric relations (2.1) and (2.2) leads to two differential equations governing the two components of the displacement u and v:

$$\frac{d\hat{v}}{d\theta} = \frac{\vartheta(\hat{m})\sin\theta}{\sqrt{C - 2\hat{f}_x\cos\theta + 2\hat{f}_y\sin\theta}} \qquad (2.14)$$

$$\frac{d\hat{u}}{d\theta} = \frac{\vartheta(\hat{m})(\cos\theta - 1)}{\sqrt{C - 2\hat{f}_x\cos\theta + 2\hat{f}_y\sin\theta}} \qquad (2.15)$$

where $\hat{u} = u/L$ and $\hat{v} = v/L$. A set of three ordinary differential equations (2.12), (2.14) and (2.15) constitutes a basis for the development of useful results presented in the following chapter.

# CHAPTER III

## DIRECT STIFFNESS METHOD FOR LARGE CURVATURE ANALYSIS

In this chapter, a set of governing differential equations established in the previous chapter is utilized to form essential ingredients (e.g. element tangent stiffness matrix and tangent stiffness matrix of the entire structure) central to the development of the direct stiffness method for large curvature analysis. To aid such development, some fundamental results are first obtained for the case of a simply supported beam and such results are subsequently employed along with the law of coordinate transformation to arrive at desirable results.

### 3.1 Results for Simply Supported Beam

Consider a prismatic, simply-supported beam of length L, moment of inertia I and Young's modulus E and subjected to end moments $\{m_1, m_2\}$ and end force $f_{x2}$ as shown in Figure 3.1.
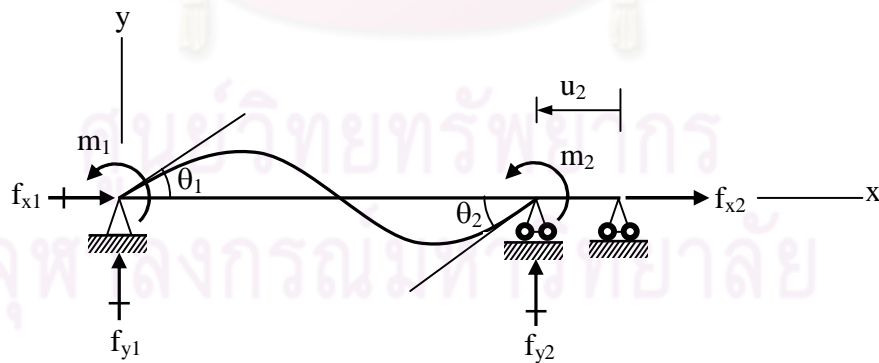


Figure 3.1 schematic of simply supported beam subjected to end moments $\{m_1, m_2,\}$ and end force $f_{x2}$

The essential boundary conditions of this particular beam are given by

$$u(\theta = \theta_1) = 0 \quad , \tag{3.1}$$

$$v(\theta = \theta_1) = 0 \quad , \tag{3.2}$$

$$v(\theta = \theta_2) = 0 \quad . \tag{3.3}$$

Similarly, the natural boundary conditions associated with the prescribed end moments $\{m_1, m_2,\}$ and end force $f_{x2}$ are given by

$$\frac{d\theta}{d\xi}(\theta = \theta_1) = \hat{m}_1 = \frac{m_1 L}{EI} \quad , \tag{3.4}$$

$$\frac{d\theta}{d\xi}(\theta = \theta_2) = \hat{m}_2 = \frac{m_2 L}{EI} \quad , \tag{3.5}$$

$$\hat{f}_x = \hat{f}_{x2} = \frac{f_{x2} L^2}{EI} \quad . \tag{3.6}$$

By imposing the moment boundary condition (3.5) along with the relation (2.11), the constant C can readily be obtained as

$$C = \hat{m}_2^2 + 2\hat{f}_x \cos\theta_2 - 2\hat{f}_y \sin\theta_2 \quad . \tag{3.7}$$

Substituting the constant C from (3.7) into the relations (2.12), (2.14) and (2.15), they now become

$$\frac{d\xi}{d\theta} = \vartheta(\hat{m}) F(\theta, \theta_2; \hat{f}_x, \hat{f}_y, \hat{m}_2) \quad , \tag{3.8}$$

$$\frac{d\hat{v}}{d\theta} = \vartheta(\hat{m})\sin\theta \, F(\theta, \theta_2; \hat{f}_x, \hat{f}_y, \hat{m}_2) \quad , \tag{3.9}$$

$$\frac{d\hat{u}}{d\theta} = \vartheta(\hat{m})(\cos\theta - 1)F(\theta, \theta_2; \hat{f}_x, \hat{f}_y, \hat{m}_2) \tag{3.10}$$

where F is a rotation-dependence function defined by

$$F(\theta, \theta_2; \hat{f}_x, \hat{f}_y, \hat{m}_2) = \frac{1}{\sqrt{\hat{m}_2^2 + 2\hat{f}_x(\cos\theta_2 - \cos\theta) - 2\hat{f}_y(\sin\theta_2 - \sin\theta)}} \quad . \tag{3.11}$$

By imposing the remaining moment boundary condition (3.4), we obtain an additional relation relating kinematical and static quantities:

$$\hat{m}_2^2 - \hat{m}_1^2 + 2\hat{f}_x(\cos\theta_2 - \cos\theta_1) - 2\hat{f}_y(\sin\theta_2 - \sin\theta_1) = 0 \quad . \tag{3.12}$$

The normalized support reactions $\{\hat{f}_{x1}, \hat{f}_{y1}, \hat{f}_{y2}\}$ can readily be computed by enforcing equilibrium of the entire member in the deformed configuration and results are given by

$$\hat{f}_{x1} = -\hat{f}_x \quad , \tag{3.13}$$

$$\hat{f}_{y1} = \frac{\hat{m}_1 + \hat{m}_2}{\hat{d}} \quad , \tag{3.14}$$

$$\hat{f}_{y2} = -\frac{\hat{m}_1 + \hat{m}_2}{\hat{d}} \tag{3.15}$$

where $\hat{f}_{x1} = f_{x1}L^2/EI$, $\hat{f}_{y1} = f_{y1}L^2/EI$, $\hat{f}_{y2} = f_{y2}L^2/EI$ and $\hat{d} = 1 + \hat{u}_2$ with $\hat{u}_2 = u_2/L$.

Next, let define $\theta^*$, $\hat{u}^*$ and $\hat{v}^*$ as the normalized rotation, the normalized displacement in x-direction and the normalized displacement in y-direction at any normalized coordinate $\xi^* = x^*/L$, respectively. By integrating equations (3.8)-(3.10) from $\theta = \theta_1$ to $\theta = \theta^*$, it leads to

$$\int_{\theta_1}^{\theta^*} \vartheta(\hat{m})F(\theta,\theta_2,\hat{f}_x,\hat{f}_y,\hat{m}_2)d\theta = \xi^* \quad , \tag{3.16}$$

$$\int_{\theta_1}^{\theta^*} \vartheta(\hat{m})\sin\theta\, F(\theta,\theta_2,\hat{f}_x,\hat{f}_y,\hat{m}_2)d\theta = \hat{v}^* \quad , \tag{3.17}$$

$$\int_{\theta_1}^{\theta^*} \vartheta(\hat{m})(\cos\theta-1)\, F(\theta,\theta_2,\hat{f}_x,\hat{f}_y,\hat{m}_2)d\theta = \hat{u}^* \tag{3.18}$$

in which the essential boundary conditions at the left end, i.e. (3.1) and (3.2), have been employed. The relations (3.16)-(3.18) provide a complete set of equations sufficient for determining the rotation and two components of the displacement at any point within the beam provided that all unknown quantities at both ends have been solved.

By considering the right end point ($\xi^* = 1$) and recalling that $\theta^* = \theta_2$, $\hat{u}^* = \hat{u}_2$ and $\hat{v}^* = 0$, equations (3.16)-(3.18) when specialized to this particular point become

$$\int_{\theta_1}^{\theta_2} \vartheta(\hat{m})F(\theta,\theta_2,\hat{f}_x,\hat{f}_y,\hat{m}_2)d\theta = 1 \quad , \tag{3.19}$$

$$\int_{\theta_1}^{\theta_2} \vartheta(\hat{m})\sin\theta\, F(\theta,\theta_2,\hat{f}_x,\hat{f}_y,\hat{m}_2)d\theta = 0 \quad , \tag{3.20}$$

$$\int_{\theta_1}^{\theta_2} \vartheta(\hat{m})(\cos\theta-1)\, F(\theta,\theta_2,\hat{f}_x,\hat{f}_y,\hat{m}_2)d\theta = \hat{u}_2 \ . \tag{3.21}$$

For a given set of end loads $\{\hat{f}_{x2},\hat{m}_1,\hat{m}_2\}$, the unknown displacement and rotations $\{\hat{u}_2,\theta_1,\theta_2\}$ can be solved from a system of nonlinear equations (3.19)-(3.20) with use of (3.6) and (3.12) to eliminate $\{\hat{f}_x,\hat{f}_y\}$. This implies that the quantities $\{\hat{f}_{x2},\hat{m}_1,\hat{m}_2\}$ constitutes a proper choice of primary unknowns if the force method is concerned. In contrast, if the displacement method is concerned as in the current investigation, the situation is reversed; i.e. the problem statement now becomes to find the end loads

$\{ \hat{f}_{x2}, \hat{m}_1, \hat{m}_2 \}$ in terms of the prescribed displacement and rotations $\{ \hat{u}_2, \theta_1, \theta_2 \}$. According to the geometric constraint posed by the member inextensibility, the problem indicated above is not well-posed or, in the other word, $\{ \hat{u}_2, \theta_1, \theta_2 \}$ cannot be specified arbitrarily. If $\{ \hat{f}_x, \theta_1, \theta_2 \}$ are prescribed instead, the end loads $\{ \hat{f}_{x2}, \hat{m}_1, \hat{m}_2 \}$ can be solved from (3.6), (3.19) and (3.20) and the end displacement $\hat{u}_2$ can subsequently be computed from (3.21). However, lack of the displacement component $\hat{u}_2$ renders a set $\{ \hat{f}_x, \theta_1, \theta_2 \}$ not well-suited for treatment by the displacement method.

To circumvent such inconvenience, we choose $\{ \hat{u}_2, \theta_1, \theta_2, \hat{f}_x \}$ as a set of primary unknowns. To allow $\hat{u}_2$ be one of independent variables, the strong requirement posed by (3.21) must be relaxed via the introduction of the residual $\mathcal{R}$ such that

$$\mathcal{R} \equiv \hat{d} - \int_{\theta_1}^{\theta_2} \vartheta(\hat{m}) \cos\theta \; F(\theta, \theta_2; \hat{f}_x, \hat{f}_y, \hat{m}_2) d\theta \quad . \tag{3.22}$$

Furnished by (3.22), for any given set $\{ \hat{u}_2, \theta_1, \theta_2, \hat{f}_x \}$, the quantities $\{ \hat{f}_{x2}, \hat{m}_1, \hat{m}_2, \mathcal{R} \}$ can always be determined from (3.6), (3.19), (3.21) and (3.22). It is worth noting that $\{ \hat{u}_2, \theta_1, \theta_2, \hat{f}_x \}$ and the corresponding $\{ \hat{f}_{x2}, \hat{m}_1, \hat{m}_2, \mathcal{R} \}$ are solutions of the boundary value problem only if the residual $\mathcal{R}$ vanishes, i.e. $\mathcal{R} = 0$.

### 3.1.1 Gradient matrix

Let $\mathbf{f}_{(s)}$ be a vector defined by $\mathbf{f}_{(s)} = [\mathbf{f}_p \; \mathbf{f}_r]^T$ where $\mathbf{f}_p = \{ \hat{f}_{x2}, \hat{m}_1, \hat{m}_2, \mathcal{R} \}$ and $\mathbf{f}_r = \{ \hat{f}_{x1}, \hat{f}_{y1}, \hat{f}_{y2} \}$ and let $\mathbf{u}_{(s)}$ be a vector defined by $\mathbf{u}_{(s)} = \{ \hat{u}_2, \theta_1, \theta_2, \hat{f}_x \}^T$. From (3.6), (3.12)-(3.15), (3.19)-(3.20) and (3.22), it can be verified that $\mathbf{f}_{(s)} = \mathbf{f}_{(s)}(\mathbf{u})$ and, from Taylor series expansion, this nonlinear function $\mathbf{f}_{(s)}$ possesses a best linear approximation in the neighborhood of any vector $\mathbf{u}_o$ given by

$$\mathbf{f}_{(s)}(\mathbf{u}) = \mathbf{f}_{(s)}(\mathbf{u}_o) + \mathbf{g}(\mathbf{u}_o)(\mathbf{u} - \mathbf{u}_o) \tag{3.23}$$

where $\mathbf{g}$ is the gradient matrix defined by

$$\mathbf{g} = \frac{\partial \mathbf{f}_{(s)}}{\partial \mathbf{u}_{(s)}} = \begin{bmatrix} \mathbf{g}_p \\ \mathbf{g}_r \end{bmatrix} \tag{3.24}$$

with the sub-matrices $\mathbf{g}_p$ and $\mathbf{g}_r$ representing the gradient of the vector $\mathbf{f}_p$ and vector $\mathbf{f}_r$ with respect to the vector $\mathbf{u}_{(s)}$, respectively. The explicit definition of the sub-matrix $\mathbf{g}_p$ is given by

$$\mathbf{g}_p = \begin{bmatrix} \partial \hat{f}_{x2}/\partial \hat{u}_2 & \partial \hat{f}_{x2}/\partial \theta_1 & \partial \hat{f}_{x2}/\partial \theta_2 & \partial \hat{f}_{x2}/\partial \hat{f}_x \\ \partial \hat{m}_1/\partial \hat{u}_2 & \partial \hat{m}_1/\partial \theta_1 & \partial \hat{m}_1/\partial \theta_2 & \partial \hat{m}_1/\partial \hat{f}_x \\ \partial \hat{m}_2/\partial \hat{u}_2 & \partial \hat{m}_2/\partial \theta_1 & \partial \hat{m}_2/\partial \theta_2 & \partial \hat{m}_2/\partial \hat{f}_x \\ \partial \mathcal{R}/\partial \hat{u}_2 & \partial \mathcal{R}/\partial \theta_1 & \partial \mathcal{R}/\partial \theta_2 & \partial \mathcal{R}/\partial \hat{f}_x \end{bmatrix} . \tag{3.25}$$

By denoting $g_{ij}$ as an entry located at the $i^{th}$ row and $j^{th}$ column of the sub-matrix $\mathbf{g}_p$, the sub-matrix $\mathbf{g}_r$ can readily be obtained, in terms of $g_{ij}$, by

$$\mathbf{g}_r = \frac{1}{\hat{d}} \begin{bmatrix} -g_{11}\hat{d} & -g_{12}\hat{d} & -g_{13}\hat{d} & -g_{14}\hat{d} \\ -\hat{s} & g_{22}+g_{32} & g_{23}+g_{33} & g_{24}+g_{34} \\ \hat{s} & -g_{22}-g_{32} & -g_{23}-g_{33} & -g_{24}-g_{34} \end{bmatrix} \tag{3.26}$$

where $\hat{s} = (\hat{m}_1 + \hat{m}_2)/\hat{d}$.

To form the gradient matrix $\mathbf{g}$, it therefore necessitates the construction of the sub-matrix $\mathbf{g}_p$. As clearly indicated by (3.6), (3.19), (3.20), and (3.22), certain entries of the sub-matrix can trivially be obtained, e.g. $g_{11} = g_{12} = g_{13} = g_{21} = g_{31} = 0$ and $g_{14} = g_{41} = 1$. With these results, the sub-matrix $\mathbf{g}_p$ now becomes

$$\mathbf{g}_p = \begin{bmatrix} \mathbf{g}_{p1} & \mathbf{g}_{p2} \\ \mathbf{g}_{p3} & \mathbf{g}_{p4} \end{bmatrix} \tag{3.27}$$

where the matrices $\mathbf{g}_{p1}$, $\mathbf{g}_{p2}$, $\mathbf{g}_{p3}$ and $\mathbf{g}_{p4}$ are defined by

$$\mathbf{g}_{p1} = \begin{bmatrix} 0 \end{bmatrix} \quad , \tag{3.28}$$

$$\mathbf{g}_{p2} = \mathbf{g}_{p3}^{T} = \begin{bmatrix} 0 & 0 & 1 \end{bmatrix} \quad , \tag{3.29}$$

$$\mathbf{g}_{p4} = \begin{bmatrix} \partial\hat{m}_1/\partial\theta_1 & \partial\hat{m}_1/\partial\theta_2 & \partial\hat{m}_1/\partial\hat{f}_x \\ \partial\hat{m}_2/\partial\theta_1 & \partial\hat{m}_2/\partial\theta_2 & \partial\hat{m}_2/\partial\hat{f}_x \\ \partial\mathcal{R}/\partial\theta_1 & \partial\mathcal{R}/\partial\theta_2 & \partial\mathcal{R}/\partial\hat{f}_x \end{bmatrix} \quad . \tag{3.30}$$

Determination of the matrix $\mathbf{g}_{p4}$ is non-trivial and theoretically requires implicit differentiations. The explicit form of such the matrix $\mathbf{g}_{p4}$ can further be derived for various cases depending on the existence and location of inflection points within the member. For instance, a single curvature member contains either no inflection point or inflection points only at its ends while a double curvature member contains an inflection within the member. Presence of the inflection point within the member poses two potential difficulties that require a careful treatment; one is associated with the singularity of the function F at the inflection point and the other corresponds to the discontinuity of the moment-dependence function $\vartheta(\hat{m})$ at the inflection point.

### 3.1.2 Determination of sub-matrix $\mathbf{g}_{p4}$

Determination of the sub-matrix $\mathbf{g}_{p4}$ is established for the following three cases: a member containing no inflection point, a member containing an inflection point at the end, and a member containing an inflection point within the member. Results for these three cases are sufficient for the development carried out further below.

#### 3.1.2.1 Member containing no inflection point

Consider a beam member where the bending moment $\hat{m}(\xi) > 0$ for $\xi \in [0, 1]$ or $\hat{m}(\xi) < 0$ for $\xi \in [0, 1]$. This particular case arises when the applied end moments $\{\hat{m}_1, \hat{m}_2\}$ are non-zero and of the opposite sign. The resulting deformed configuration of the beam possesses a single curvature and, in addition, $\vartheta(\hat{m})$ becomes a constant function

with its value equal to either 1 or -1 depending on the sign of $\hat{m}$, i.e. $\vartheta(\hat{m}) = 1$ for $\hat{m} > 0$ and $\vartheta(\hat{m}) = -1$ for $\hat{m} < 0$. It is worth noting that the function F, defined by (3.11), is well-behaved in the sense that the quantity within the square root is always greater than zero; this results directly from the fact that $\hat{m} \neq 0$ for the entire beam. Such desirable feature of F renders all involved integrals nonsingular and, therefore, allows a standard procedure be employed in their treatment.

For convenience in further development, let re-express the governing equations (3.19) and (3.20) in a form

$$\Gamma_1(\theta_1, \theta_2, \hat{f}_x, \hat{f}_y, \hat{m}_2) = \vartheta \int_{\theta_1}^{\theta_2} F(\theta, \theta_2, \hat{f}_x, \hat{f}_y, \hat{m}_2) d\theta - 1 = 0 \quad , \tag{3.31}$$

$$\Gamma_2(\theta_1, \theta_2, \hat{f}_x, \hat{f}_y, \hat{m}_2) = \vartheta \int_{\theta_1}^{\theta_2} \sin\theta \, F(\theta, \theta_2, \hat{f}_x, \hat{f}_y, \hat{m}_2) d\theta = 0 \tag{3.32}$$

and recall from (3.22) that

$$\mathscr{R} = \mathscr{R}(\theta_1, \theta_2, u_2, \hat{f}_x, \hat{f}_y, \hat{m}_2) = \hat{d} - \vartheta \int_{\theta_1}^{\theta_2} \cos\theta \, F(\theta, \theta_2; \hat{f}_x, \hat{f}_y, \hat{m}_2) d\theta \quad . \tag{3.33}$$

From the auxiliary relation (3.12), it can be concluded that

$$\hat{f}_y = \hat{f}_y(\theta_1, \theta_2, \hat{f}_x, \hat{m}_1, \hat{m}_2) \quad . \tag{3.34}$$

With use of (3.33), equations (3.31) and (3.32) implicitly define the normalized end moments $\{ \hat{m}_1, \hat{m}_2 \}$ as functions of $\{ \theta_1, \theta_2, \hat{f}_x \}$, i.e.

$$\hat{m}_1 = \hat{m}_1(\theta_1, \theta_2, \hat{f}_x) \quad , \tag{3.35}$$

$$\hat{m}_2 = \hat{m}_2(\theta_1, \theta_2, \hat{f}_x) \quad . \tag{3.36}$$

By taking derivative of (3.31)-(3.33) with respect to $\{\theta_1, \theta_2, \hat{f}_x\}$ along with employing (3.34)-(3.36) and the chain rule of differentiation, we obtain the relation

$$\mathbf{S}\mathbf{g}_{p4} = -\mathbf{D} \tag{3.37}$$

where the matrices $\mathbf{S}$ and $\mathbf{D}$ are given by

$$\mathbf{S} = \begin{bmatrix} \dfrac{\partial \Gamma_1}{\partial \hat{f}_y}\dfrac{\partial \hat{f}_y}{\partial \hat{m}_1} & \dfrac{\partial \Gamma_1}{\partial \hat{m}_2} + \dfrac{\partial \Gamma_1}{\partial \hat{f}_y}\dfrac{\partial \hat{f}_y}{\partial \hat{m}_2} & 0 \\[2ex] \dfrac{\partial \Gamma_2}{\partial \hat{f}_y}\dfrac{\partial \hat{f}_y}{\partial \hat{m}_1} & \dfrac{\partial \Gamma_2}{\partial \hat{m}_2} + \dfrac{\partial \Gamma_2}{\partial \hat{f}_y}\dfrac{\partial \hat{f}_y}{\partial \hat{m}_2} & 0 \\[2ex] \dfrac{\partial \mathcal{R}}{\partial \hat{f}_y}\dfrac{\partial \hat{f}_y}{\partial \hat{m}_1} & \dfrac{\partial \mathcal{R}}{\partial \hat{m}_2} + \dfrac{\partial \mathcal{R}}{\partial \hat{f}_y}\dfrac{\partial \hat{f}_y}{\partial \hat{m}_2} & 1 \end{bmatrix}, \tag{3.38}$$

$$\mathbf{D} = \begin{bmatrix} \dfrac{\partial \Gamma_1}{\partial \theta_1} + \dfrac{\partial \Gamma_1}{\partial \hat{f}_y}\dfrac{\partial \hat{f}_y}{\partial \theta_1} & \dfrac{\partial \Gamma_1}{\partial \theta_2} + \dfrac{\partial \Gamma_1}{\partial \hat{f}_y}\dfrac{\partial \hat{f}_y}{\partial \theta_2} & \dfrac{\partial \Gamma_1}{\partial \hat{f}_x} + \dfrac{\partial \Gamma_1}{\partial \hat{f}_y}\dfrac{\partial \hat{f}_y}{\partial \hat{f}_x} \\[2ex] \dfrac{\partial \Gamma_2}{\partial \theta_1} + \dfrac{\partial \Gamma_2}{\partial \hat{f}_y}\dfrac{\partial \hat{f}_y}{\partial \theta_1} & \dfrac{\partial \Gamma_2}{\partial \theta_2} + \dfrac{\partial \Gamma_2}{\partial \hat{f}_y}\dfrac{\partial \hat{f}_y}{\partial \theta_2} & \dfrac{\partial \Gamma_2}{\partial \hat{f}_x} + \dfrac{\partial \Gamma_2}{\partial \hat{f}_y}\dfrac{\partial \hat{f}_y}{\partial \hat{f}_x} \\[2ex] -\dfrac{\partial \mathcal{R}}{\partial \theta_1} - \dfrac{\partial \mathcal{R}}{\partial \hat{f}_y}\dfrac{\partial \hat{f}_y}{\partial \theta_1} & -\dfrac{\partial \mathcal{R}}{\partial \theta_2} - \dfrac{\partial \mathcal{R}}{\partial \hat{f}_y}\dfrac{\partial \hat{f}_y}{\partial \theta_2} & -\dfrac{\partial \mathcal{R}}{\partial \hat{f}_x} - \dfrac{\partial \mathcal{R}}{\partial \hat{f}_y}\dfrac{\partial \hat{f}_y}{\partial \hat{f}_x} \end{bmatrix}. \tag{3.39}$$

Upon using the explicit function form of $\{\Gamma_1, \Gamma_2, \mathcal{R}\}$, the matrix S and D can be obtained explicitly by

$$\mathbf{S} = \begin{bmatrix} \dfrac{\vartheta(i_2 - i_1 s_2)\hat{m}_1}{s_2 - s_1} & -\dfrac{\vartheta(i_2 - i_1 s_1)\hat{m}_2}{s_2 - s_1} & 0 \\[2ex] \dfrac{\vartheta(i_4 - i_2 s_2)\hat{m}_1}{s_2 - s_1} & -\dfrac{\vartheta(i_4 - i_2 s_1)\hat{m}_2}{s_2 - s_1} & 0 \\[2ex] \dfrac{\vartheta(i_5 - i_3 s_2)\hat{m}_1}{s_2 - s_1} & -\dfrac{\vartheta(i_5 - i_3 s_1)\hat{m}_2}{s_2 - s_1} & 1 \end{bmatrix}, \tag{3.40}$$

$$\mathbf{D} = \begin{bmatrix} -\dfrac{\vartheta(i_2 - i_1 s_2)\lambda_1}{s_2 - s_1} + \dfrac{1}{\hat{m}_1} & \dfrac{\vartheta(i_2 - i_1 s_2)\lambda_2}{s_2 - s_1} + \dfrac{1}{\hat{m}_2} & \vartheta\dfrac{i_2(c_1 - c_2) + i_1 s_{12}}{s_2 - s_1} + \vartheta i_3 \\[2ex] -\dfrac{\vartheta(i_4 - i_2 s_2)\lambda_1}{s_2 - s_1} + \dfrac{s_1}{\hat{m}_1} & \dfrac{\vartheta(i_4 - i_2 s_2)\lambda_2}{s_2 - s_1} + \dfrac{s_2}{\hat{m}_2} & \vartheta\dfrac{i_4(c_1 - c_2) + i_2 s_{12}}{s_2 - s_1} + \vartheta i_5 \\[2ex] -\dfrac{\vartheta(i_5 - i_3 s_2)\lambda_1}{s_2 - s_1} + \dfrac{c_1}{\hat{m}_1} & \dfrac{\vartheta(i_5 - i_2 s_3)\lambda_2}{s_2 - s_1} + \dfrac{c_2}{\hat{m}_2} & \vartheta\dfrac{i_5(c_1 - c_2) + i_3 s_{12}}{s_2 - s_1} + \vartheta i_6 \end{bmatrix} \qquad (3.41)$$

where $s_1 = \sin\theta_1$, $s_2 = \sin\theta_2$, $s_{12} = \sin(\theta_1 - \theta_2)$, $c_1 = \cos\theta_1$, $c_2 = \cos\theta_2$, $\lambda_1 = \hat{f}_x s_1 + \hat{f}_y c_1$, $\lambda_2 = \hat{f}_x s_2 + \hat{f}_y c_2$ and integrals $\{i_1, i_2, i_3, i_4, i_5, i_6\}$ are denoted by

$$i_1 = \int_{\theta_1}^{\theta_2} F^3(\theta, \theta_2; \hat{f}_x, \hat{f}_y, \hat{m}_2)d\theta \quad , \qquad\qquad (3.42)$$

$$i_2 = \int_{\theta_1}^{\theta_2} F^3(\theta, \theta_2; \hat{f}_x, \hat{f}_y, \hat{m}_2)\sin\theta d\theta \quad , \qquad\qquad (3.43)$$

$$i_3 = \int_{\theta_1}^{\theta_2} F^3(\theta, \theta_2; \hat{f}_x, \hat{f}_y, \hat{m}_2)\cos\theta d\theta \quad , \qquad\qquad (3.44)$$

$$i_4 = \int_{\theta_1}^{\theta_2} F^3(\theta, \theta_2; \hat{f}_x, \hat{f}_y, \hat{m}_2)\sin^2\theta d\theta \quad , \qquad\qquad (3.45)$$

$$i_5 = \int_{\theta_1}^{\theta_2} F^3(\theta, \theta_2; \hat{f}_x, \hat{f}_y, \hat{m}_2)\sin\theta\cos\theta d\theta \quad , \qquad\qquad (3.46)$$

$$i_6 = \int_{\theta_1}^{\theta_2} F^3(\theta, \theta_2; \hat{f}_x, \hat{f}_y, \hat{m}_2)\cos^2\theta d\theta \quad . \qquad\qquad (3.47)$$

By solving a system of linear equations (3.37), we obtain an explicit expression of the matrix $\mathbf{g}_{p4}$ in a form

$$\mathbf{g}_{p4} = -\mathbf{S}^{-1}\mathbf{D} = \begin{bmatrix} \dfrac{2i_2 s_1 - i_1 s_1^2 - i_4}{\vartheta \zeta_3 \hat{m}_1^2} + \dfrac{\lambda_1}{\hat{m}_1} & \dfrac{i_2(s_1 + s_2) - i_1 s_1 s_2 - i_4}{\vartheta \zeta_3 \hat{m}_1 \hat{m}_2} & \dfrac{\zeta_1 s_1 + \zeta_2}{\zeta_3 \hat{m}_1} - \dfrac{c_1}{\hat{m}_1} \\[3mm] \dfrac{i_2(s_1 + s_2) - i_1 s_1 s_2 - i_4}{\vartheta \zeta_3 \hat{m}_1 \hat{m}_2} & \dfrac{2i_2 s_2 - i_1 s_2^2 - i_4}{\vartheta \zeta_3 \hat{m}_2^2} + \dfrac{\lambda_2}{\hat{m}_2} & \dfrac{\zeta_1 s_2 + \zeta_2}{\zeta_3 \hat{m}_2} - \dfrac{c_2}{\hat{m}_2} \\[3mm] \dfrac{\zeta_1 s_1 + \zeta_2}{\zeta_3 \hat{m}_1} - \dfrac{c_1}{\hat{m}_1} & \dfrac{\zeta_1 s_2 + \zeta_2}{\zeta_3 \hat{m}_2} - \dfrac{c_2}{\hat{m}_2} & \dfrac{2i_2 i_3 i_5 - i_3^2 i_4 - i_1 i_5^2}{\vartheta \zeta_3} - \dfrac{i_6}{\vartheta} \end{bmatrix} \qquad (3.48)$$

where $\zeta_1 = i_2 i_3 - i_1 i_5$, $\zeta_1 = i_2 i_5 - i_3 i_4$ and $\zeta_3 = i_2^2 - i_1 i_4$. Clearly, the matrix $\mathbf{g}_{p4}$ is essentially symmetric and it can further be verified that it is additionally positive definite.

### 3.1.2.2 Member containing interior inflection point

Consider a beam member where there exists an inflection point at an interior point $\xi_z \in (0, 1)$ or, equivalently, the bending moment vanishes at $\xi_z \in (0, 1)$ and $\hat{m}(\xi_1)\hat{m}(\xi_2) < 0$ for $\xi_1 \in [0, \xi_z)$ and $\xi_2 \in (\xi_z, 1]$. This particular case arises when the applied end moments $\{\hat{m}_1, \hat{m}_2\}$ are non-zero and of the same sign. The resulting deformed configuration of the beam possesses a double curvature; i.e. the curvature on both sides of the inflection point is of the opposite sign. As a result, the moment-dependence function $\vartheta$ is discontinuous at $\xi_z$ and takes different values on both sides of the inflection point. For the applied end moments $\hat{m}_1 > 0$, $\hat{m}_2 < 0$, it results in $\vartheta = -1$ for $\xi \in [0, \xi_z)$ and $\vartheta = 1$ for $\xi \in (\xi_z, 1]$ and, for $\hat{m}_1 < 0$, $\hat{m}_2 > 0$, it results in $\vartheta = 1$ for $\xi \in [0, \xi_z)$ and $\vartheta = -1$ for $\xi \in (\xi_z, 1]$. Schematic of the beam associated with the former case is shown in Figure 3.2.

At the inflection point, a special condition associated with vanishing of the bending moment is given by

$$\frac{d\theta}{d\xi}(\theta = \theta_z) = 0 \quad . \qquad (3.49)$$

where $\theta_z$ denotes the rotation at the inflection point. By enforcing this special condition, the constant C can be obtained from (2.11) as
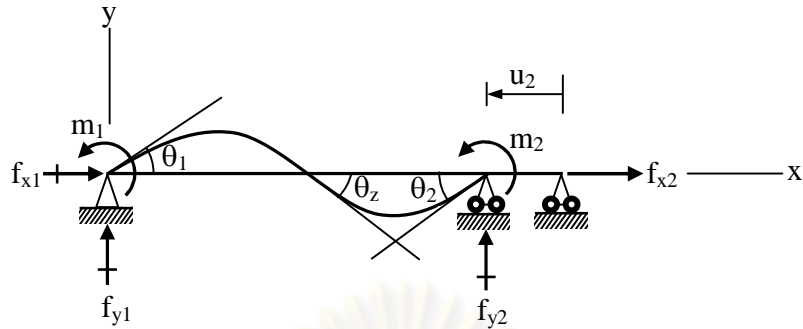
Figure 3.2 Schematic of simply supported beam subjected to end moments of same sign

$$C = 2\hat{f}_x\cos\theta_z - 2\hat{f}_y\sin\theta_z \quad . \tag{3.50}$$

By substituting the constant C into (2.12), (2.14) and (2.15), it leads to

$$\frac{d\xi}{d\theta} = \Im(\hat{m})F_z(\theta, \theta_z; \hat{f}_x, \hat{f}_y) \quad , \tag{3.51}$$

$$\frac{d\hat{v}}{d\theta} = \Im(\hat{m})\sin\theta\, F_z(\theta, \theta_z; \hat{f}_x, \hat{f}_y) \quad , \tag{3.52}$$

$$\frac{d\hat{u}}{d\theta} = \Im(\hat{m})(\cos\theta - 1)F_z(\theta, \theta_z; \hat{f}_x, \hat{f}_y) \tag{3.53}$$

where the function $F_z$ is defined by

$$F_z(\theta, \theta_z; \hat{f}_x, \hat{f}_y) = \frac{1}{\sqrt{2\hat{f}_x(\cos\theta_z - \cos\theta) - 2\hat{f}_y(\sin\theta_z - \sin\theta)}} \quad . \tag{3.54}$$

By integrating equations (3.51)-(3.53) over the entire beam, we obtain

$$\psi\left[ -\int_{\theta_1}^{\theta_z} F_z(\theta, \theta_z; \hat{f}_x, \hat{f}_y)d\theta + \int_{\theta_z}^{\theta_2} F_z(\theta, \theta_z; \hat{f}_x, \hat{f}_y)d\theta \right] = 1 \quad , \tag{3.55}$$

$$\psi\left[-\int_{\theta_1}^{\theta_z}\sin\theta\, F_z(\theta,\theta_z;\hat{f}_x,\hat{f}_y)d\theta + \int_{\theta_z}^{\theta_2}\sin\theta\, F_z(\theta,\theta_z;\hat{f}_x,\hat{f}_y)d\theta\right] = 0 \quad, \tag{3.56}$$

$$\psi\left[-\int_{\theta_1}^{\theta_z}\left(\cos\theta-1\right)F_z(\theta,\theta_z;\hat{f}_x,\hat{f}_y)d\theta + \int_{\theta_z}^{\theta_2}\left(\cos\theta-1\right)F_z(\theta,\theta_z;\hat{f}_x,\hat{f}_y)d\theta\right] = \hat{u}_2 \tag{3.57}$$

where a constant $\psi$ is defined by

$$\psi = \begin{cases} -1 & , & \hat{m}_1,\hat{m}_2 < 0 \\ 1 & , & \hat{m}_1,\hat{m}_2 > 0 \end{cases} \quad. \tag{3.58}$$

It is evident from (3.54) that the function $F_z$ is singular at the inflection point; thus, all singular integrals appearing in (3.55)-(3.57) require special treatments. To overcome such difficulty, a series of variable transformations is introduced to remove and regularize such singularity. By defining quantities

$$\hat{f}_s^2 = \sqrt{\hat{f}_x^2 + \hat{f}_y^2} \quad, \quad \cos\theta_o = \frac{\hat{f}_x}{\hat{f}_s^2} \quad, \quad \sin\theta_o = -\frac{\hat{f}_y}{\hat{f}_s^2} \quad, \tag{3.59}$$

terms appearing in the square root in (3.54) can be expressed as

$$\hat{f}_x\cos\theta - \hat{f}_y\sin\theta = \hat{f}_s^2\cos(\theta-\theta_o) \quad, \tag{3.60}$$

$$\hat{f}_x\cos\theta_z - \hat{f}_y\sin\theta_z = \hat{f}_s^2\cos(\theta_z-\theta_o) \quad. \tag{3.61}$$

After substituting identities (3.60) and (3.61) into (3.54), the function $F_z$ now becomes

$$F_z(\theta,\theta_z,\theta_o;\hat{f}_s) = \frac{1}{\sqrt{2\hat{f}_s^2\left[\cos(\theta_z-\theta_o)-\cos(\theta-\theta_o)\right]}} \quad. \tag{3.62}$$

Upon change of a variable $\bar{\theta} = \pi + (\theta - \theta_o)$ and use of an identity $\cos\bar{\theta} = 1 - 2\sin^2(\bar{\theta}/2)$, we then obtain

$$F_z(\bar{\theta}, \bar{\theta}_z; \hat{f}_s) = \frac{1}{\sqrt{4\hat{f}_s^2\left[\sin^2\left(\dfrac{\bar{\theta}_z}{2}\right) - \sin^2\left(\dfrac{\bar{\theta}}{2}\right)\right]}} \tag{3.63}$$

where $\bar{\theta}_z = \pi + (\theta_z - \theta_o)$. Finally, we introduce another variable transformation $\bar{p}\sin\phi = \sin(\bar{\theta}/2)$ where $\bar{p} = \sin(\bar{\theta}_z/2)$. The function $F_z$ in (3.63) now becomes

$$F_z(\phi; \bar{p}, \hat{f}_s) = \frac{1}{\sqrt{4\hat{f}_s^2(\bar{p}^2 - \bar{p}^2\sin^2\phi)}} = \frac{1}{2\hat{f}_s\bar{p}\cos\phi} \qquad . \tag{3.64}$$

From the relations $\bar{\theta} = \pi + (\theta - \theta_o)$ and $\bar{p}\sin\phi = \sin(\bar{\theta}/2)$, we obtain the differential relation between $\theta$ to $\phi$ as

$$d\theta = d\bar{\theta} = \frac{2\bar{p}\cos\phi}{\cos(\bar{\theta}/2)}d\phi = \frac{2\psi\bar{p}\cos\phi}{\sqrt{1 - \bar{p}^2\sin^2\phi}}d\phi \qquad . \tag{3.65}$$

Note that to obtain the relation (3.65) we have used the following identity

$$\cos(\bar{\theta}/2) = -\psi\sqrt{1 - \bar{p}^2\sin^2\phi} \qquad . \tag{3.66}$$

The parameter $\psi$ appearing on the right hand side of (3.66) is used to indicate the sign of $\cos(\bar{\theta}/2)$. If the applied end moments $\{\hat{m}_1, \hat{m}_2\}$ are positive, the shear force within the beam is also positive and this renders the angle $\bar{\theta}/2$ falling into the quadrants 2 or 3 or, equivalently, $\cos(\bar{\theta}/2) < 0$. In the contrary, ff the applied end moments $\{\hat{m}_1, \hat{m}_2\}$ are negative, the shear force within the beam is also negative and this renders the angle $\bar{\theta}/2$ falling into the quadrant 1 or, equivalently, $\cos(\bar{\theta}/2) > 0$. By using (3.64)-(3.66), equations (3.55)-(3.57) become

$$\int_{\phi_1}^{\pi/2} f_o(\phi;\overline{p})d\phi + \int_{\phi_2}^{\pi/2} f_o(\phi;\overline{p})d\phi = \hat{f}_s \quad , \tag{3.67}$$

$$\int_{\phi_1}^{\pi/2} f_v(\phi,\theta_o;\overline{p})d\phi + \int_{\phi_2}^{\pi/2} f_v(\phi,\theta_o;\overline{p})d\phi = 0 \quad , \tag{3.68}$$

$$\int_{\phi_1}^{\pi/2} f_u(\phi,\theta_o;\overline{p})d\phi + \int_{\phi_2}^{\pi/2} f_u(\phi,\theta_o;\overline{p})d\phi = \hat{f}_s\hat{u}_2 \tag{3.69}$$

where $\overline{p}\sin\phi_1 = \sin(\overline{\theta}_1/2)$, $\overline{p}\sin\phi_2 = \sin(\overline{\theta}_2/2)$, $\overline{\theta}_1 = \pi + (\theta_1 - \theta_o)$, $\overline{\theta}_2 = \pi + (\theta_2 - \theta_o)$ and

$$f_o(\phi;\overline{p}) = \frac{1}{\sqrt{1-\overline{p}^2\sin^2\phi}} \quad , \tag{3.70}$$

$$f_v(\phi,\theta_o;\overline{p}) = \frac{\sin\theta_o}{\sqrt{1-\overline{p}^2\sin^2\phi}} - 2\sin\theta_o\sqrt{1-\overline{p}^2\sin^2\phi} - 2\psi\overline{p}\cos\theta_o\sin\phi \quad , \tag{3.71}$$

$$f_u(\phi,\theta_o;\overline{p}) = \frac{\cos\theta_o-1}{\sqrt{1-\overline{p}^2\sin^2\phi}} - 2\cos\theta_o\sqrt{1-\overline{p}^2\sin^2\phi} + 2\psi\overline{p}\sin\theta_o\sin\phi \quad . \tag{3.72}$$

Once all unknowns at both end of the member are resolved, the rotation, normalized displacement in x-direction and normalized displacement in y-direction at any interior point $\xi^* = x^*/L \notin (0,1)$, denoted by $\theta^*$, $\hat{u}^*$ and $\hat{v}^*$, can readily be obtained by integrating (3.51)-(3.53) from $\xi = 0$ to $\xi = \xi^*$ along with the use of (3.64)-(3.66). The final expressions are given by

$$\xi^*\hat{f}_s = \begin{cases} \displaystyle\int_{\phi_1}^{\phi^*} f_o(\phi;\overline{p})d\phi & , \ 0 < \xi^* < \xi_z \\[4mm] \displaystyle\int_{\phi_1}^{\pi/2} f_o(\phi;\overline{p})d\phi + \int_{\phi^*}^{\pi/2} f_o(\phi;\overline{p})d\phi & , \ \xi_z < \xi^* < 1 \end{cases} \tag{3.73}$$

$$\hat{v}^*\hat{f}_s = \begin{cases} \displaystyle\int_{\phi_1}^{\phi^*} f_v(\phi,\theta_o;\overline{p})d\phi & , \ 0 < \xi^* < \xi_z \\[4mm] \displaystyle\int_{\phi_1}^{\pi/2} f_v(\phi,\theta_o;\overline{p})d\phi + \int_{\phi^*}^{\pi/2} f_v(\phi,\theta_o;\overline{p})d\phi & , \ \xi_z < \xi^* < 1 \end{cases} \tag{3.74}$$

$$\hat{u}^* \hat{f}_s = \begin{cases} \displaystyle\int_{\phi_1}^{\phi^*} f_u(\phi, \theta_o; \overline{p}) d\phi & , \ 0 < \xi^* < \xi_z \\[4mm] \displaystyle\int_{\phi_1}^{\pi/2} f_u(\phi, \theta_o; \overline{p}) d\phi + \int_{\phi^*}^{\pi/2} f_u(\phi, \theta_o; \overline{p}) d\phi & , \ \xi_z < \xi^* < 1 \end{cases} \tag{3.75}$$

where $\sin(\overline{\theta}^*/2) = \overline{p} \sin \phi^*$ and $\overline{\theta}^* = \pi + (\theta^* - \theta_o)$. Finally, the normalized support reactions $\{\hat{f}_{x1}, \hat{f}_{y1}, \hat{f}_{y2}\}$ can be computed from (3.13)-(3.15).

By imposing the remaining two moment boundary conditions at both ends of the beam in addition to the boundary condition (3.6), it leads to two auxiliary equations

$$\delta_1(\theta_1, \theta_z, \hat{f}_x, \hat{f}_y, \hat{m}_1) = \hat{m}_1^2 + 2\hat{f}_x(\cos\theta_1 - \cos\theta_z) - 2\hat{f}_y(\sin\theta_1 - \sin\theta_z) = 0 \quad , \tag{3.76}$$

$$\delta_2(\theta_2, \theta_z, \hat{f}_x, \hat{f}_y, \hat{m}_2) = \hat{m}_2^2 + 2\hat{f}_x(\cos\theta_2 - \cos\theta_z) - 2\hat{f}_y(\sin\theta_2 - \sin\theta_z) = 0 \quad . \tag{3.77}$$

The residual function for this particular case is given by

$$\mathcal{R} = \hat{\mathcal{R}}(\phi_1, \phi_2, \theta_o, \hat{u}_2, \hat{f}_s, \overline{p}) = \hat{u}_2 + \frac{1}{\hat{f}_s} \left[ \int_{\phi_1}^{\pi/2} f_u(\phi, \theta_o; \overline{p}) d\phi + \int_{\phi_2}^{\pi/2} f_u(\phi, \theta_o; \overline{p}) d\phi \right] \tag{3.78}$$

The governing equations (3.67) and (3.68) can alternatively be expressed as

$$\Gamma_o(\phi_1, \phi_2, \hat{f}_s, \overline{p}) = \int_{\phi_1}^{\pi/2} f_o(\phi; \overline{p}) d\phi + \int_{\phi_2}^{\pi/2} f_o(\phi; \overline{p}) d\phi - \hat{f}_s = 0 \quad , \tag{3.79}$$

$$\Gamma_v(\phi_1, \phi_2, \hat{f}_s, \overline{p}) = \int_{\phi_1}^{\pi/2} f_v(\phi, \theta_o; \overline{p}) d\phi + \int_{\phi_2}^{\pi/2} f_v(\phi, \theta_o; \overline{p}) d\phi = 0 \quad . \tag{3.80}$$

From the relations (3.79) and (3.80) along with the transformations $\overline{\theta} = \pi + (\theta - \theta_o)$ and $\overline{p}\sin\phi = \sin(\overline{\theta}/2)$, it implies that $\theta_z$ and $\hat{f}_y$ are implicit functions of $\{\theta_1, \theta_2, \hat{f}_x\}$, i.e.

$$\theta_z = \theta_z(\theta_1, \theta_2, \hat{f}_x) \quad , \tag{3.81}$$

$$\hat{f}_y = \hat{f}_y(\theta_1, \theta_2, \hat{f}_x) \quad . \tag{3.82}$$

By using conditions (3.76) and (3.77) along with (3.81) and (3.82), the end moments $\hat{m}_1$ and $\hat{m}_2$ are implicit functions of $\{\theta_1, \theta_2, \hat{f}_x\}$, i.e. $\hat{m}_1 = \hat{m}_1(\theta_1, \theta_2, \hat{f}_x)$ and $\hat{m}_2 = \hat{m}_2(\theta_1, \theta_2, \hat{f}_x)$. By taking derivative of (3.76) and (3.77) with respect to $\theta_1$, $\theta_2$ and $\hat{f}_x$, it leads to:

$$\begin{bmatrix} \dfrac{\partial \hat{m}_1}{\partial \theta_1} & \dfrac{\partial \hat{m}_1}{\partial \theta_2} & \dfrac{\partial \hat{m}_1}{\partial \hat{f}_x} \\[2mm] \dfrac{\partial \hat{m}_2}{\partial \theta_1} & \dfrac{\partial \hat{m}_2}{\partial \theta_2} & \dfrac{\partial \hat{m}_2}{\partial \hat{f}_x} \end{bmatrix} = \begin{bmatrix} \lambda_1/\hat{m}_1 & 0 & (c_z - c_1)/\hat{m}_1 \\ 0 & \lambda_2/\hat{m}_2 & (c_z - c_2)/\hat{m}_2 \end{bmatrix} + \begin{bmatrix} -\lambda_z/\hat{m}_1 & (s_1 - s_z)/\hat{m}_1 \\ -\lambda_z/\hat{m}_2 & (s_2 - s_z)/\hat{m}_2 \end{bmatrix} \mathbf{A} \tag{3.83}$$

where $s_z = \sin\theta_z$, $c_z = \cos\theta_z$, $\lambda_z = \hat{f}_x s_z + \hat{f}_y c_z$ and the matrix $\mathbf{A}$ is defined by

$$\mathbf{A} = \begin{bmatrix} \dfrac{\partial \theta_z}{\partial \theta_1} & \dfrac{\partial \theta_z}{\partial \theta_2} & \dfrac{\partial \theta_z}{\partial \hat{f}_x} \\[2mm] \dfrac{\partial \hat{f}_y}{\partial \theta_1} & \dfrac{\partial \hat{f}_y}{\partial \theta_2} & \dfrac{\partial \hat{f}_y}{\partial \hat{f}_x} \end{bmatrix} \tag{3.84}$$

From (3.78) and (3.81)-(3.82), it implies that $\mathcal{R} = \mathcal{R}(\theta_1, \theta_2, \hat{f}_x)$. By differentiating (3.78) with respect to $\theta_1$, $\theta_2$ and $\hat{f}_x$, we then obtain

$$\begin{bmatrix} \dfrac{\partial \mathcal{R}}{\partial \theta_1} & \dfrac{\partial \mathcal{R}}{\partial \theta_2} & \dfrac{\partial \mathcal{R}}{\partial \hat{f}_x} \end{bmatrix} = \mathbf{B} + \mathbf{CA} \tag{3.85}$$

where the matrices $\mathbf{B}$ and $\mathbf{C}$ are given by

$$\mathbf{B} = \begin{bmatrix} \dfrac{\partial \hat{\mathcal{R}}}{\partial \theta_1} & \dfrac{\partial \hat{\mathcal{R}}}{\partial \theta_2} & \dfrac{\partial \hat{\mathcal{R}}}{\partial \hat{f}_x} \end{bmatrix} \quad , \quad \mathbf{C} = \begin{bmatrix} \dfrac{\partial \hat{\mathcal{R}}}{\partial \theta_z} & \dfrac{\partial \hat{\mathcal{R}}}{\partial \hat{f}_y} \end{bmatrix} \tag{3.86}$$

Note that all entries of the matrices $\mathbf{B}$ and $\mathbf{C}$ can be obtained from the function form of $\hat{\mathcal{R}}$ defined by (3.78) along with the transformations $\bar{\theta} = \pi + (\theta - \theta_o)$ and $\bar{p}\sin\phi = \sin(\bar{\theta}/2)$

(see explicit results in Appendix A). To compute all entries of the matrix **A**, we differentiate equations (3.79) and (3.80) with respect to $\theta_1$, $\theta_2$ and $\hat{f}_x$ and this results in a system of equations:

$$\mathbf{DA} = \mathbf{F} \tag{3.87}$$

where the matrices **D** and **F** are given by

$$\mathbf{D} = \begin{bmatrix} \dfrac{\partial\Gamma_o}{\partial\theta_z} & \dfrac{\partial\Gamma_o}{\partial\hat{f}_y} \\[2ex] \dfrac{\partial\Gamma_v}{\partial\theta_z} & \dfrac{\partial\Gamma_v}{\partial\hat{f}_y} \end{bmatrix} \quad , \tag{3.88}$$

$$\mathbf{F} = -\begin{bmatrix} \dfrac{\partial\Gamma_o}{\partial\theta_1} & \dfrac{\partial\Gamma_o}{\partial\theta_2} & \dfrac{\partial\Gamma_o}{\partial\hat{f}_x} \\[2ex] \dfrac{\partial\Gamma_v}{\partial\theta_1} & \dfrac{\partial\Gamma_v}{\partial\theta_2} & \dfrac{\partial\Gamma_v}{\partial\hat{f}_x} \end{bmatrix} \quad . \tag{3.89}$$

All entries of **D** and **F** can be obtained from the function form of $\Gamma_o$ and $\Gamma_v$ defined by (3.79) and (3.80) along with the transformations $\bar{\theta} = \pi + (\theta - \theta_o)$ and $\bar{p}\sin\phi = \sin(\bar{\theta}/2)$ (see explicit results in Appendix A). Once **A** is solved from (3.87), it is substituted into (3.83) and (3.85) to obtain all entries of the matrix $\mathbf{g}_{p4}$. Due to the complexity of the function form resulting from the variable transformations, the matrices **B**, **C**, **D** and **F** are computed numerically.

### 3.1.2.3 Member containing inflection point at the end

Finally, consider a beam member containing an inflection point only at one of its ends or, equivalently, the bending moment possesses the same sign throughout the member and vanishes only at one of its ends. This particular case arises when one of the applied end moments $\{\hat{m}_1, \hat{m}_2\}$ vanishes. The resulting deformed configuration of the beam possesses a single curvature and, in addition, the moment-dependence function $\vartheta$

becomes a constant function with its value equal to either 1 or -1 depending on the sign of non-vanishing applied end moments $\{\hat{m}_1, \hat{m}_2\}$. Without loss of generality, the development presented below focuses only on the member containing an inflection point at the right end. While results for the member containing an inflection point at the left end are also needed, the treatment of such member follows the same procedure.

Now, let restrict attention to the case that the beam is subjected only to non-zero $\hat{m}_1$ whereas $\hat{m}_2$ vanishes. Specifically, the beam possesses a positive curvature if and only if $\hat{m}_1 < 0$ and possesses a negative curvature if and only if $\hat{m}_1 > 0$. It is worth noting that the case treated here is a special case of a double curvature beam discussed in subsection 3.1.2.2; in particular, $\theta_z = \theta_2$, $\xi_z = 1$, and the point of singularity move to the right end. As a consequence, basic equations and procedures adopted in the previous case can, after a proper specialization, be applied to this particular case. Due to the moment-dependence function taking a single value throughout the member, there is no need to separate all involved integrals that are evaluated over the entire member into two parts. By replacing $\theta_z = \theta_2$ into (3.54), we obtain a new function, called $F_{z1}$, given by

$$F_{z1}(\theta, \theta_z; \hat{f}_x, \hat{f}_y) = \frac{1}{\sqrt{2\hat{f}_x(\cos\theta_2 - \cos\theta) - 2\hat{f}_y(\sin\theta_2 - \sin\theta)}} \quad . \tag{3.90}$$

It is evident that the function $F_{z1}$ is singular at the right end of the beam. The governing equations (3.55)-(3.57), when specialized to this particular case, now take the following form

$$-\psi \int_{\theta_1}^{\theta_2} F_z(\theta, \theta_z; \hat{f}_x, \hat{f}_y) d\theta = 1 \quad , \tag{3.91}$$

$$-\psi \int_{\theta_1}^{\theta_2} \sin\theta \, F_z(\theta, \theta_z; \hat{f}_x, \hat{f}_y) d\theta = 0 \quad , \tag{3.92}$$

$$-\psi \int_{\theta_1}^{\theta_2} \left( \cos\theta - 1 \right) F_z(\theta, \theta_z; \hat{f}_x, \hat{f}_y) d\theta = \hat{u}_2 \qquad (3.93)$$

where $\psi = 1$ for $\hat{m}_1 < 0$ and $\psi = -1$ for $\hat{m}_1 > 0$. By introducing the same type of variable transformations as employed in the previous case, i.e. $\bar{\theta} = \pi + (\theta - \theta_o)$ and $\bar{p}\sin\phi = \sin(\bar{\theta}/2)$, equations (3.91)-(3.93) become

$$\int_{\phi_1}^{\pi/2} f_o(\phi; \bar{p}) d\phi = \hat{f}_s \qquad , \qquad (3.94)$$

$$\int_{\phi_1}^{\pi/2} f_v(\phi, \theta_o; \bar{p}) d\phi = 0 \qquad , \qquad (3.95)$$

$$\int_{\phi_1}^{\pi/2} f_u(\phi, \theta_o; \bar{p}) d\phi = \hat{f}_s \hat{u}_2 \qquad (3.96)$$

where $\bar{p}\sin\phi_1 = \sin(\bar{\theta}_1/2)$, $\bar{\theta}_1 = \pi + (\theta_1 - \theta_o)$, and functions $f_o, f_v, f_u$ are defined by (3.70)-(3.72).

In addition, the rotation, normalized displacement in x-direction and normalized displacement in y-direction at any interior point $\xi^* = x^*/L \notin (0,1)$, denoted by $\theta^*$, $\hat{u}^*$ and $\hat{v}^*$, can readily be obtained in a similar manner and the final expressions are given by

$$\xi^* \hat{f}_s = \int_{\phi_1}^{\phi^*} f_o(\phi; \bar{p}) d\phi \qquad , \qquad (3.97)$$

$$\hat{v}^* \hat{f}_s = \int_{\phi_1}^{\phi^*} f_v(\phi, \theta_o; \bar{p}) d\phi \qquad , \qquad (3.98)$$

$$\hat{u}^* \hat{f}_s = \int_{\phi_1}^{\phi^*} f_u(\phi, \theta_o; \bar{p}) d\phi \qquad (3.99)$$

where $\sin(\bar{\theta}^*/2) = \bar{p}\sin\phi^*$ and $\bar{\theta}^* = \pi + (\theta^* - \theta_o)$. Finally, the normalized support reactions $\{\hat{f}_{x1}, \hat{f}_{y1}, \hat{f}_{y2}\}$ can be computed from (3.13)-(3.15).

Since the end moment $\hat{m}_2$ is prescribed equal to zero, the rotation at the right end $\theta_2$ is no longer an independent quantity but can be obtained in terms of other independent unknowns via the constraint $\hat{m}_2 = 0$. Let redefine $\mathbf{f}$ such that $\mathbf{f} = [\mathbf{f}_p \ \mathbf{f}_r]^T$ where $\mathbf{f}_p = \{ \hat{f}_{x2}, \hat{m}_1, \mathscr{R} \}$ and $\mathbf{f}_r = \{ \hat{f}_{x1}, \hat{f}_{y1}, \hat{f}_{y2} \}$ and redefine $\mathbf{u}$ such that $\mathbf{u} = \{ \hat{u}_2, \theta_1, \hat{f}_x \}^T$. Consistent with these new definitions, the reduced gradient matrix takes the form $\overline{\mathbf{g}} = [\overline{\mathbf{g}}_p^T \ \overline{\mathbf{g}}_r^T]^T$ where the sub-matrices $\overline{\mathbf{g}}_p$ and $\overline{\mathbf{g}}_r$ are of dimensions 3x3 and given by

$$\overline{\mathbf{g}}_p = \begin{bmatrix} \overline{\mathbf{g}}_{p1} & \overline{\mathbf{g}}_{p2} \\ \overline{\mathbf{g}}_{p3} & \overline{\mathbf{g}}_{p4} \end{bmatrix} \quad . \tag{3.100}$$

$$\overline{\mathbf{g}}_r = \frac{1}{\hat{d}} \begin{bmatrix} -\overline{g}_{11}\hat{d} & -\overline{g}_{12}\hat{d} & -\overline{g}_{13}\hat{d} \\ -\hat{s} & \overline{g}_{22} & \overline{g}_{23} \\ \hat{s} & -\overline{g}_{22} & -\overline{g}_{23} \end{bmatrix} = \frac{1}{\hat{d}} \begin{bmatrix} 0 & 0 & -\hat{d} \\ -\hat{s} & \overline{g}_{22} & \overline{g}_{23} \\ \hat{s} & -\overline{g}_{22} & -\overline{g}_{23} \end{bmatrix} \tag{3.101}$$

where $\hat{s} = (\hat{m}_1 + \hat{m}_2)/\hat{d}$, $\overline{g}_{ij}$ denotes an entry located at the i$^{th}$ row and j$^{th}$ column of the sub-matrix $\overline{\mathbf{g}}_p$ and

$$\overline{\mathbf{g}}_{p1} = [0] \quad , \tag{3.102}$$

$$\overline{\mathbf{g}}_{p2} = \overline{\mathbf{g}}_{p3}^T = [0 \quad 1] \quad , \tag{3.103}$$

$$\overline{\mathbf{g}}_{p4} = \begin{bmatrix} \partial\hat{m}_1/\partial\theta_1 & \partial\hat{m}_1/\partial\hat{f}_x \\ \partial\mathscr{R}/\partial\theta_1 & \partial\mathscr{R}/\partial\hat{f}_x \end{bmatrix} . \tag{3.104}$$

It still remains to compute the matrix $\overline{\mathbf{g}}_{p4}$ and a procedure similar to that employed in section 3.1.2.2 is utilized.

By imposing the remaining moment boundary condition at the left end of the beam in addition to the boundary condition (3.6), it leads to an auxiliary equation

$$\delta_1(\theta_1, \theta_2, \hat{f}_x, \hat{f}_y, \hat{m}_1) = \hat{m}_1^2 + 2\hat{f}_x(\cos\theta_1 - \cos\theta_2) - 2\hat{f}_y(\sin\theta_1 - \sin\theta_2) = 0 \tag{3.105}$$

The residual function resulting from (3.96) is given by

$$\mathcal{R} = \hat{\mathcal{R}}(\phi_1, \theta_o, \hat{u}_2, \hat{f}_s, \overline{p}) = \hat{u}_2 + \frac{1}{\hat{f}_s} \int_{\phi_1}^{\pi/2} f_u(\phi, \theta_o; \overline{p}) d\phi \qquad (3.106)$$

The governing equations (3.94) and (3.95) can alternatively be expressed as

$$\Gamma_o(\phi_1, \hat{f}_s, \overline{p}) = \int_{\phi_1}^{\pi/2} f_o(\phi; \overline{p}) d\phi - \hat{f}_s = 0 \quad , \qquad (3.107)$$

$$\Gamma_v(\phi_1, \hat{f}_s, \overline{p}) = \int_{\phi_1}^{\pi/2} f_v(\phi, \theta_o; \overline{p}) d\phi = 0 \qquad . \qquad (3.108)$$

From the relations (3.107) and (3.108) along with the transformations $\overline{\theta} = \pi + (\theta - \theta_o)$ and $\overline{p}\sin\phi = \sin(\overline{\theta}/2)$, it implies that $\theta_2$ and $\hat{f}_y$ are implicit functions of $\{\theta_1, \hat{f}_x\}$, i.e.

$$\theta_2 = \theta_2(\theta_1, \hat{f}_x) \quad , \qquad (3.109)$$

$$\hat{f}_y = \hat{f}_y(\theta_1, \hat{f}_x) \qquad . \qquad (3.110)$$

By using conditions (3.105) along with (3.109) and (3.110), the end moment $\hat{m}_1$ is an implicit function of $\{\theta_1, \hat{f}_x\}$, i.e. $\hat{m}_1 = \hat{m}_1(\theta_1, \hat{f}_x)$. By taking derivative of (3.105) with respect to $\theta_1$ and $\hat{f}_x$, it gives rise to

$$\left[ \frac{\partial \hat{m}_1}{\partial \theta_1} \quad \frac{\partial \hat{m}_1}{\partial \hat{f}_x} \right] = \left[ \lambda_1 / \hat{m}_1 \quad (c_z - c_1) / \hat{m}_1 \right] + \left[ -\lambda_z / \hat{m}_1 \quad (s_1 - s_z) / \hat{m}_1 \right] \overline{A} \qquad (3.111)$$

where the matrix $\overline{A}$ is defined by

$$\bar{\mathbf{A}} = \begin{bmatrix} \dfrac{\partial \theta_2}{\partial \theta_1} & \dfrac{\partial \theta_2}{\partial \hat{f}_x} \\[3mm] \dfrac{\partial \hat{f}_y}{\partial \theta_1} & \dfrac{\partial \hat{f}_y}{\partial \hat{f}_x} \end{bmatrix} \tag{3.112}$$

From (3.106) and (3.109)-(3.110), it implies that $\mathcal{R} = \mathcal{R}(\theta_1, \hat{f}_x)$. By differentiating (3.106) with respect to $\theta_1$ and $\hat{f}_x$, we then obtain

$$\begin{bmatrix} \dfrac{\partial \mathcal{R}}{\partial \theta_1} & \dfrac{\partial \mathcal{R}}{\partial \hat{f}_x} \end{bmatrix} = \bar{\mathbf{B}} + \bar{\mathbf{C}}\bar{\mathbf{A}} \tag{3.113}$$

where the matrices **B** and **C** are given by

$$\bar{\mathbf{B}} = \begin{bmatrix} \dfrac{\partial \hat{\mathcal{R}}}{\partial \theta_1} & \dfrac{\partial \hat{\mathcal{R}}}{\partial \hat{f}_x} \end{bmatrix} \quad , \quad \bar{\mathbf{C}} = \begin{bmatrix} \dfrac{\partial \hat{\mathcal{R}}}{\partial \theta_2} & \dfrac{\partial \hat{\mathcal{R}}}{\partial \hat{f}_y} \end{bmatrix} \tag{3.114}$$

Note that all entries of the matrices $\bar{\mathbf{B}}$ and $\bar{\mathbf{C}}$ can be obtained from the function form of $\hat{\mathcal{R}}$ defined by (3.106) along with the transformations $\bar{\theta} = \pi + (\theta - \theta_o)$ and $\bar{p}\sin\phi = \sin(\bar{\theta}/2)$ (see explicit results in Appendix B). To compute all entries of the matrix $\bar{\mathbf{A}}$, we differentiate equations (3.107) and (3.108) with respect to $\theta_1$ and $\hat{f}_x$ and this results in a system of equations:

$$\bar{\mathbf{D}}\bar{\mathbf{A}} = \bar{\mathbf{F}} \tag{3.115}$$

where the matrices $\bar{\mathbf{D}}$ and $\bar{\mathbf{F}}$ are given by

$$\bar{\mathbf{D}} = \begin{bmatrix} \dfrac{\partial \Gamma_o}{\partial \theta_2} & \dfrac{\partial \Gamma_o}{\partial \hat{f}_y} \\[3mm] \dfrac{\partial \Gamma_v}{\partial \theta_2} & \dfrac{\partial \Gamma_v}{\partial \hat{f}_y} \end{bmatrix} \quad , \tag{3.116}$$

$$\overline{\mathbf{F}} = -\begin{bmatrix} \dfrac{\partial \Gamma_o}{\partial \theta_1} & \dfrac{\partial \Gamma_o}{\partial \theta_2} \\[2ex] \dfrac{\partial \Gamma_v}{\partial \theta_1} & \dfrac{\partial \Gamma_v}{\partial \theta_2} \end{bmatrix} \quad . \tag{3.117}$$

All entries of $\overline{\mathbf{D}}$ and $\overline{\mathbf{F}}$ can be obtained from the function form of $\Gamma_o$ and $\Gamma_v$ defined by (3.107) and (3.108) along with the transformations $\overline{\theta} = \pi + (\theta - \theta_o)$ and $\overline{p}\sin\phi = \sin(\overline{\theta}/2)$ (see explicit results in Appendix B). Once $\overline{\mathbf{A}}$ is solved from (3.115), it is substituted into (3.111) and (3.113) to obtain all entries of the matrix $\overline{\mathbf{g}}_{p4}$. Due to the complexity of the function form resulting from the variable transformations, the matrices $\overline{\mathbf{B}}$, $\overline{\mathbf{C}}$, $\overline{\mathbf{D}}$ and $\overline{\mathbf{F}}$ are computed numerically.

## 3.2 Local Element Tangent Stiffness Matrix

Consider now a member with more general boundary conditions as shown schematically in Figure 3.3. Let $\{x, y\}$ be a local coordinate system of the undeformed member and $\{x^*, y^*\}$ is the coordinate system of the deformed member defined such that a chord connecting its end points always lies on the $x^*$ axis. With this specific choice of $\{x^*, y^*\}$, behavior of the member observed from this coordinate system is identical to that of the simply-support beam

The normalized end loads and normalized end displacements and rotations are denoted by $\{\hat{f}_{x1}, \hat{f}_{y1}, \hat{m}_1, \hat{f}_{x2}, \hat{f}_{y2}, \hat{m}_2\}$ and $\{\hat{u}_1, \hat{v}_1, \theta_1, \hat{u}_2, \hat{v}_2, \theta_2\}$, in the $\{x,y\}$ system and by $\{\hat{f}_{x1}^*, \hat{f}_{y1}^*, \hat{m}_1^*, \hat{f}_{x2}^*, \hat{f}_{y2}^*, \hat{m}_2^*\}$ and $\{\hat{u}_2^*, \theta_1^*, \theta_2^*\}$ in the $\{x^*, y^*\}$ system. From geometric consideration of the deformed configuration, $\{\hat{u}_2^*, \theta_1^*, \theta_2^*\}$ can be expressed in terms of $\{\hat{u}_1, \hat{v}_1, \theta_1, \hat{u}_2, \hat{v}_2, \theta_2\}$ by

$$\theta_1^* = \theta_1 - \phi \quad , \tag{3.118}$$

$$\theta_2^* = \theta_2 - \phi \quad , \tag{3.119}$$
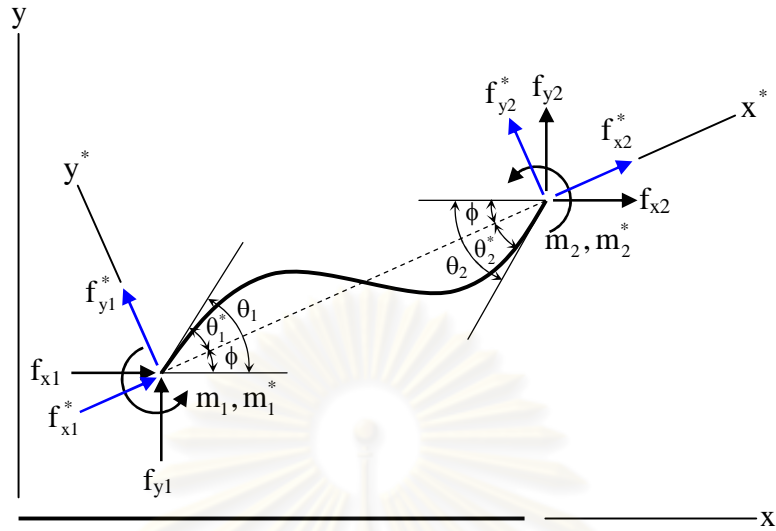
Figure 3.3 Schematic of undeformed and deformed configurations of member subjected to general boundary conditions.

$$\hat{u}_2^* = (1 + \hat{u}_2 - \hat{u}_1)\cos\phi - (\hat{v}_2 - \hat{v}_1)\sin\phi - 1 \tag{3.120}$$

where $\phi$ is a chord rotation defined by

$$(1 + \hat{u}_2 - \hat{u}_1)\sin\phi - (\hat{v}_2 - \hat{v}_1)\cos\phi = 0 \quad . \tag{3.121}$$

Let $\hat{f}_x^*$ be the internal force in $x^*$-direction and $\mathcal{R}^*$ be the residual defined in the $\{x^*, y^*\}$ system in the same way as given by (3.22). In the $\{x, y\}$ system, we choose $\{\hat{f}_x, \mathcal{R}\}$ such that

$$\hat{f}_x = \hat{f}_x^* \quad , \tag{3.122}$$

$$\mathcal{R} = \mathcal{R}^* \quad . \tag{3.123}$$

By applying the coordinate transformation, a vector $\mathbf{f} = \{\hat{f}_{x1}, \hat{f}_{y1}, \hat{m}_1, \hat{f}_{x2}, \hat{f}_{y2}, \hat{m}_2, \mathcal{R}\}$ is related to a vector $\mathbf{f}^* = \{\hat{f}_{x2}^*, \hat{m}_1^*, \hat{m}_2^*, \mathcal{R}^*, \hat{f}_{x1}^*, \hat{f}_{y1}^*, \hat{f}_{y2}^*\}$ by

$$\mathbf{f} = \mathbf{R}(\phi)\mathbf{f}^* \tag{3.124}$$

where $\mathbf{R}(\phi)$ is a transformation matrix of dimension 7x7 given by

$$\mathbf{R}(\phi) = \begin{bmatrix} 0 & 0 & 0 & 0 & c_\phi & -s_\phi & 0 \\ 0 & 0 & 0 & 0 & s_\phi & c_\phi & 0 \\ 0 & 1 & 0 & 0 & 0 & 0 & 0 \\ c_\phi & 0 & 0 & 0 & 0 & 0 & -s_\phi \\ s_\phi & 0 & 0 & 0 & 0 & 0 & c_\phi \\ 0 & 0 & 1 & 0 & 0 & 0 & 0 \\ 0 & 0 & 0 & 1 & 0 & 0 & 0 \end{bmatrix} \tag{3.125}$$

with $s_\phi = \sin\phi$ and $c_\phi = \cos\phi$. By defining $\mathbf{u} = \{\hat{u}_1, \hat{v}_1, \theta_1, \hat{u}_2, \hat{v}_2, \theta_2, \hat{f}_x\}$ and $\mathbf{u}^* = \{\hat{u}_2^*, \theta_1^*, \theta_2^*, \hat{f}_x^*\}$ and then recalling (3.118)-(3.123), we obtain the relation $\mathbf{u}^* = \mathbf{u}^*(\mathbf{u})$. From the fact that behavior of the member in the $\{x^*, y^*\}$ system is identical to that for the simply supported beam, $\mathbf{f}^*$ and $\mathbf{u}^*$ are related by $\mathbf{f}^* = \mathbf{f}^*(\mathbf{u}^*)$. Combing (3.124), $\mathbf{u}^* = \mathbf{u}^*(\mathbf{u})$ and $\mathbf{f}^* = \mathbf{f}^*(\mathbf{u}^*)$ leads to the relation

$$\mathbf{f} = \mathbf{f}(\mathbf{u}) = \mathbf{R}(\phi)\,\mathbf{f}^*(\mathbf{u}^*(\mathbf{u})) \quad . \tag{3.126}$$

Upon use of Taylor series expansion, the nonlinear function $\mathbf{f}$ defined by (3.126) possesses a best linear approximation in the neighborhood of a given vector $\mathbf{u}_o$ as

$$\mathbf{f}(\mathbf{u}) = \mathbf{f}(\mathbf{u}_o) + \mathbf{k}_\ell(\mathbf{u}_o)(\mathbf{u} - \mathbf{u}_o) \tag{3.127}$$

where $\mathbf{k}_\ell$ is a local element tangent stiffness matrix of the member given by

$$\mathbf{k}_\ell = \frac{\partial \mathbf{R}}{\partial \phi}\mathbf{f}^*\frac{\partial \phi}{\partial \mathbf{u}} + \mathbf{R}\,\mathbf{g}\frac{\partial \mathbf{u}^*}{\partial \mathbf{u}} \quad . \tag{3.128}$$

Note that the relation $\mathbf{g} = \partial\mathbf{f}^*/\partial\mathbf{u}^*$ has been utilized.

For the case that the member contains an inflection point at the right end, the end moment $\hat{m}_2$ vanishes and the corresponding end rotation $\theta_2$ is eliminated from a set of unknowns. In particular, let define the reduced vectors $\overline{\mathbf{f}}$, $\overline{\mathbf{f}}^*$, $\overline{\mathbf{u}}$ and $\overline{\mathbf{u}}^*$ such that $\overline{\mathbf{f}} = \{\hat{f}_{x1}, \hat{f}_{y1}, \hat{m}_1, \hat{f}_{x2}, \hat{f}_{y2}, \mathcal{R}\}$, $\overline{\mathbf{f}}^* = \{\hat{f}_{x2}^*, \hat{m}_1^*, \mathcal{R}^*, \hat{f}_{x1}^*, \hat{f}_{y1}^*, \hat{f}_{y2}^*\}$, $\overline{\mathbf{u}} = \{\hat{u}_1, \hat{v}_1, \theta_1, \hat{u}_2, \hat{v}_2, \hat{f}_x\}$ and $\overline{\mathbf{u}}^* = \{\hat{u}_2^*, \theta_1^*, \theta_2^*, \hat{f}_x^*\}$. By applying the coordinate transformation, a relation between the reduced vectors $\overline{\mathbf{f}}$ and $\overline{\mathbf{f}}^*$ is given by

$$\overline{\mathbf{f}} = \overline{\mathbf{R}}(\phi)\,\overline{\mathbf{f}}^* \tag{3.129}$$

where $\overline{\mathbf{R}}(\phi)$ is a reduced transformation matrix of dimensions 6x6 given by

$$\overline{\mathbf{R}}(\phi) = \begin{bmatrix} 0 & 0 & 0 & c_\phi & -s_\phi & 0 \\ 0 & 0 & 0 & s_\phi & c_\phi & 0 \\ 0 & 1 & 0 & 0 & 0 & 0 \\ c_\phi & 0 & 0 & 0 & 0 & -s_\phi \\ s_\phi & 0 & 0 & 0 & 0 & c_\phi \\ 0 & 0 & 1 & 0 & 0 & 0 \end{bmatrix}. \tag{3.130}$$

By using the relations (3.118) and (3.119)-(3.123), we obtain the relation $\overline{\mathbf{u}}^* = \overline{\mathbf{u}}^*(\overline{\mathbf{u}})$ and, from the fact that behavior of the member in the $\{x^*, y^*\}$ system is identical to that for the simply supported beam, $\overline{\mathbf{f}}^*$ and $\overline{\mathbf{u}}^*$ are related by $\overline{\mathbf{f}}^* = \overline{\mathbf{f}}^*(\overline{\mathbf{u}}^*)$. Combing (3.129), $\overline{\mathbf{u}}^* = \overline{\mathbf{u}}^*(\overline{\mathbf{u}})$ and $\overline{\mathbf{f}}^* = \overline{\mathbf{f}}^*(\overline{\mathbf{u}}^*)$ yields

$$\overline{\mathbf{f}} = \overline{\mathbf{f}}(\overline{\mathbf{u}}) = \overline{\mathbf{R}}(\phi)\,\overline{\mathbf{f}}^*(\overline{\mathbf{u}}^*(\overline{\mathbf{u}}))\ . \tag{3.131}$$

From Taylor series expansion, the nonlinear function $\overline{\mathbf{f}}$ defined by (3.131) possesses a best linear approximation in the neighborhood of a given vector $\overline{\mathbf{u}}_o$ as

$$\overline{\mathbf{f}}\,(\,\overline{\mathbf{u}}\,) = \overline{\mathbf{f}}\,(\,\overline{\mathbf{u}}_{o}\,) + \overline{\mathbf{k}}_{\ell}\,(\,\overline{\mathbf{u}}_{o}\,)(\,\overline{\mathbf{u}} - \overline{\mathbf{u}}_{o}\,) \tag{3.132}$$

where $\overline{\mathbf{k}}_{\ell}$ is a reduced, local element tangent stiffness matrix of the member containing the inflection point at the right end and is given by

$$\overline{\mathbf{k}}_{\ell} = \frac{\partial \overline{\mathbf{R}}}{\partial \phi}\,\overline{\mathbf{f}}^{*}\,\frac{\partial \phi}{\partial \overline{\mathbf{u}}} + \overline{\mathbf{R}}\,\overline{\mathbf{g}}\,\frac{\partial \overline{\mathbf{u}}^{*}}{\partial \overline{\mathbf{u}}}\ . \tag{3.133}$$

in which the relation $\overline{\mathbf{g}} = \partial \overline{\mathbf{f}}^{*}/\partial \overline{\mathbf{u}}^{*}$ has been used. Note that the reduced, local element tangent stiffness matrix is of dimensions 6x6.

The reduced, local element tangent stiffness matrix of the member containing an inflection point at the left end can be obtained in a similar fashion.

### 3.3 Global Element Tangent Stiffness Matrix

Let the orientation of the member in undeformed configuration be denoted by an angle $\beta$ between the local x-axis (defined in section 3.2) and the global X-axis. The element tangent stiffness matrix referring to the global coordinate system {X, Y} can be obtained using the following standard coordinate transformation formula

$$\mathbf{k}_{g} = \mathbf{Q}^{T}\mathbf{k}_{\ell}\mathbf{Q} \tag{3.134}$$

where $\mathbf{k}_{g}$ is the global element tangent stiffness matrix and $\mathbf{Q}$ is a transformation matrix given by

$$\mathbf{Q} = \begin{bmatrix} c_{\beta} & s_{\beta} & 0 & 0 & 0 & 0 & 0 \\ -s_{\beta} & c_{\beta} & 0 & 0 & 0 & 0 & 0 \\ 0 & 0 & 1 & 0 & 0 & 0 & 0 \\ 0 & 0 & 0 & c_{\beta} & s_{\beta} & 0 & 0 \\ 0 & 0 & 0 & -s_{\beta} & c_{\beta} & 0 & 0 \\ 0 & 0 & 0 & 0 & 0 & 1 & 0 \\ 0 & 0 & 0 & 0 & 0 & 0 & 1 \end{bmatrix} \tag{3.135}$$

in which $s_\beta = \sin\beta$ and $c_\beta = \cos\beta$.

Similarly, the reduced, global element tangent stiffness matrix for the beam containing an inflection point at the right end is given by

$$\bar{\mathbf{k}}_{g} = \bar{\mathbf{Q}}^{\mathrm{T}}\bar{\mathbf{k}}_{l}\,\bar{\mathbf{Q}} \tag{3.136}$$

where $\bar{\mathbf{k}}_{g}$ is the reduced, global element tangent stiffness matrix and $\bar{\mathbf{Q}}$ is a reduced transformation matrix given by

$$\bar{\mathbf{Q}} = \begin{bmatrix} c_\beta & s_\beta & 0 & 0 & 0 & 0 \\ -s_\beta & c_\beta & 0 & 0 & 0 & 0 \\ 0 & 0 & 1 & 0 & 0 & 0 \\ 0 & 0 & 0 & c_\beta & s_\beta & 0 \\ 0 & 0 & 0 & -s_\beta & c_\beta & 0 \\ 0 & 0 & 0 & 0 & 0 & 1 \end{bmatrix} \tag{3.137}$$

The reduced, global element tangent stiffness matrix of the member containing an inflection point at the left end can be obtained in a similar fashion. The reduced transformation matrix $\bar{\mathbf{Q}}$ for this particular case is given by

$$\bar{\mathbf{Q}} = \begin{bmatrix} c_\beta & s_\beta & 0 & 0 & 0 & 0 \\ -s_\beta & c_\beta & 0 & 0 & 0 & 0 \\ 0 & 0 & c_\beta & s_\beta & 0 & 0 \\ 0 & 0 & -s_\beta & c_\beta & 0 & 0 \\ 0 & 0 & 0 & 0 & 1 & 0 \\ 0 & 0 & 0 & 0 & 0 & 1 \end{bmatrix} \tag{3.138}$$

## 3.4 Global Structure Tangent Stiffness Equations

The global tangent stiffness equations of the structure can readily be obtained by a direct assembly procedure of the element tangent stiffness equation. The strategy employs two key ingredients: the compatibility of the displacement and rotation at nodes

and at ends of the members and equilibrium of external loads and member end forces at nodes. The resulting equations are given by

$$\mathbf{P} = \mathbf{P}_o + \mathbf{K}_t(\mathbf{U} - \mathbf{U}_o) \tag{3.139}$$

where $\mathbf{P}$ is a vector of nodal loads and zero residuals of all members, $\mathbf{U}$ is a vector of nodal displacements and rotations and the internal axial force of all members, $\{\mathbf{P}_o, \mathbf{U}_o\}$ are vectors at the reference state, and $\mathbf{K}_t$ is the global tangent stiffness matrix of the entire structure. The matrix $\mathbf{K}_t$ can be obtained from a direct assembly of the global element tangent stiffness matrices $\mathbf{k}_g$, given by (3.134), and the reduced global element tangent stiffness matrices $\bar{\mathbf{k}}_g$, given by (3.136), of all members.

## 3.5 Numerical Implementation

In this section, we briefly describe the numerical integration technique used to evaluate all integrals in the governing equations and the iterative strategy for solving a system of nonlinear equations.

### 3.5.1 Numerical integration

In the construction of the gradient matrix $\mathbf{g}$ and the reduced gradient matrix $\bar{\mathbf{g}}$, it is required an evaluation of elliptic integrals and other integrals of the same kind. Since the involved integrands are very complex, a direct analytical integration is impractical or sometimes impossible. This therefore necessitates the use of a numerical integration technique to approximate such integrals. Since all involved integrals are already regularized such that the integrands are well-behaved and non-singular, they can efficiently be integrated by a standard Gaussian quadrature. To ensure the accuracy of integrated results, the quadrature is tested for all types of integrals by varying the number of integration points. It has been found that a relatively low number of integration points is needed to obtain sufficiently accurate numerical results.

### 3.5.2 Newton-Raphson technique

A system of nonlinear equations governing behavior of the entire structure is nonlinear and mathematically complex due partly to the use of exact kinematics. An explicit solution of such system of nonlinear equations does not exist and this necessitates the use of an iterative method to construct approximate solutions instead. In the current investigation, a standard Newton-Ralphson method is utilized along with the direct stiffness strategy to solve such nonlinear equations. The structure tangent stiffness equation (3.139) constitutes the best linear approximation of the governing nonlinear functions in the neighborhood of the reference state and is employed in the iterative procedure to progressively improve the numerical solutions. The accuracy of the approximate solutions is controlled by limiting the norm of the residual force vector within a specified tolerance.

# CHAPTER IV

## VERIFICATION AND RESULTS

As a means to verify both the formulation and numerical implementation and also demonstrate the capability and versatility of the current technique, extensive numerical experiments are performed for various flexure-dominating structures. In a verification procedure, a set of simple boundary value problems is first investigated and results are compared with existing analytical solutions and, subsequently, more complex structures are analyzed and results are verified by those obtained from a reliable technique, finite element method (FEM). Finally, the verified technique is utilized to examine various aspects and behaviors of several structures undergoing large displacement and rotation; structures containing multiple members and inflection points are treated.

### 4.1 Verification with analytical solution

In this section, we consider structures where the bending moment is piecewise constant while the internal axial force and shear force identically vanish. For this particular case, differential equations governing the deflected shape are significantly simplified such that the corresponding analytical solution can readily be obtained via a direct integration method. In addition, to emphasize the independence of a level of mesh refinement, results obtained from the current technique are reported for a series of meshes.

#### 4.1.1 Cantilever beam subjected to end moment

Consider a cantilever beam of length L and flexural rigidity EI and subjected to the end moment M at the tip while fixed at the left end as shown schematically in Figure 4.1(a). In the analysis, three uniform meshes, as depicted in Figure 4.1(b), are adopted; in particular, Mesh-1, Mesh-2 and Mesh-3 contain 1, 2 and 4 members of equal length, respectively.
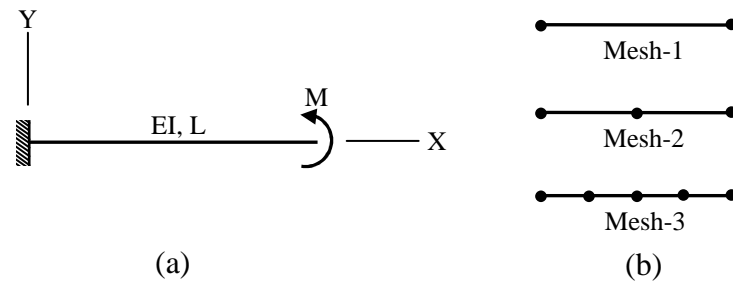
Figure 4.1 (a) Schematic of cantilever beam subjected to end moment and (b) three meshes employed in the analysis

For this particular case, the governing equations for the rotation ($\theta$), normalized displacement in the X-direction ($\hat{u}$) and normalized displacement in the Y-direction ($\hat{v}$) reduce to

$$\frac{d\theta}{d\xi} = \hat{m} \tag{4.1}$$

$$\frac{d\hat{u}}{d\theta} = \frac{\cos\theta - 1}{\hat{m}} \tag{4.2}$$

$$\frac{d\hat{v}}{d\theta} = \frac{\sin\theta}{\hat{m}} \tag{4.3}$$

where $\hat{m} = ML/EI$. By perform a direct integration of (4.1)-(4.3) along with the use of boundary conditions at the fixed end, we obtain the displacement and rotation at any point $\xi = x/L$, $x \in [0, L]$ as

$$\theta = \hat{m}\xi \tag{4.4}$$

$$\hat{u} = \frac{\sin(\hat{m}\xi)}{\hat{m}} - \xi \tag{4.5}$$

$$\hat{v} = \frac{1 - \cos(\hat{m}\xi)}{\hat{m}} \tag{4.6}$$

The exact solution of a deflected shape of the beam given by (4.3)-(4.6) is reported in Figure 4.2 for $\hat{m} \in \{0.5, 1, 1.5, 2, 3\}$ along with numerical results obtained by the current technique; normalized coordinates of the deflected shape for each mesh are reported only at the nodal points. It is evident from this set of results that the current technique yields highly accurate displacement at the nodal points (indistinguishable from the analytical solution) and such accuracy exhibits no dependence on the level of mesh refinement. It is worth noting that such a crucial feature of the current technique results directly from the use of the exact element tangent stiffness matrix and no approximation of a form of the solution and governing equations.
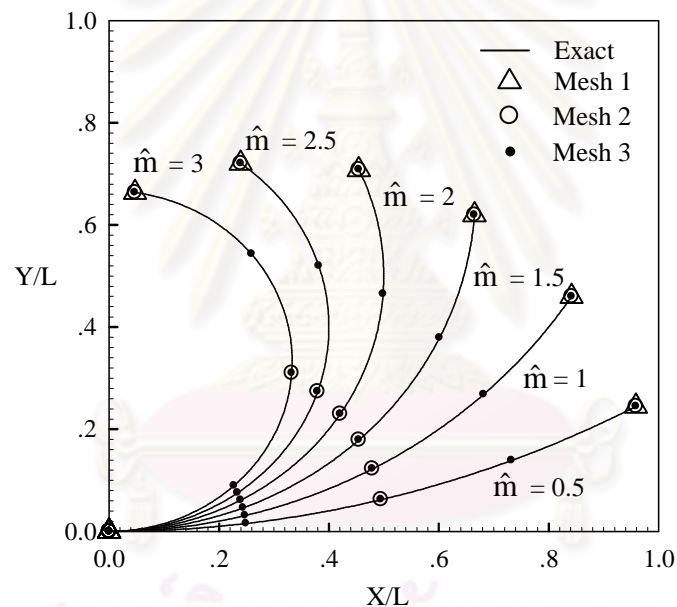


Figure 4.2 Deflected shape of cantilever beam subjected to end moment where
$$X/L = \xi + \hat{u} \text{ and } Y/L = \hat{v}$$

The rotation and displacement at the tip of the beam are also obtained and reported as a function of the normalized end moment $\hat{m}$ in Figure 4.3. Similar to the previous set of results, the current technique (for Mesh-1) yields very accurate numerical solutions for any value of the normalized end moment $\hat{m}$. It is also found that the horizontal and vertical displacements at the tip are nonlinear functions of the applied end moment $\hat{m}$ while the end rotation varies linearly with respect to $\hat{m}$. In

particular, the vertical displacement increases monotonically until it reaches the maximum at a particular value of the bending moment and after that it gradually decreases. In the contrary, the magnitude of the horizontal displacement increases monotonically for the entire range of $\hat{m}$ treated. The observed behavior is clearly illustrated by the deflected shape shown in Figure 4.2.
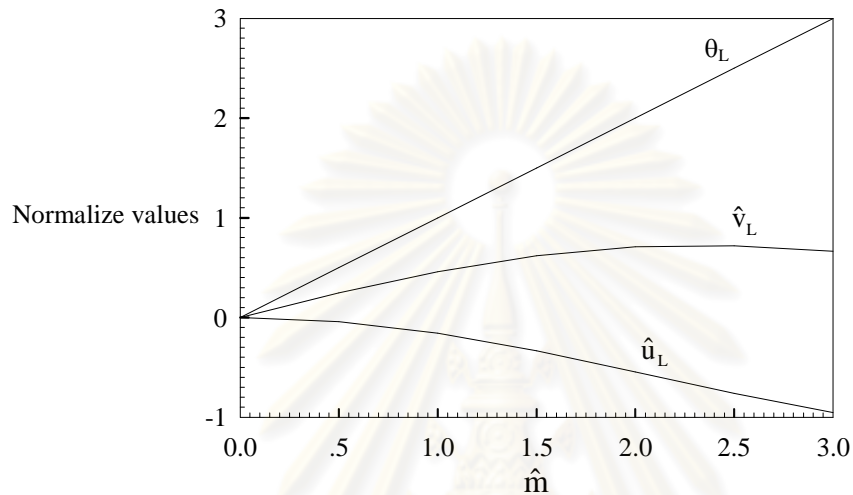


Figure 4.3 Relations between the displacement and rotation at the tip and the applied end moment.

### 4.1.2 Cantilever beam subjected to two moments

Consider next the same cantilever beam of length L and flexural rigidity EI but subjected to two moments 1.5M and -M, the former applied at the tip and the latter applied at the mid span as shown in Figure 4.4 (a). Note for this particular case that the bending moment within the left half of the beam is equal to 0.5M while in the right half, the bending moment is equal to -M. Three uniform meshes (consisting of 2, 4 and 8 members of equal length) employed in the analysis are illustrated in Figure 4.4(b). Results are obtained for various values of the normalized applied moment $\hat{m} = ML/EI \in \{1, 2, 3, 4, 5\}$.

Since the bending moment is constant for the left and right halves of the beam, the governing equations (4.1)-(4.3) are applicable to both portions. Upon a direct integration of such equations along with the use of boundary conditions at the fixed end and continuity conditions at the mid span, it leads to the close form solution for

the rotation, the displacement in X-direction and the displacement in Y-direction at any point $\xi = x/L, \; x \in [0, L]$ :

$$\theta = \begin{cases} 0.5\hat{m}\xi & , \quad 0 \le \xi \le 0.5 \\ \hat{m}(0.75 - \xi) & , \quad 0.5 \le \xi \le 1 \end{cases} \tag{4.7}$$

$$\hat{u} = \begin{cases} \dfrac{2\sin(0.5\hat{m}\xi)}{\hat{m}} - \xi & , \quad 0 \le \xi \le 0.5 \\ \dfrac{\sin(0.25\hat{m}) + \sin((0.75 - \xi)\hat{m})}{\hat{m}} + \xi - 1 & , \quad 0.5 \le \xi \le 1 \end{cases} \tag{4.8}$$

$$\hat{v} = \begin{cases} \dfrac{2 - 2\cos(0.5\hat{m}\xi)}{\hat{m}} & , \quad 0 \le \xi \le 0.5 \\ \dfrac{2 - 3\cos(0.25\hat{m}) + \cos((0.75 - \xi)\hat{m})}{\hat{m}} & , \quad 0.5 \le \xi \le 1 \end{cases} \tag{4.9}$$



(a)



(b)
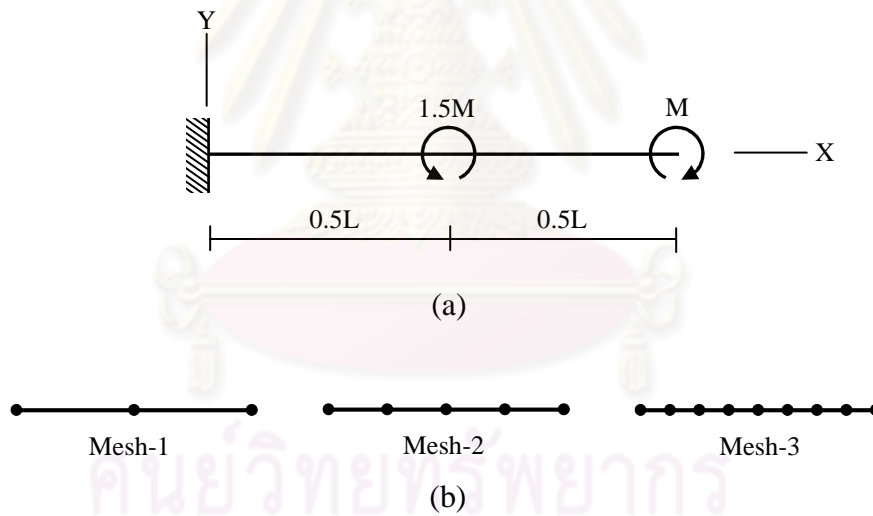
Figure 4.4 (a) Schematic of cantilever beam subjected to moments at the mid span and at the tip and (b) three meshes adopted in the analysis

The deflected shapes of the beam for different values of $\hat{m}$ are shown in Figure 4.5. The numerical results obtained for each mesh are reported only at the nodal points and compared with the analytical solution given by (4.7)-(4.9). As evident from this set of results, the numerical solutions exhibit excellent agreement with the benchmark solution with no dependence on the level of mesh refinement. For

this particular problem, the bending moment and curvature of the left half is twice of and opposite to that of the right half. As the applied moment $\hat{m}$ increases, the deflected shape of the beam is significantly different from its original shape and obviously different from that predicted by linear analysis.
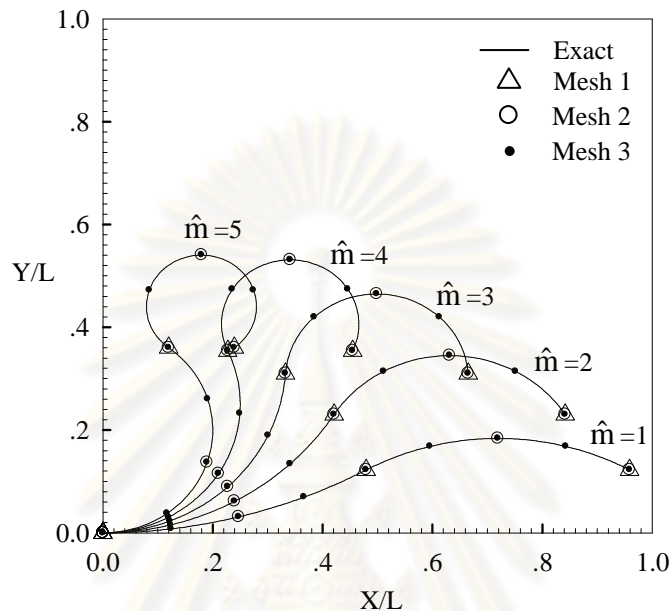


Figure 4.5 Deflected shape of cantilever beam subjected to two moments where
$$X/L = \xi + \hat{u} \text{ and } Y/L = \hat{v}$$

### 4.1.3 Frame subjected to moments

Finally, consider a more complex problem corresponding to a rigid frame consisting of a single column and two overhanging beams as shown schematically in Figure 4.6(a). The column and the two beams are of the same length L and the same flexural rigidity EI and the frame is subjected to three moments $\{M_1, M_2, M_3\}$ where $M_1$ and $M_2$ are applied at the free end of the beams and $M_3$ is applied at the junction of the beams and the column. In the analysis, we choose $\{M_1, M_2, M_3\}$ such that $M_1 = M_2 = 2EI/L$ and $M_3 = -5EI/L$ and three meshes (consisting of 3, 6, and 12 members) are adopted as shown in Figure 4.6(b). For this special loading condition, it yields a constant bending moment within the beam $B_1$, the beam $B_2$ and the column $C_1$ and zero internal axial and shear forces over the entire structure. Similar to the first two cases, the analytical solution for the rotation and displacement at any point within the

structure can readily be obtained by applying the governing equations (4.1)-(4.3) to the beams $B_1$ and $B_2$ and the column $C_1$ along with the use of the boundary conditions at the fixed base and the continuity conditions at the junction.
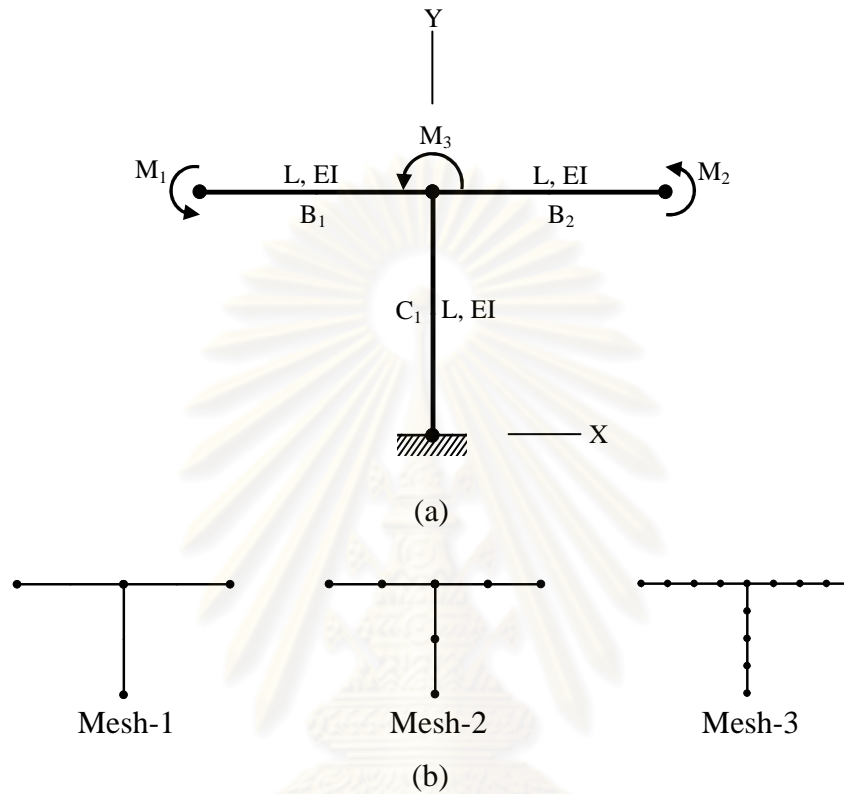


Figure 4.6(a) Schematic of rigid frame subjected to three moments and (b) three meshes adopt in the analysis

The deflected shape and the original shape of the rigid frame are reported in Figure 4.7. Again, numerical results for the displacement at the nodal points obtained from all three meshes coincide with the analytical solutions and, in addition, no dependence on the level of mesh refinement is observed. As evident from the deflected shape, the beams $B_1$ and $B_2$ and the column $C_1$ possess a single curvature; in particular, the curvature of the beam $B_1$ is opposite to that of the beam $B_2$.

From above three verifications, the developed technique yields numerical results that are identical to existing analytical solutions. While the possible small error may be introduced in the evaluation of integrals by standard Gaussian quadrature and

nonlinear solver by Newton-Ralpson iteration, it is controllable and can be reduced by either increasing the number of integration points or the level of solution tolerance. The independence of the level of mesh refinement is an attractive feature of the current technique that allows the optimal number of members be used in the analysis without altering the accuracy of obtained results.

It is noted that all three problems considered above are associated only with structures containing no inflection point within the member and possessing a piecewise constant bending moment and no internal axial and shear force. More verification is still needed for structures consisting of members possessing non-uniform internal forces and/or containing an inflection point.
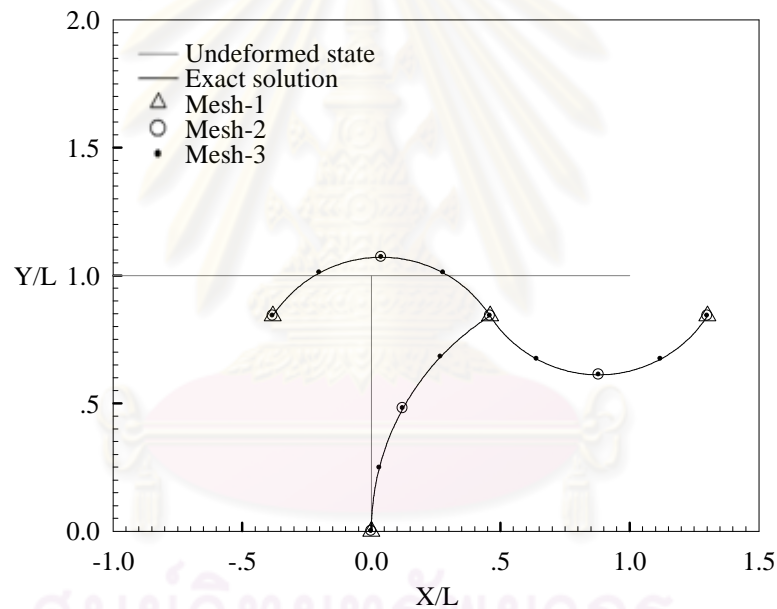


Figure 4.7 Deflected shape of rigid frame subjected to three moments where
$$X/L = \xi + \hat{u} \text{ and } Y/L = \hat{v}$$

## 4.2 Verification with finite element method

In this section, verifications of the current technique are conducted for more complex structures (e.g. structures containing inflection points and/or possessing non-uniform and non-zero internal forces) that are lack of analytical solution. As a means for comparison, the benchmark solutions are constructed by a reliable computational technique called a finite element method (FEM). To ensure the accuracy of the

benchmark solutions, their convergence is first investigated and a sufficiently refined mesh is then utilized. As a result of the independence of mesh refinement, numerical results presented further below are obtained from a possible coarsest mesh. Solutions at interior points of the member can readily be obtained from equations (3.16)-(3.18) or (3.73)-(3.75) or (3.97)-(3.99) after all unknown quantities at the ends were determined.

### 4.2.1 Simply-supported beam subjected to end moments and axial force

Consider a simply-supported beam of length L and constant flexural rigidity EI as shown in Figure 4.8. The beam is subjected to two counterclockwise $M_1$ and $M_2$ at both ends and the axial force $f_x$ at the right end. For this particular case, the beam contains an interior inflection point and, additionally, the bending moment, axial force and shear force exist and are non-uniform.
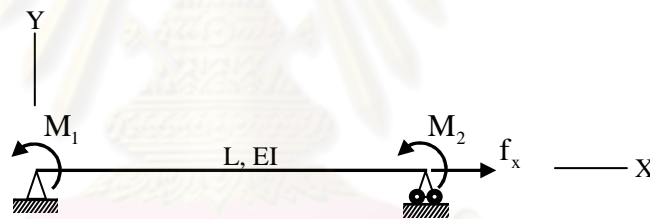


Figure 4.8 Schematic of simply supported beam subjected to end moments and axial force

In the analysis, we treat following two loading conditions: case-I associated with $M_1 = M_2 = 8.8EI/L$ and $f_x = 0$ and case-II corresponding to $M_1 = 4EI/L$, $M_2 = 5EI/L$ and $f_x = -4.5EI/L^2$. The beam is discretized into a single member that contains an inflection point.

Deflected shapes of the beam are reported in Figure 4.9 for the case-I and case-II. As compared with the benchmark solutions constructed by the FEM. results obtained from the current technique are highly accurate and nearly indistinguishable from the benchmark solutions with the error less than a fraction of one percent.
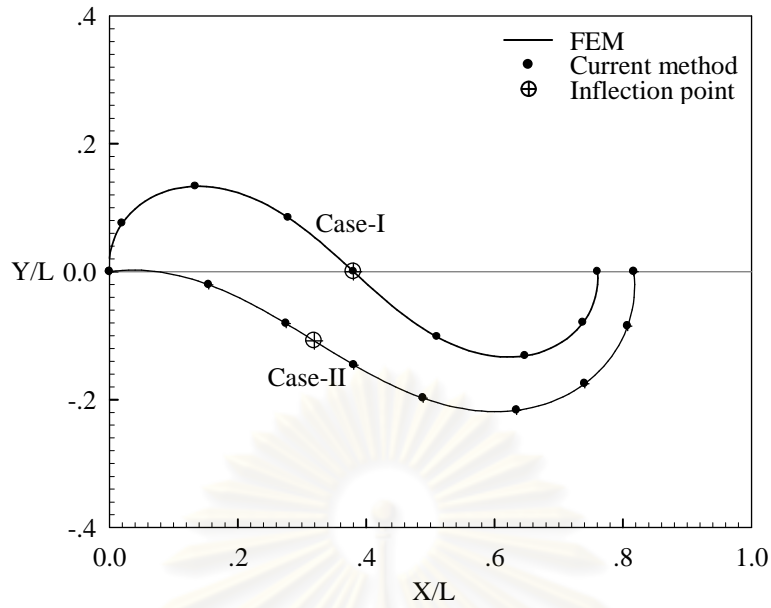
Figure 4.9 Schematic of deflected shape of simply supported beam subjected
to two loading conditions
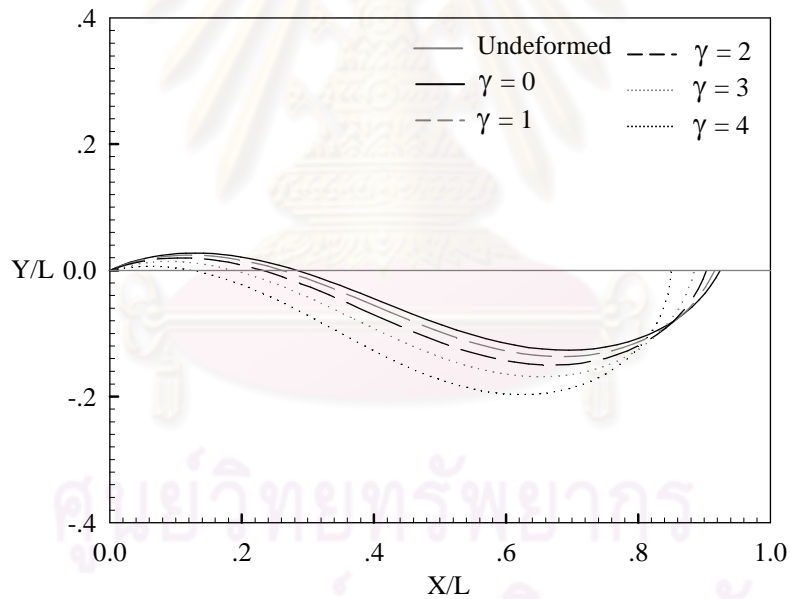


Figure 4.10 Schematic of deflected shape of simply supported beam for various
values of compressive force

To further investigate the influence of the axial compressive force $f_x$ on the
deflected shape of the beam, we fix the applied end moments to $M_1 = 4EI/L$, $M_2 =$
$5EI/L$ and vary $f_x$ such that $\gamma = f_x L^2 / EI \in \{0, 1, 2, 3, 4\}$. The deflected shape obtained
for each value of $f_x$ is reported in Figure 4.10. From these results, it can be concluded

that presence of the axial force significantly influences the deflected shape of the beam. In particular, as $f_x$ increases the inflection point gradually moves to the pinned support and the deflected shape starts to resemble the buckling shape of the first mode. In addition, the horizontal displacement of the roller support increases monotonically with respect to $f_x$.

### 4.2.2 Portal rigid frame subjected to horizontal force

To further verify the current technique and also demonstrate its capability in the treatment of structures comprising multiple members, we consider a portal frame that consists of two identical columns and one beam of the same length L and the same flexural rigidity EI as shown schematically in Figure 4.11. The frame is completely fixed at the base and subjected to a horizontal concentrated force P at the top.
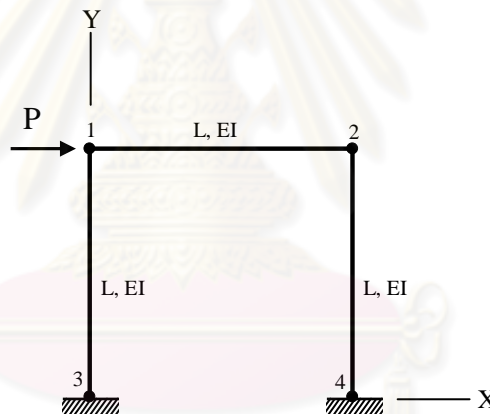


Figure 4.11 Schematic of portal frame subjected to a horizontal concentrated force at the top.

In the analysis, the structure is discretized into three members and four nodes as shown in Figure 4.11 and the horizontal force is taken such that $PL^2/EI = 15$. Note that a large value of the force P is chosen in order to amplify the influence of the nonlinear geometry and, as a result, augment the complexity of the problem. The deflected shapes of the frame are obtained from the current method and the FEM and results are then reported in Figure 4.12. The benchmark solution from the FEM is obtained by using a very fine mesh containing 100 members for each beam and

column, and coordinates of the deflected shape obtained from the current technique are plotted only at nodal points. Results indicate that the current technique gives rise to very accurate numerical solution and nearly coincide with those from the FEM. Although the computed results are presented only at the nodal points, coordinates of all interior points of all members can readily be obtained when quantities at their ends are known. Since nodal quantities can be solved very accurately, solutions within the member possess the comparable level of accuracy; if they were plotted in Figure 4.12, no distinction from results from the FEM will be observed.
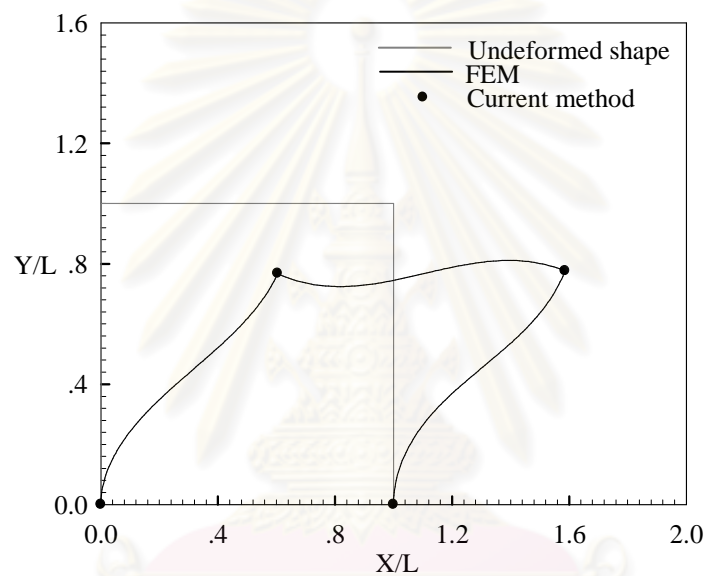


Figure 4.12 Deflected shape of portal frame subjected to horizontal concentrated force at the top
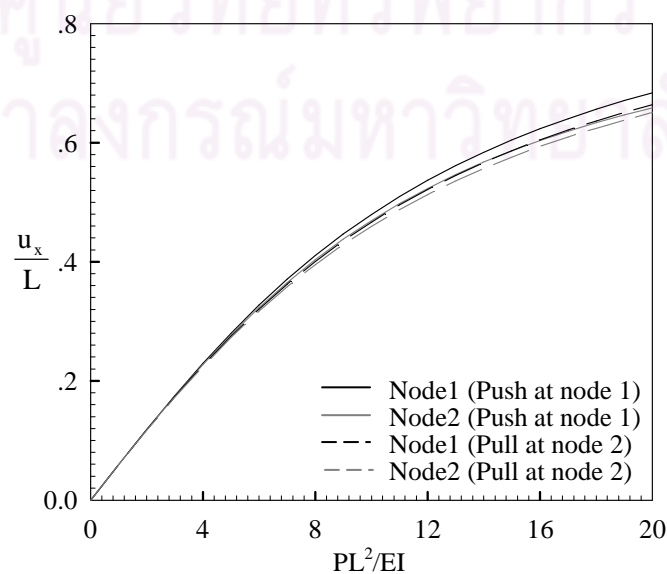


(a)
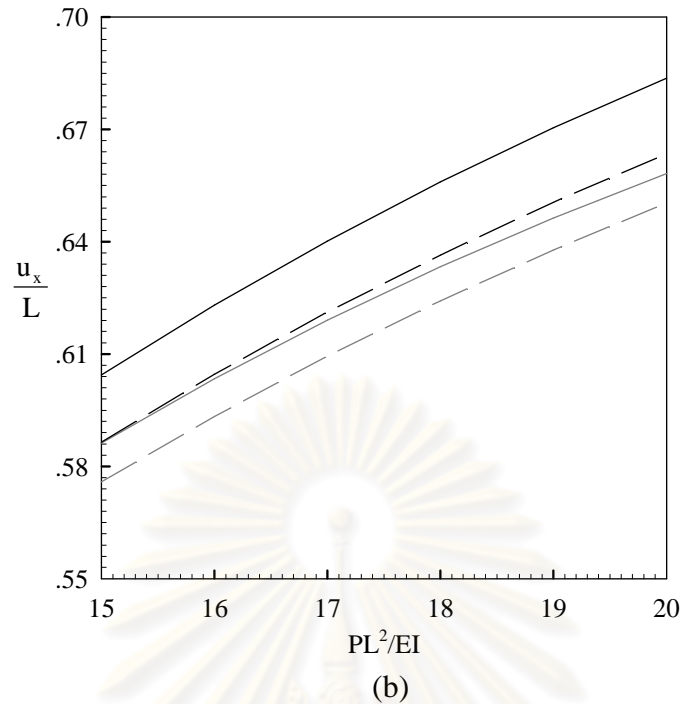
Figure 4.13 (a) Normalized horizontal displacement of node 1 and node 2 versus normalized applied force and (b) the same relation but plotted in magnified scale

Next, we examine the influence of the location and magnitude of the horizontal concentrated force P on the horizontal displacement of node 1 and node 2. Two locations of the applied force, node 1 and node 2, are considered in this investigation. It is worth noting that the linear analysis predicts no difference among the horizontal displacements at node 1 and node 2 and this observation is independent of the location of the applied force P. Nevertheless, the different behavior is captured when the large curvature analysis is employed. The normalized horizontal displacements $u_x/L$ at node 1 and node 2 for different locations of the applied force P are displayed in Figure 4.13. Due to the inextensibility assumption, as the beam member undergoes deflection, the horizontal projected length is always less than its original length. This therefore renders the horizontal displacements of node 1 always larger than that of node 2. Furthermore, when comparing the horizontal displacement at the same node but changing the location of the force P instead, results from analysis indicate certain discrepancy. Such discrepancy is insignificant for small values of P but becomes more

apparent when P increases. In addition, nonlinearity of the load-displacement relation is observed for large values of P.
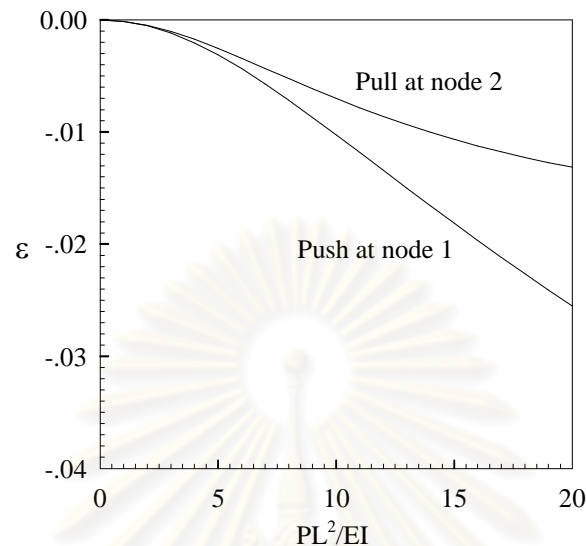


Figure 4.14 Relation between reduction of normalized horizontal projected length and normalized applied force

To clearly illustrate the reduction of the horizontal projected length of the beam, we also plot the difference between the normalized horizontal displacements at node 2 and node 1, denoted by $\varepsilon$, versus the normalized applied force as shown in Figure 4.14. From these results, the horizontal projected length for the case P is applied at node 1 is always shorter than that for the case P is applied at node 2 and such difference becomes more apparent when the force P increases. This is due to the fact that when the force P is applied at node 1, the beam is in compression and the P-$\Delta$ effect significantly amplifies the elastic shortening. In contrast, when the force P is applied at node 2, the beam is in tension and such axial force trends to stretch the beam and therefore reduces the elastic shortening.

### 4.2.3 Portal rigid frame subjected to horizontal and vertical forces

Consider the same structure as treated in the previous example but now subjected to both the horizontal force P and the vertical force V as shown

schematically in Figure 4.15. Again, in the analysis, a mesh consisting of one beam member and two column members is utilized.
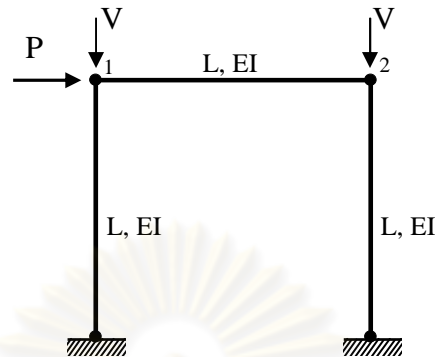


Figure 4.15 Schematic of portal frame subjected to horizontal and vertical forces

First, we obtain the deflected shape of the frame under the applied loads $PL^2/EI = 4$ and $VL^2/EI = 5$ and the result is reported in Figure 4.16(a). In this plot, two other sets of results, one obtained from linear analysis and the other obtained from $2^{nd}$ order analysis, are also included. It is obvious from these results that the deflected shapes obtained from the three analyses exhibit significant discrepancy. In particular, the linear analysis underestimates the horizontal displacement at the top of the frame and no information on the downward movement is predicted while the $2^{nd}$ order analysis considerably overestimates the horizontal movement of the top of the beam and, similarly, it still lack information on the downward movement due to the linear kinematics assumption.

Next, we investigate the influence of the vertical force V on the horizontal displacement of node 1 of the frame and demonstrate the capability of the linear and $2^{nd}$ order analyses in comparison with the current method (that is based on large curvature analysis). Figure 4.16(b) shows the plot of the normalized horizontal displacement versus the normalized vertical force for the constant horizontal force $PL^2/EI = 4$. From large curvature analysis, it is found that while maintaining the horizontal force constant but increasing the vertical force, the horizontal displacement at the top of the frame increases monotonically and exhibits strong dependence on the value of the vertical force V. This is owing to an additional bending moment induced

by the P-$\Delta$ effect. It is also important to point out that the linear analysis yields the solution that is independent of the vertical load V while the $2^{nd}$ order analysis can capture the axial-bending coupling but it yields very inaccurate results especially for large values (
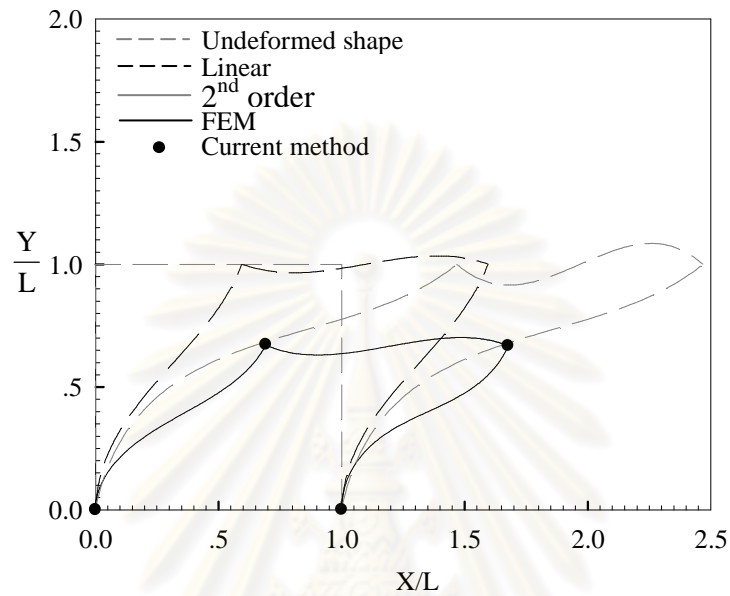


(a)
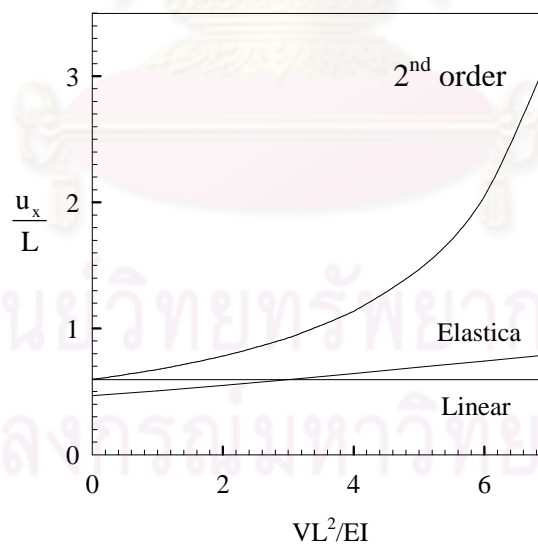


(b)

Figure 4.16 (a) Deflected shape of the frame obtained from different types of analysis and (b) normalized horizontal displacement at node 1 versus normalized vertical force

### 4.2.4 Gable frame subjected to horizontal force at the tip

Consider next a structure of more complex geometry in terms of member orientations as shown in Figure 4.17. The gable frame consists of two vertical members of length L and flexural rigidity EI and two inclined members of length $\sqrt{2}L$ and flexural rigidity EI and it is subjected to a horizontal concentrated force P at the vertex. In the analysis, a mesh consisting of four members, two vertical and two inclined members, is adopted.
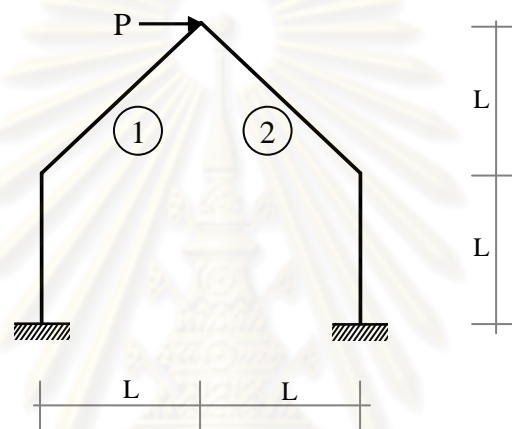


Figure 4.17 Schematic of gable frame subjected to horizontal load at the vertex.

As an additional verification of the current technique, we first obtain results for a particular applied force $P = 4EI/L^2$ and then compared with those obtained from FEM in Figure 4.18. Again, it can be concluded that results computed from the current technique exhibit excellent agreement with the benchmark solution. In addition, the deflected shape obtained from linear analysis is significantly different from that obtained from the large curvature analysis; in particular, the horizontal displacement of the frame is over predicted while there is no information of the downward movement of the vertex. This implies that as the structure undergoes large displacement and rotation, the linear analysis no longer yields results of sufficient accuracy. It is also found that the deflected shapes of the gable frame (predicted by the large curvature analysis) for the force $P = 6EI/L^2$ and $P = 15EI/L^2$ are very

different; strong dependence of the applied load on the deformed configuration of the structure becomes apparent when the level of applied loads is sufficiently large.
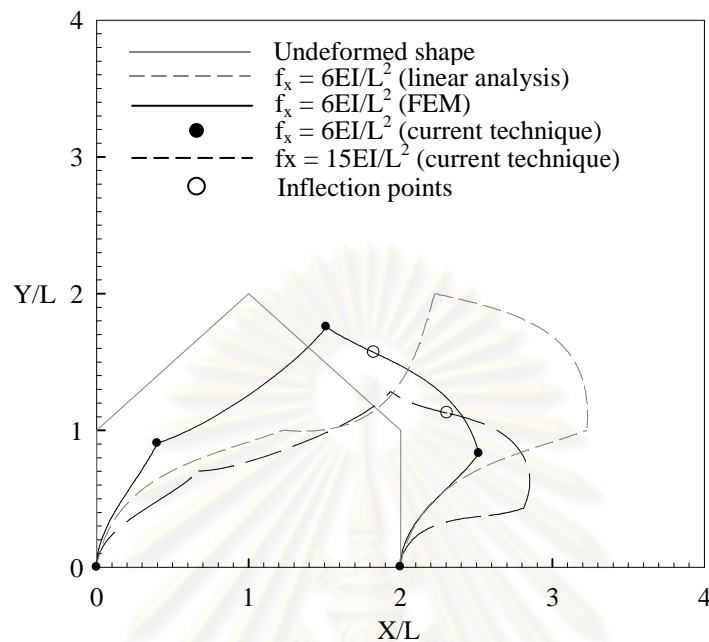


Figure 4.18 Deflected shape of gable frame subjected to horizontal force at vertex

Next, we investigate the location of the inflection point within the two inclined members. Within the context of linear analysis along with the use of anti-symmetry, it can readily be deduced that both inclined members possess a single curvature and always contain an inflection point at the vertex. In contrast, the large curvature analysis predicts different solutions. As the horizontal force P increases, the inflection point moves from the vertex into the member 2 and, as a results, the member 1 possesses a single curvature while the member 2 possesses a double curvature. Figure 4.19 indicates the relation between the position of the inflection point and the normalized applied force. Note that a parameter $\varpi$ is defined $\varpi = 100(\bar{L}/\sqrt{2}L)$ where $\bar{L}$ is the length of the portion of the member 2 that is on the left of the inflection point. As clearly demonstrated by these results, the rate of movement of the inflection point with respect to the applied force is large at the beginning and then starts to drop as the applied force increases.

Another important aspect observed in the analysis of this particular structure is that the anti-symmetry of the structure that is applicable to the linear analysis is

completely destroyed as the structure deformed and can no longer be employed in the large curvature analysis.
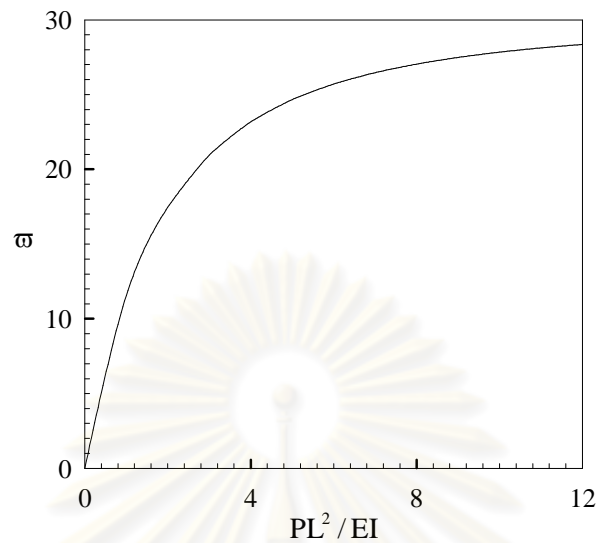


Figure 4.19 Relation between position of inflection point and normalized applied force

### 4.2.5 Multi-storey rigid frame subjected to lateral forces
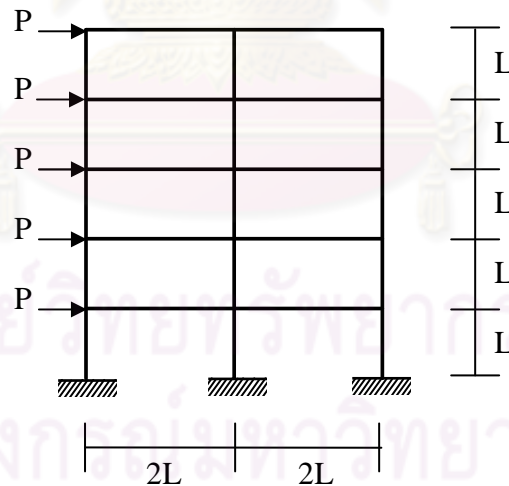


Figure 4.20 Schematic of multi-storey frame subjected to lateral forces

As a final example, consider a multi-storey rigid frame as shown schematically in Figure 4.20. In addition to verification of the current technique, this example serves to demonstrate its capability to treat a structure consisting of several members. The frame consists of columns of the same length L and flexural rigidity EI

and beams of the same length 2L and flexural rigidity EI, and it is subjected to a set of later forces of the same magnitude P as indicated in Figure 4.20. In the analysis, the structure is discretized into 15 column members and 10 beam members.
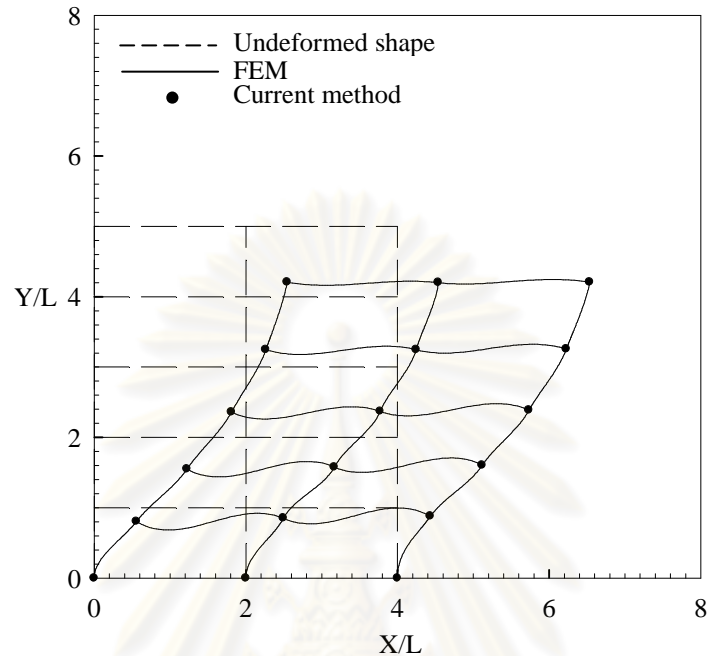


Figure 4.21 Deflected shape of multi-storey frame subjected to lateral forces

For purpose of verification, we first perform the analysis for $PL^2/EI = 2.5$. The deflected shapes of the frame obtained from the current technique and FEM are reported in Figure 4.21. It can be concluded that computed numerical results are nearly indistinguishable from the benchmark solution. This implies that the current technique yields highly accurate results without mesh refinement. To further confirm such high accuracy, numerical values of the lateral and vertical displacements at three nodes on the top floor of the frame and the reactive forces at its three supports are shown in Table 4.1 and Table 4.2, respectively. It is evident from this set of results that errors of numerical results relative to the benchmark solutions are only small fractions of one percent.

To further investigate the difference between results obtained from linear analysis and large curvature analysis, we perform analysis of the structure for a range of the applied load $PL^2/EI \in [0, 2.5]$. The horizontal displacement at the central node

of each floor and the horizontal and vertical reactive forces versus the applied load are reported in Figure 4.22 and Figure 4.23, respectively.

Table 4.1 Nodal displacements at top floor of multi-storey frame

| | Normalized horizontal displacement | | | Normalized vertical displacement | | |
|---|---|---|---|---|---|---|
| | FEM | Current method | Error (%) | FEM | Current Method | Error (%) |
| Left node | 2.54630 | 2.54622 | 0.00314 | -0.79503 | -0.79501 | 0.00269 |
| Central node | 2.54120 | 2.54113 | 0.00286 | -0.80120 | -0.80118 | 0.00216 |
| Right node | 2.53590 | 2.53586 | 0.00155 | -0.79562 | -0.79559 | 0.00352 |

Table 4.2 Reactive forces at three supports of multi-storey frame.

| | Normalized horizontal reactive force | | | Normalized vertical reactive force | | |
|---|---|---|---|---|---|---|
| | FEM | Current method | Error (%) | FEM | Current Method | Error (%) |
| Left node | -9.00390 | -9.00415 | -0.00281 | -5.80340 | -5.80359 | 0.00332 |
| Central node | -4.52140 | -4.52134 | -0.00130 | -0.31481 | -0.31514 | 0.10383 |
| Right node | 1.02530 | 1.02549 | 0.01893 | 6.11870 | 6.11873 | 0.00048 |

Results shown in Figure 4.22 indicates that for small values of applied loads the horizontal displacements at each floor obtained from linear analysis and large curvature analysis are comparable but a significant discrepancy of those results become more apparent for large values of applied loads. It can also be pointed out that the large curvature analysis provides information on the increase of structural stiffness due to geometric nonlinearity; in particular, as the applied loads increase, the slope of the displacement-load curve decreases monotonically.
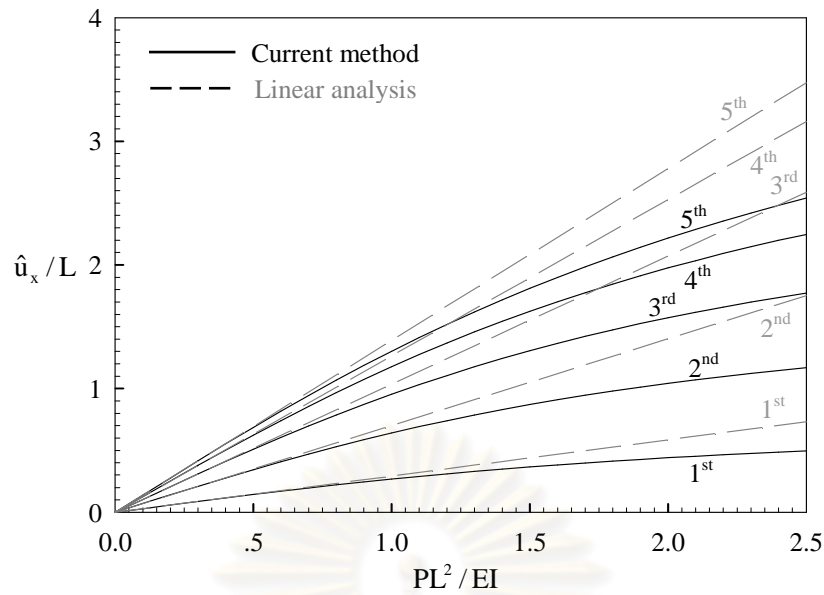
Figure 4.22 Normalized horizontal displacements at central node of each floor versus normalized horizontal force.

Regarding to linear analysis, the reactive forces at the three supports vary linearly with respect to the applied load P and, from anti-symmetric properties of the given structure, the vertical reactive force at the central support vanishes and the magnitude of horizontal and vertical reactive forces at the left and right supports are identical. However, the large curvature analysis predicts significantly distinct solutions. The horizontal reactive forces at the left and right supports are not the same and exhibit major difference from those predicted by the linear analysis while the vertical reactive forces show somewhat less discrepancy. It is noticed in addition that the negative horizontal reactive force at the right support changes to positive values when the displacement becomes large; this aspect of behavior cannot be captured by the linear analysis. Remark also that for the central support, a nonzero but small vertical reactive force is predicted from the large curvature analysis.

Regarding to linear analysis, the reactive forces at the three supports vary linearly with respect to the applied load P and, from anti-symmetric properties of the given structure, the vertical reactive force at the central support vanishes and the magnitude of horizontal and vertical reactive forces at the left and right supports are identical. However, the large curvature analysis predicts significantly distinct solutions. The horizontal reactive forces at the left and right supports are not the same

and exhibit major difference from those predicted by the linear analysis while the vertical reactive forces show somewhat less discrepancy. It is noticed in addition that the negative horizontal reactive force at the right support changes to positive values when the displacement becomes large; this aspect of behavior cannot be captured by the linear analysis. Remark also that for the central support, a nonzero but small vertical reactive force is predicted from the large curvature analysis.



Figure 4.23 (a) Normalized horizontal reactive force and (b) normalized vertical reactive force versus normalized applied load. Symbols {l, m, r} and {L, M, R} are used to indicate results from linear and large curvature analyses for left, central and right supports, respectively.

As demonstrated by extensive numerical experiments on various structures (e.g. simple or complex geometries, single or multiple members, containing inflection point(s) or no inflection points, small or large values of applied loads, etc.), the current technique has proven to yield highly accurate numerical results without any mesh refinement. As compared with either existing analytical solutions or benchmark solutions constructed by a reliable numerical method, i.e. FEM, small errors in the order of a fraction of one percent have been observed. It is worth to emphasize again that the current technique exploits no approximation of the form of the solution and governing equations; as a consequence, only potential sources of errors are due to the numerical integration of involved integrals and the solution tolerance employed in Newton-Ralphson iteration.

## 4.3 Other interesting results

In this section, a verified technique is employed to investigate behavior of various structures undergoing large displacement and rotations, e.g. nonlinear load-displacement relations, deformed configuration as a function of applied loads, change of locations of inflection points, etc.

### 4.3.1 Square box rigid frame subjected to pair of horizontal forces

Consider a square box rigid frame as shown in Figure 4.24(a). The frame consists of two horizontal member and two vertical members of the same length L and the same flexural rigidity EI and is subjected to a pair of opposite, horizontal forces P at the mid span of the vertical members. The frame is constrained against the rigid body movement by a pinned support and roller support as indicated in Figure 4.24(a). Since a pair of applied loads is self equilibrated, there is no reactive force induced at the two supports. Figure 4.24(b) shows a generic deflected shape of the frame under the application of forces and $\bar{L}$ denotes the distance between the mid spans of the two vertical members.
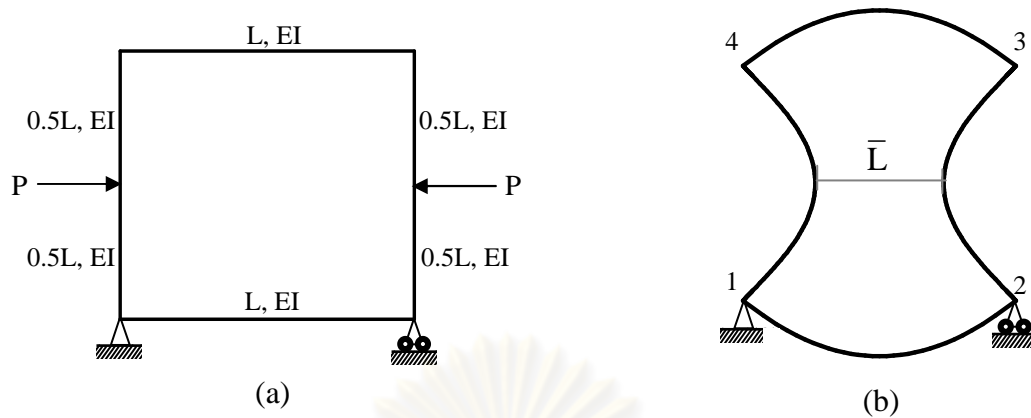
Figure 4.24 (a) Schematic of square box rigid frame subjected to a pair of horizontal forces and (b) deflected shape of the frame
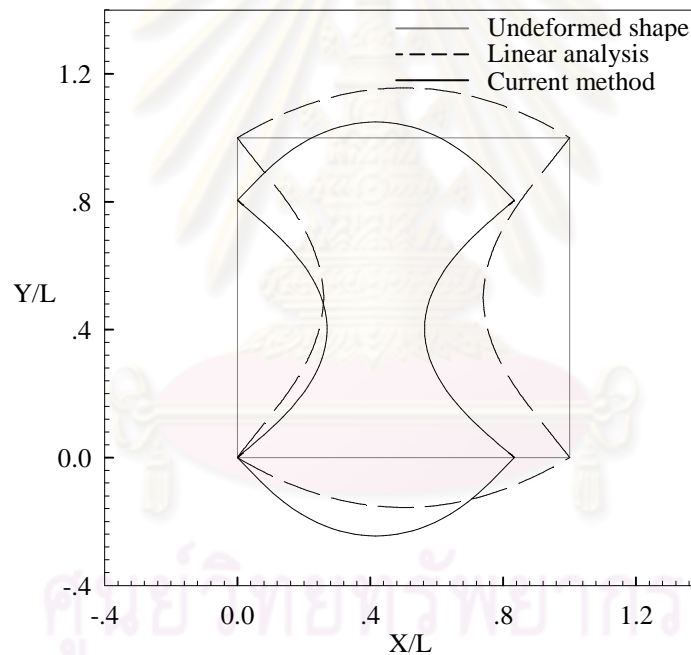


Figure 4.25 Deflected shape of square box rigid frame subjected to a pair of horizontal forces

In the analysis, the structure is discretized into 4 members, 2 vertical and 2 horizontal members. The deflected shapes of the frame obtained from linear and large curvature analyses are reported, for $PL^2/EI = \alpha = 20$, in Figure 4.25. As indicated by these results, the linear analysis predicts a deflected shape with no movement of nodes 1, 2, 3 and 4 while the large curvature analysis yields significant different deflected

shape. In particular, the displacements at the nodal points obtained from the current technique are nonzero and this results primarily from the elastic shortening due to members undergoing large curvature. The deflected shape of the frame from large curvature analysis for various values of the applied loads is shown in Figure 4.26. Clearly, the deflected shape of the frame exhibits strong dependence on the magnitude of the applied loads.
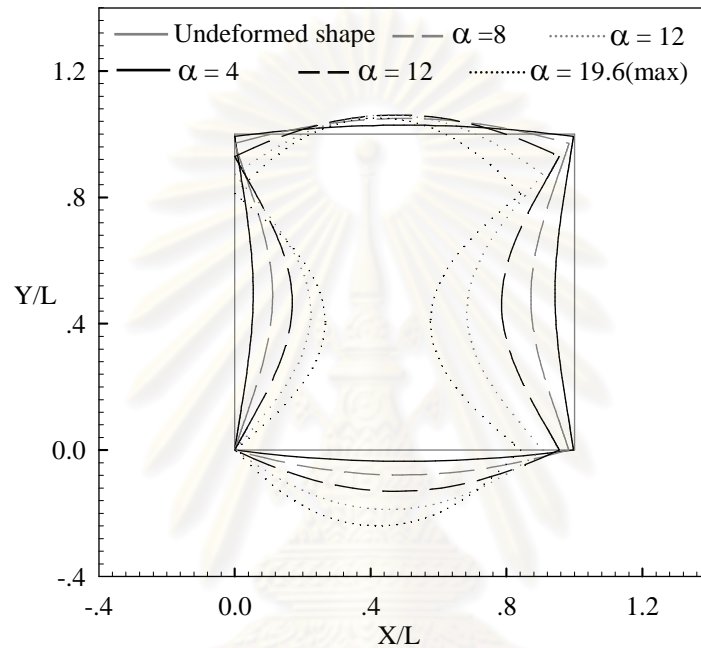


Figure 4.26 Deflected shapes of square box rigid frame for various values of applied forces

Next, we examine the relation between the distance $\bar{L}$ and the applied horizontal forces P. As reported in Figure 4.27, the linear analysis yields a linear relationship between $\bar{L}$ and P and such a linear regime is also observed in the large curvature analysis provided that the applied load P is sufficiently small. However, for large values of P, the current technique predicts a nonlinear behavior and, in addition, significant deviation from linear results is observed. Remark that the distance $\bar{L}$ obtained from large curvature analysis is always less than that obtained from linear analysis. This is due to the fact that for the linear case, the nodal points 2 and 3 are not allowed to move in the horizontal direction in order to maintain inextensibility (in the sense of linearized kinematics) of the two horizontal members.
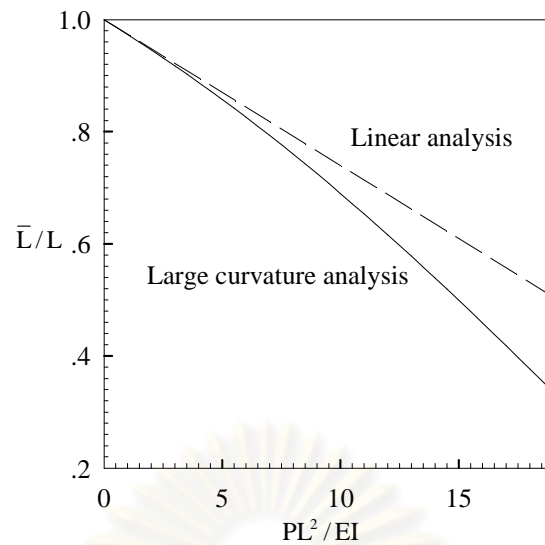
Figure 4.27 Relation between normalized distance $\overline{L}/L$ and normalized applied force

Figure 4.28 shows the relation between the horizontal displacement at the mid span of the left vertical member and the applied loads. It is evident that results from both linear and large curvature analyses are slightly different and such discrepancy results directly from the elastic shortening due to the left vertical member undergoing large curvature.
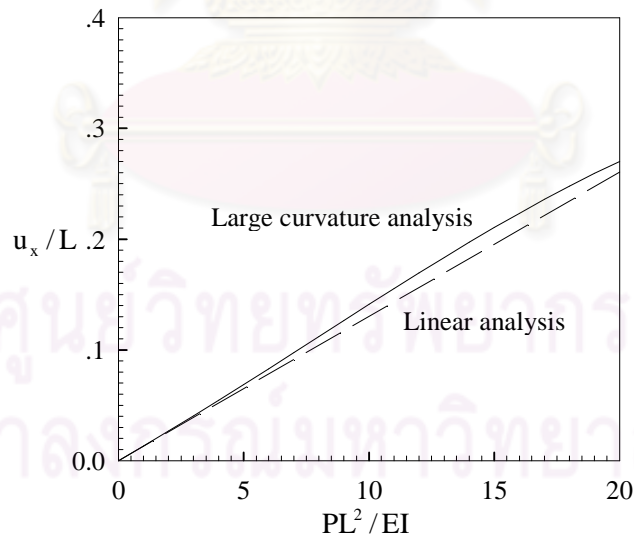


Figure 4.28 Relation between horizontal displacement at mid span of the left vertical member and applied loads

### 4.3.2 Opened square box subjected to pair of vertical forces

Consider an opened square box rigid frame as shown in Figure 4.29. The frame possesses the same geometry as that of the previous example except at the top where it contains two identical overhanging beams. The flexural rigidity EI is constant throughout the structure and the frame is subjected to a pair of opposite vertical forces P as indicated in Figure 4.29 (a). The generic deflected shape of the structure under such applied loads is shown schematically in Figure 4.29(b). As clearly illustrated by the undeformed configuration of the structure, anti-symmetry of the structure can be employed to reduce computational effort in the linear analysis. However, as the structure undergoes displacement and deformation, the anti-symmetry of the structure is completely destroyed and can no longer be applied. To perform analysis by the current technique, a mesh consisting of 3 horizontal members and 2 vertical members is adopted.



(a)                                                              (b)
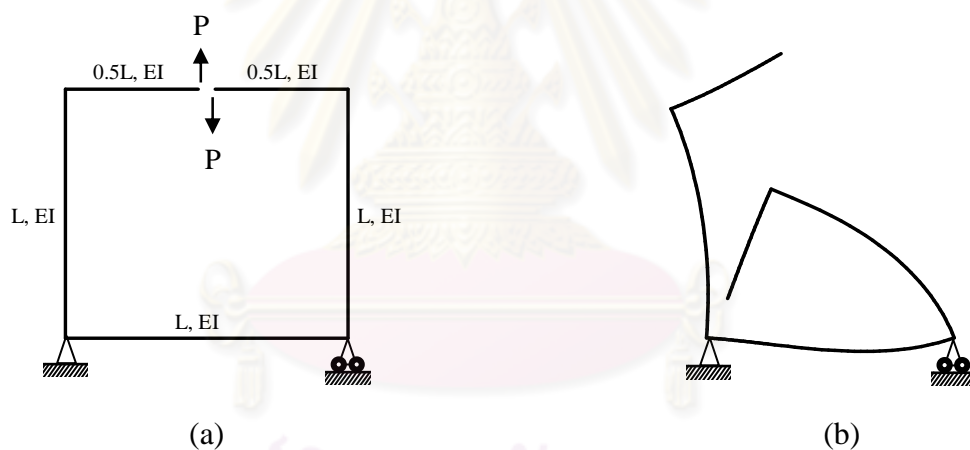
Figure 4.29 (a) Schematic of opened square box subjected to a pair of vertical forces and (b) generic deflected shape of the frame

Numerical results are obtained for various values of the applied force P ranging from zero to $1.8EI/L^2$ and reported in Figure 4.30. In particular, Figure 4.30(c) illustrates the evolution of the deflected shape as the applied load P increases. Clearly, for large values of the applied load P, the deflected shape is substantially different from the original undeformed configuration. It can also be observed that all members, except the bottom member, possess a single curvature.
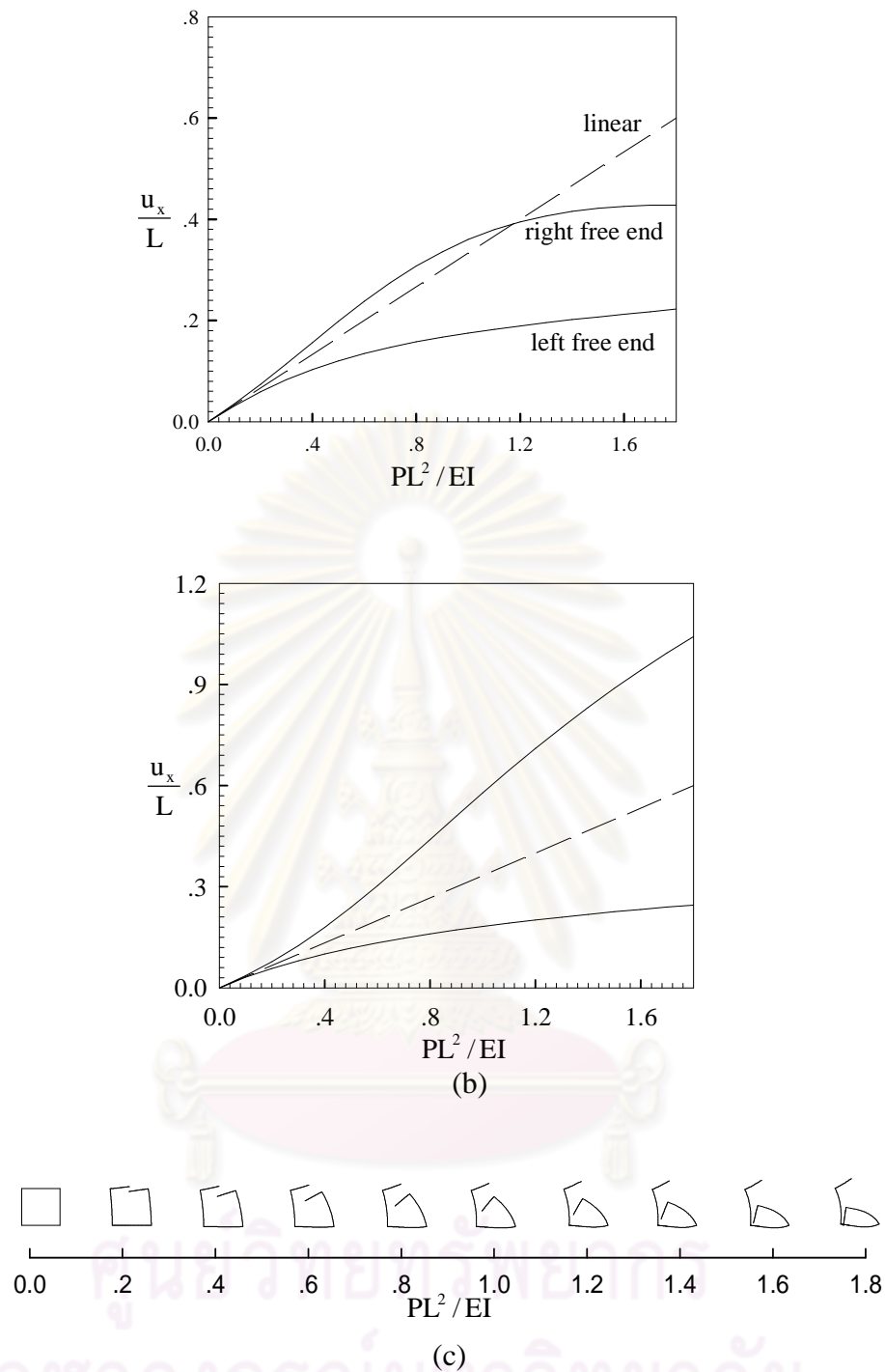
Figure 4.30 (a) Normalized horizontal displacement and (b) normalized vertical displacement versus normalized applied load, (c) a series of deflected shape of frame

The horizontal and vertical displacements at the left and right free ends are depicted in Figure 4.30(a) and 4.30(b), respectively. Unlike the linear case, the horizontal and vertical displacements at the left and right free ends predicted by the current technique are very different and exhibit a strong nonlinearity on the applied

load. Such nonlinearity and discrepancy from linear results become more evident as the applied load is sufficiently large. In addition, both the horizontal and vertical displacements at the left free end are always larger than those at the right free end. The rate of change of the horizontal displacement with respect to the applied load (commonly known as the tangent flexibility) for the right free end is less than that for the left free end for small values of applied load P, but as the applied load P is sufficiently large, such rate of change gradually decreases and reverses the trend. In contrast, the rate of change of the vertical displacement for the right free end is greater than that for the left free end for an entire range of the applied load considered in the analysis. Another observation is that the inflection point present within the bottom beam moves from the mid span toward the left supports. This results from that as the structure undergoes deformation, the actual moment arm of the force acting at the left free end (measuring from the pinned support) decreases while the actual moment arm of the force acting at the right free end (measuring from the roller support) increases.

### 4.3.3 Simply-supported beam subjected to unequal end moments

As a final example, we investigate the movement of an inflection point within the member as the loading condition changes. Consider a simply-supported beam of length L and flexural rigidity EI and subjected to counterclockwise end moments $M_1$ and $M_2$, respectively, as shown in Figure 4.31. From linear analysis, the bending moment diagram is linear throughout the beam and thus there exists a point (called an inflection point) where the bending moment vanishes. It can further be verified that the location of an inflection point remains unchanged as long as the ratio between the two end moments is the same. In this investigation, we will prove, within the context of large curvature analysis, that this phenomenon is no longer valid.



Figure 4.31 Schematic of simply-supported beam subjected to two counterclockwise end moments

In the analysis, a mesh consisting only one member is utilized and values of the applied end moments are chosen such that $M_1L/EI = 3$ and $M_2 = \eta M_1$ where $1 \leq \eta \leq 2$. The end moment $M_1$ is chosen sufficiently high to ensure that the beam undergoes large displacement and rotation, and the non-dimensional parameter $\eta$ is chosen to be greater than or equal to 1 simply to force the inflection point moving to left support. Figure 4.32 shows a series of deflected shapes of the beam for various values of the loading parameter $\eta$. Small circle symbols appearing in the plot indicate locations of the inflection point. As evident from these results, as the ratio between the end moments $\eta = M_2/M_1$ increases, the inflection point moves from the mid span (for $\eta = 1$) towards the left support. To explore further, let define two parameters $r_1$ and $r_2$ such that

$$r_1 = \frac{s_R}{s_L} \qquad ; \qquad r_2 = \frac{s_{pR}}{s_{pL}} \qquad\qquad\qquad (4.10)$$

where $s_L$ is the arc length of a portion of the beam on the left of the inflection point, $s_R$ is the arc length of a portion of the beam on the right of the inflection point, $s_{pL}$ is the horizontal projected length of a portion of the beam on the left of the inflection point and $s_{pR}$ is the horizontal projected length of a portion of the beam on the right of the inflection point. The relation between the two parameters $r_1$ and $r_2$ and the loading parameter is reported in Figure 4.33.

As clearly demonstrated in Figure (4.33), the ratio $r_1$ is a nonlinear function of the loading parameter $\eta$ with the slope greater than one while the ratio $r_2$ varies linearly with respect to $\eta$ and, in addition, the constant slope is unity. The former observation implies that the large curvature analysis predicts a greater rate of movement of the inflection point towards the end possessing a smaller moment than that by the linear analysis. In contrast, the latter finding concludes that if the spatial coordinates is utilized in stead of the material coordinates in the identification of the inflection point, both linear and large curvature analyses yield the same conclusion.
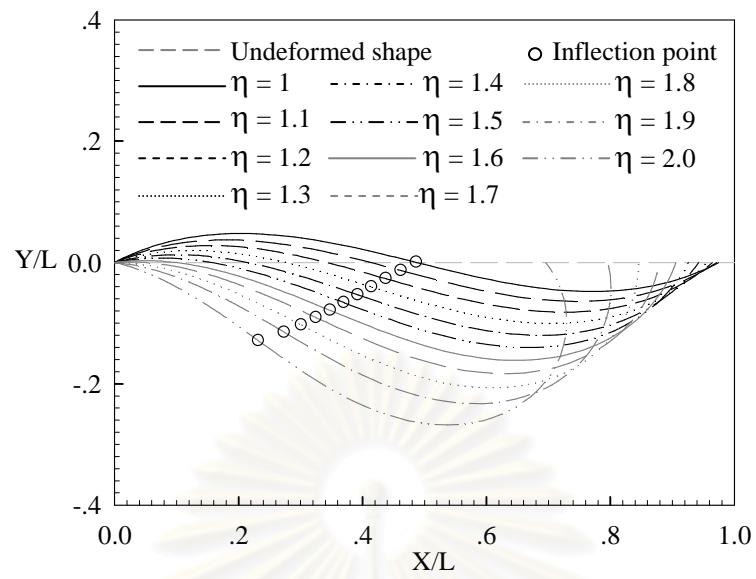
Figure 4.32 Deflected shape of simply-supported beam for various values of loading

parameter η
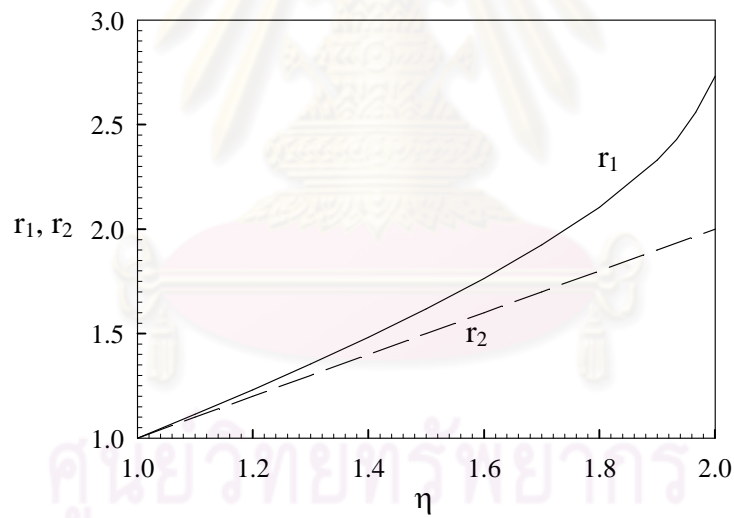


Figure 4.33 Relation between the parameters $r_1$ and $r_2$ and loading parameter η

# CHAPTER V

## CONCLUSION

### 5.1 Summary

A simple, systematic method has been developed for analysis of flexure-dominating structures undergoing large displacement and rotation. The technique is based primarily on a standard direct stiffness strategy and Newton-Ralphson iteration. The element tangent stiffness matrix essential for the development of the direct stiffness method has been constructed by directly solving the nonlinear governing differential equations. In particular, the gradient matrix of a simply-supported beam has first been established and subsequently been employed as a basis for the development of the tangent stiffness matrix for following three types of members: a single curvature member containing no inflection point, a single curvature member containing an inflection point at the end, and a double curvature member containing an interior inflection point. It is worth noting that the resulting tangent stiffness matrix possesses two attractive features: (i) it is exact in the sense that it involves no approximation of a solution form or governing equations and (ii) all entries of the matrix are given in an explicit form concerning the elliptic integrals or other integrals of the same kind. The former feature enhances the rate of convergence of a nonlinear solver and, when properly incorporated with the evaluation of exact residuals, it can in principle yield numerical solutions of the same quality as an analytical solution. The latter feature is well-suited for numerical evaluation of the tangent stiffness matrix by a standard Gaussian quadrature.

In addition, the length constraint posed by the member inextensibility has directly been incorporated in the construction of the element tangent stiffness matrix and this increases dimensions of the matrix by one. Such direct integration of the length constraint allows the nodal displacements be treated as primary unknowns and, as a consequence, this is well-suited for the stiffness method. The tangent stiffness matrix of the entire structure has been obtained via a direct assembly procedure. This

crucial ingredient has been utilized in the iterative process of a nonlinear solver by Newton-Ralphson iteration.

The proposed technique is a semi-analytical approach where all ingredients essential for the development of a direct stiffness method (e.g. element tangent stiffness matrix and residual vector) are derived from exact governing equations but all entries of the tangent stiffness matrix must be evaluated numerically and a resulting system of algebraic nonlinear equations must also be solved by a numerical technique. Hence, the accuracy of numerical solutions obtained from the current technique depends primarily on the accuracy of the numerical integration and the accuracy of the solution solver via the specified tolerance. Upon an extensive and careful study of the number of integration points and solution tolerance, the current technique has yielded highly accurate numerical solutions. Another crucial feature of the current technique is that there is no requirement on mesh refinement in order to achieve the desirable accuracy. This feature minimizes the number of members in the structure discretization to reduce the computational cost.

From extensive verifications via the comparison with either analytical solutions or benchmark solutions constructed from the finite element method (FEM), the current technique has proven to yield highly accurate numerical solutions and confirmed the independence of the level of mesh refinement. The observed errors are only a small fraction of one percent. Although the finite element method employed can solve the same problem, analysis must be performed using either a series of meshes or a sufficiently fine mesh to ensure the convergence of numerical solutions. In addition, such method still possesses some limitations such as an ability to perform the analysis over a limited range of applied loads.

As evident from extensive numerical experiments on various structures, the current technique has offered two crucial benefits. Firstly, the method proposes a simple and systematic means capable of modeling large structures when exact kinematics is presumed and, secondly, it is solidly confirmed to yield "exact" numerical solutions (within round off errors and errors caused by a numerical quadrature and nonlinear solver) that are independence of the level of mesh refinement. One practical contribution of the current investigation is that it provide an

accurate computational tool well-suited for analysis of structures undergoing large displacement and rotation, e.g. very flexible structures, moment-resisting cables, slender drill string rods, etc. According to its high accuracy, the proposed technique can also be employed to generate benchmark solutions for a comparison purpose.

## 5.2 Limitations and possible extensions

The key formulation underlying the current technique is still restricted to structures made from linearly elastic materials. Such limitation can pose some potential drawbacks (e.g. yields numerical results of insufficient accuracy, misleads the response prediction, provides no information on some aspects etc.) when the technique is applied to analyze certain structures. In general, the deformation induced within the structure undergoing large displacement and rotation is not small and this can generate stress exceeding the proportional limit of a constituting material; as a result, a linear relation between the deformation and internal force is no longer applicable. To capture this situation accurately, the material nonlinearity must properly be incorporated, in addition to the geometric nonlinearity, into the development of a mathematical model. Extension of the current development to treat material nonlinearity is in fact nontrivial and deserves a careful treatment.

In addition, either elongation or shortening along the axis of the member is not allowed in the current development. This restriction posed by the inextensibility assumption is no longer acceptable when the structure under consideration can undergo both axial and bending deformations of comparable magnitude. To capable of treating such structures, the inextensibility assumption must be removed and nontrivial modifications must be taken into account and requires further investigation.

# REFERENCES

Banerjee, A., Bhattacharaya, B. and Mallik, A.K. 2008. Large deflection of cantilever beams with geometric non-linearity: Analytical and numerical approaches. International Journal of Non-Linear Mechanics. 43: 366-376.

Dado, M., Al-Sadder, S. and Abuzeid, O. 2004. Post-buckling behavior of two elastica columns linked with a rotational spring. Int. J. of Nonlin. Mech. 39: 1579-1587.

Gallagher, R.H., Ziemian, R.D., and McGuire, W. 2000. Matrix Structural Analysis. New Jersey: Courier Dover Publications.

Hu, Y.J., Zhu, Y. and Cheng, C.J. DQEM for large deformation analysis of structure with discontinuity conditions and initial displacements. Engrg. Struct. Article in press.

Kirchhoff, G.R. 1859. On the equilibrium and the moments of an infinitely thin bar. J. Math. (Crelle). 56.

Krawinkler, H. and Seneviratna, G. D. 1998. Pros and cons of a pushover analysis of seismic performance evaluation. Engrg. Struct. 20: 452-464.

Lee, K. 2001. Post-buckling of uniform cantilever column under a combined load. Int. J. Nonlin. Mech. 36: 813-816.

Li, Q.S. 2001. Exact solutions for buckling of non-uniform columns under axial concentrated and distributed loading. Eur. J. Mech. A/Solids. 20: 485-500.

Madhusudan, B.P., Rajeev, V.R. and Rao, B.N. 2003. Post-buckling of cantilever columns having variable cross section under a combined load. Int. J. Nonlin. Mech. 38: 1513-1522.

Phungpaingam, B. and Chucheepsakul S. 2002. Large deflection of a viariable-arc-length beam subjected to an inclined follower force. The 8th National Convention on Civil Engineering. 8: STR 370-375.

Sampaio, J.H. and Hundhausen, J.R. 1998. A mathematical model and analytical solution for buckling of inclined beam-columns. Appl. Math. Model. 22: 405-421.

Shavartman, B.S. 2007. Large deflections of a cantilever beam subjected to a follower force. Journal of sound and vibration. 304: 969-973.

Silvestre, N. and Camotim, D. 2007. Elastic buckling and second-order behaviour of pitched-roof steel frames. J. of Const. Steel Research. 63: 804-818.

Suwansheewasiri, A. and Chucheepsakul, S. 2004. Buckling and post-buckling analysis of elastic frames under non-follower forces by elliptic integral method. The 9th National Convention on Civil Engineering. 9: STR 138-143.

Timoshenko, S.P. 1953. History of Strength of Materials. New York: McGraw-Hill.

Timoshenko, S.P. and Gere, J.M. 1972. Theory of Elastic Stability, 2nd Edition. New York: McGraw-Hill.

Vaz, M.A. and Silva, D.F.C. 2003. Post-buckling analysis of slender elastic rods subjected to terminal forces. Int. J. Nonlin. Mech. 38: 483-492.

Wang, C.Y. 1997. Post-buckling of a clamped simply supported elastica. Int. J. Nonlin. Mech. 32: 1115-1122.

Wang, J., Chen, J.K. and Liao, S. 2006. An explicit solution of the large deformation of a cantilever beam under point load at the free tip. Journal of Computational and Applied Mathematics. 212: 320-330.

West, H.H. 2002. Fundamentals of Structural Analysis, John Wiley & Sons, New Jersey.

**APPENDICES**

## APPENDIX A

This section presents explicit results for all entries of matrices **B**, **C**, **D** and **F**. By recalling that $\sin\phi_1 = \sin(\overline{\theta}_1/2)/\sin(\overline{\theta}_z/2)$ and then differentiating this relation with respect to $\{\overline{\theta}_1, \overline{\theta}_z\}$, we obtain

$$\frac{\partial\phi_1}{\partial\overline{\theta}_1} = \frac{\cos(\overline{\theta}_1/2)}{2\sin(\overline{\theta}_z/2)\cos\phi_1} \quad , \tag{A.1}$$

$$\frac{\partial\phi_1}{\partial\overline{\theta}_z} = \frac{-\tan\phi_1}{2\tan(\overline{\theta}_z/2)} \quad . \tag{A.2}$$

Similarly by taking derivative of $\sin\phi_2 = \sin(\overline{\theta}_2/2)/\sin(\overline{\theta}_z/2)$ with respect to $\{\overline{\theta}_2, \overline{\theta}_z\}$, it leads to

$$\frac{\partial\phi_2}{\partial\overline{\theta}_2} = \frac{\cos(\overline{\theta}_2/2)}{2\sin(\overline{\theta}_z/2)\cos\phi_2} \quad , \tag{A.3}$$

$$\frac{\partial\phi_2}{\partial\overline{\theta}_z} = \frac{-\tan\phi_2}{2\tan(\overline{\theta}_z/2)} \quad . \tag{A.4}$$

By differentiating $\overline{p} = \sin(\overline{\theta}_z/2)$ with respect to $\overline{\theta}_z$, it yields

$$\frac{\partial\overline{p}}{\partial\overline{\theta}_z} = \frac{1}{2}\cos\frac{\overline{\theta}_z}{2} . \tag{A.5}$$

From the relations $\overline{\theta}_1 = \pi + (\theta_1 - \theta_o)$, $\overline{\theta}_2 = \pi + (\theta_2 - \theta_o)$ and $\overline{\theta}_z = \pi + (\theta_z - \theta_o)$, we obtain

$$\frac{\partial\overline{\theta}_1}{\partial\theta_o} = \frac{\partial\overline{\theta}_2}{\partial\theta_o} = \frac{\partial\overline{\theta}_z}{\partial\theta_o} = -1 \quad , \tag{A.6}$$

$$\frac{\partial\overline{\theta}_1}{\partial\theta_1} = \frac{\partial\overline{\theta}_2}{\partial\theta_2} = \frac{\partial\overline{\theta}_z}{\partial\theta_z} = 1 \quad . \tag{A.7}$$

By taking derivatives of $\theta_o = \sin^{-1}(-\hat{f}_y/\sqrt{\hat{f}_x^2 + \hat{f}_y^2})$ with respect to $\{\hat{f}_x, \hat{f}_y\}$, it leads to

$$\frac{\partial \theta_o}{\partial \hat{f}_x} = \frac{-\hat{f}_y}{\hat{f}_x^2 + \hat{f}_y^2} \quad , \tag{A.8}$$

$$\frac{\partial \theta_o}{\partial \hat{f}_y} = \frac{-\hat{f}_x}{\hat{f}_x^2 + \hat{f}_y^2} \quad . \tag{A.9}$$

By taking derivatives of $f_s^2 = \sqrt{\hat{f}_x^2 + \hat{f}_y^2}$ with respect to $\{\hat{f}_x, \hat{f}_y\}$, it yields

$$\frac{\partial f_s}{\partial \hat{f}_x} = \frac{\hat{f}_x}{f_s^3} \quad , \tag{A.10}$$

$$\frac{\partial f_s}{\partial \hat{f}_y} = \frac{\hat{f}_y}{f_s^3} \quad . \tag{A.11}$$

By employing (A.1)-(A.2) and (A.6)-(A.11), we obtain

$$\frac{\partial \phi_1}{\partial \theta_1} = \frac{\partial \phi_1}{\partial \overline{\theta}_1} \frac{\partial \overline{\theta}_1}{\partial \theta_1} = \frac{\cos(\overline{\theta}_1/2)}{2\sin(\overline{\theta}_z/2)\cos\phi_1} \quad , \tag{A.12}$$

$$\frac{\partial \phi_1}{\partial \hat{f}_x} = \frac{\partial \phi_1}{\partial \overline{\theta}_1} \frac{\partial \overline{\theta}_1}{\partial \theta_o} \frac{\partial \theta_o}{\partial \hat{f}_x} + \frac{\partial \phi_1}{\partial \overline{\theta}_z} \frac{\partial \overline{\theta}_z}{\partial \theta_o} \frac{\partial \theta_o}{\partial \hat{f}_x} = \left( \frac{\cos(\overline{\theta}_1/2)}{2\sin(\overline{\theta}_z/2)\cos\phi_1} - \frac{\tan\phi_1}{2\tan(\overline{\theta}_z/2)} \right) \frac{\hat{f}_y}{\hat{f}_x^2 + \hat{f}_y^2} \quad , \tag{A.13}$$

$$\frac{\partial \phi_1}{\partial \theta_z} = \frac{\partial \phi_1}{\partial \overline{\theta}_z} \frac{\partial \overline{\theta}_z}{\partial \theta_z} = \frac{-\tan\phi_1}{2\tan(\overline{\theta}_z/2)} \quad , \tag{A.14}$$

$$\frac{\partial \phi_1}{\partial \hat{f}_y} = \frac{\partial \phi_1}{\partial \overline{\theta}_1} \frac{\partial \overline{\theta}_1}{\partial \theta_o} \frac{\partial \theta_o}{\partial \hat{f}_y} + \frac{\partial \phi_1}{\partial \overline{\theta}_z} \frac{\partial \overline{\theta}_z}{\partial \theta_o} \frac{\partial \theta_o}{\partial \hat{f}_y} = \left( \frac{\cos(\overline{\theta}_1/2)}{2\sin(\overline{\theta}_z/2)\cos\phi_1} - \frac{\tan\phi_1}{2\tan(\overline{\theta}_z/2)} \right) \frac{\hat{f}_x}{\hat{f}_x^2 + \hat{f}_y^2} \quad . \tag{A.15}$$

By employing (A.3)-(A.4) and (A.6)-(A.11), we obtain

$$\frac{\partial \phi_2}{\partial \theta_2} = \frac{\partial \phi_2}{\partial \overline{\theta}_2} \frac{\partial \overline{\theta}_2}{\partial \theta_2} = \frac{\cos(\overline{\theta}_2/2)}{2\sin(\overline{\theta}_z/2)\cos\phi_2} \quad , \tag{A.16}$$

$$\frac{\partial \phi_2}{\partial \hat{f}_x} = \frac{\partial \phi_2}{\partial \overline{\theta}_2} \frac{\partial \overline{\theta}_2}{\partial \theta_o} \frac{\partial \theta_o}{\partial \hat{f}_x} + \frac{\partial \phi_2}{\partial \overline{\theta}_2} \frac{\partial \overline{\theta}_z}{\partial \theta_o} \frac{\partial \theta_o}{\partial \hat{f}_x} = \left( \frac{\cos(\overline{\theta}_2/2)}{2\sin(\overline{\theta}_z/2)\cos\phi_2} - \frac{\tan\phi_2}{2\tan(\overline{\theta}_z/2)} \right) \frac{\hat{f}_y}{\hat{f}_x^2 + \hat{f}_y^2} \quad , \tag{A.17}$$

$$\frac{\partial \phi_2}{\partial \theta_z} = \frac{\partial \phi_2}{\partial \overline{\theta}_2} \frac{\partial \overline{\theta}_z}{\partial \theta_z} = \frac{-\tan\phi_2}{2\tan(\overline{\theta}_z/2)} \quad , \tag{A.18}$$

$$\frac{\partial \phi_2}{\partial \hat{f}_y} = \frac{\partial \phi_2}{\partial \overline{\theta}_2} \frac{\partial \overline{\theta}_2}{\partial \theta_o} \frac{\partial \theta_o}{\partial \hat{f}_y} + \frac{\partial \phi_2}{\partial \overline{\theta}_2} \frac{\partial \overline{\theta}_z}{\partial \theta_o} \frac{\partial \theta_o}{\partial \hat{f}_y} = \left( \frac{\cos(\overline{\theta}_2/2)}{2\sin(\overline{\theta}_z/2)\cos\phi_2} - \frac{\tan\phi_2}{2\tan(\overline{\theta}_z/2)} \right) \frac{\hat{f}_x}{\hat{f}_x^2 + \hat{f}_y^2} \quad . \tag{A.19}$$

By employing (A.5)-(A.11), we obtain

$$\frac{\partial \overline{p}}{\partial \theta_z} = \frac{\partial \overline{p}}{\partial \overline{\theta}_z} \frac{\partial \overline{\theta}_z}{\partial \theta_z} = \frac{1}{2}\cos\frac{\overline{\theta}_z}{2} \quad , \tag{A.20}$$

$$\frac{\partial \overline{p}}{\partial \hat{f}_x} = \frac{\partial \overline{p}}{\partial \overline{\theta}_z} \frac{\partial \overline{\theta}_z}{\partial \theta_o} \frac{\partial \theta_o}{\partial \hat{f}_x} = \frac{1}{2}\cos\frac{\overline{\theta}_z}{2} \frac{\hat{f}_y}{\hat{f}_x^2 + \hat{f}_y^2} \quad , \tag{A.21}$$

$$\frac{\partial \overline{p}}{\partial \hat{f}_y} = \frac{\partial \overline{p}}{\partial \overline{\theta}_z} \frac{\partial \overline{\theta}_z}{\partial \theta_o} \frac{\partial \theta_o}{\partial \hat{f}_y} = \frac{1}{2}\cos\frac{\overline{\theta}_z}{2} \frac{\hat{f}_x}{\hat{f}_x^2 + \hat{f}_y^2} \quad , \tag{A.22}$$

By taking derivatives of (3.78) with respect to $\{ \phi_1, \phi_2, \theta_o, \hat{f}_s, \overline{p} \}$, we obtain

$$\frac{\partial \hat{\mathcal{R}}}{\partial \phi_1} = \frac{-1}{f_s} \left( 2\cos\theta_o \sqrt{1 - \overline{p}^2\sin^2\phi_1} + 2\psi\sin\theta_o \overline{p}\sin\phi_1 + \frac{(1 - \cos\theta_o)}{\sqrt{1 - \overline{p}^2\sin^2\phi_1}} \right) \quad , \tag{A.23}$$

$$\frac{\partial \hat{\mathcal{R}}}{\partial \phi_2} = \frac{-1}{f_s} \left( 2\cos\theta_o \sqrt{1 - \overline{p}^2\sin^2\phi_2} + 2\psi\sin\theta_o \overline{p}\sin\phi_2 + \frac{(1 - \cos\theta_o)}{\sqrt{1 - \overline{p}^2\sin^2\phi_2}} \right) \quad , \tag{A.24}$$

$$\frac{\partial \hat{\mathcal{R}}}{\partial \overline{p}} = \int\limits_{\phi_1}^{\pi/2} \frac{\partial f_u}{\partial \overline{p}} \, d\phi + \int\limits_{\phi_2}^{\pi/2} \frac{\partial f_u}{\partial \overline{p}} \, d\phi$$

$$= \int\limits_{\phi_1}^{\pi/2} \frac{2\overline{p}\cos\theta_o}{\sqrt{1-\overline{p}^2\sin^2\phi}} + 2\psi\sin\theta_o\sin\phi - \frac{\overline{p}(1-\cos\theta_o)}{\sqrt{1-\overline{p}^2\sin^2\phi}^3} \, d\phi$$

$$+ \int\limits_{\phi_2}^{\pi/2} \frac{2\overline{p}\cos\theta_o}{\sqrt{1-\overline{p}^2\sin^2\phi}} + 2\psi\sin\theta_o\sin\phi - \frac{\overline{p}(1-\cos\theta_o)}{\sqrt{1-\overline{p}^2\sin^2\phi}^3} \, d\phi \quad , \tag{A.25}$$

$$\frac{\partial \hat{\mathcal{R}}}{\partial \theta_o} = \int\limits_{\phi_1}^{\pi/2} \frac{\partial f_u}{\partial \theta_o} \, d\phi - \int\limits_{\phi_2}^{\pi/2} \frac{\partial f_u}{\partial \theta_o} \, d\phi$$

$$= \int\limits_{\phi_1}^{\pi/2} -2\sin\theta_o\sqrt{1-\overline{p}^2\sin^2\phi} + 2\psi\cos\theta_o\overline{p}\sin\phi + \frac{\sin\theta_o}{\sqrt{1-\overline{p}^2\sin^2\phi}} \, d\phi$$

$$- \int\limits_{\phi_2}^{\pi/2} -2\sin\theta_o\sqrt{1-\overline{p}^2\sin^2\phi} + 2\psi\cos\theta_o\overline{p}\sin\phi + \frac{\sin\theta_o}{\sqrt{1-\overline{p}^2\sin^2\phi}} \, d\phi \quad , \tag{A.26}$$

$$\frac{\partial \hat{\mathcal{R}}}{\partial f_s} = \frac{1}{f_s^2}\left(-\int\limits_{\phi_1}^{\pi/2} f_u \, d\phi + \int\limits_{\phi_2}^{\pi/2} f_u \, d\phi\right)$$

$$= \frac{1}{f_s^2}\left(-\int\limits_{\phi_1}^{\pi/2} 2\cos\theta_o\sqrt{1-\overline{p}^2\sin^2\phi_1} + 2\psi\sin\theta_o\overline{p}\sin\phi_1 + \frac{(1-\cos\theta_o)}{\sqrt{1-\overline{p}^2\sin^2\phi_1}} \, d\phi\right.$$

$$\left.- \int\limits_{\phi_2}^{\pi/2} 2\cos\theta_o\sqrt{1-\overline{p}^2\sin^2\phi_1} + 2\psi\sin\theta_o\overline{p}\sin\phi_1 + \frac{(1-\cos\theta_o)}{\sqrt{1-\overline{p}^2\sin^2\phi_1}} \, d\phi\right) \quad . \tag{A.27}$$

Similarly, by taking derivatives of (3.79) with respect to { $\phi_1, \phi_2, \hat{f}_s, \overline{p}$ } and (3.80) with respect to { $\phi_1, \phi_2, \theta_o, \overline{p}$ }, it yields

$$\frac{\partial \Gamma_o}{\partial \phi_1} = -\frac{1}{\sqrt{1-\overline{p}^2\sin^2\phi_1}} \quad , \tag{A.28}$$

$$\frac{\partial \Gamma_o}{\partial \phi_2} = -\frac{1}{\sqrt{1-\overline{p}^2\sin^2\phi_2}} \quad , \tag{A.29}$$

$$\frac{\partial \Gamma_o}{\partial \overline{p}} = \int\limits_{\phi_1}^{\pi/2} \frac{\overline{p}}{\sqrt{1-\overline{p}^2\sin^2\phi}^3} \, d\phi + \int\limits_{\phi_2}^{\pi/2} \frac{\overline{p}}{\sqrt{1-\overline{p}^2\sin^2\phi}^3} \, d\phi \quad , \tag{A. 30}$$

$$\frac{\partial \Gamma_o}{\partial f_s} = -1 \quad , \tag{A.31}$$

$$\frac{\partial \Gamma_v}{\partial \phi_1} = 2 \sin \theta_o \sqrt{1 - \overline{p}^2 \sin^2 \phi_1} - 2\psi \cos \theta_o \overline{p} \sin \phi_1 - \frac{\sin \theta_o}{\sqrt{1 - \overline{p}^2 \sin^2 \phi_1}} \quad , \tag{A.32}$$

$$\frac{\partial \Gamma_v}{\partial \phi_2} = 2 \sin \theta_o \sqrt{1 - \overline{p}^2 \sin^2 \phi_2} - 2\psi \cos \theta_o \overline{p} \sin \phi_2 - \frac{\sin \theta_o}{\sqrt{1 - \overline{p}^2 \sin^2 \phi_2}} \quad , \tag{A.33}$$

$$\begin{aligned}
\frac{\partial \Gamma_v}{\partial \overline{p}} &= \int_{\phi_1}^{\pi/2} \frac{\partial f_v}{\partial \overline{p}} \, d\phi + \int_{\phi_2}^{\pi/2} \frac{\partial f_v}{\partial \overline{p}} \, d\phi \\
&= \int_{\phi_1}^{\pi/2} \frac{-2\overline{p} \sin \theta_o}{\sqrt{1 - \overline{p}^2 \sin^2 \phi}} - 2\psi \cos \theta_o \sin \phi - \frac{\overline{p} \sin \theta_o}{\sqrt{1 - \overline{p}^2 \sin^2 \phi}^3} \, d\phi \\
&\quad + \int_{\phi_2}^{\pi/2} \frac{-2\overline{p} \sin \theta_o}{\sqrt{1 - \overline{p}^2 \sin^2 \phi}} - 2\psi \cos \theta_o \sin \phi - \frac{\overline{p} \sin \theta_o}{\sqrt{1 - \overline{p}^2 \sin^2 \phi}^3} \, d\phi \quad , \tag{A.34}
\end{aligned}$$

$$\begin{aligned}
\frac{\partial \Gamma_v}{\partial \theta_o} &= \int_{\phi_1}^{\pi/2} \frac{\partial f_v}{\partial \theta_o} \, d\phi - \int_{\pi/2}^{\phi_2} \frac{\partial f_v}{\partial \theta_o} \, d\phi \\
&= \int_{\phi_1}^{\pi/2} 2 \cos \theta_o \sqrt{1 - \overline{p}^2 \sin^2 \phi} + 2\psi \sin \theta_o \overline{p} \sin \phi - \frac{\cos \theta_o}{\sqrt{1 - \overline{p}^2 \sin^2 \phi}} \, d\phi \\
&\quad + \int_{\phi_2}^{\pi/2} 2 \cos \theta_o \sqrt{1 - \overline{p}^2 \sin^2 \phi} + 2\psi \sin \theta_o \overline{p} \sin \phi - \frac{\cos \theta_o}{\sqrt{1 - \overline{p}^2 \sin^2 \phi}} \, d\phi \quad . \tag{A.35}
\end{aligned}$$

By exploiting above information and chain rule for differentiation, entries of the matrix **B** can readily be obtained as

$$\frac{\partial \hat{\mathcal{R}}}{\partial \theta_1} = \frac{\partial \hat{\mathcal{R}}}{\partial \phi_1} \frac{\partial \phi_1}{\partial \theta_1} \quad , \tag{A.36}$$

$$\frac{\partial \hat{\mathcal{R}}}{\partial \theta_2} = \frac{\partial \hat{\mathcal{R}}}{\partial \phi_2} \frac{\partial \phi_2}{\partial \theta_2} \quad , \tag{A.37}$$

$$\frac{\partial \hat{\mathcal{R}}}{\partial \hat{f}_x} = \frac{\partial \hat{\mathcal{R}}}{\partial \phi_1} \frac{\partial \phi_1}{\partial \hat{f}_x} + \frac{\partial \hat{\mathcal{R}}}{\partial \phi_2} \frac{\partial \phi_2}{\partial \hat{f}_x} + \frac{\partial \hat{\mathcal{R}}}{\partial \overline{p}} \frac{\partial \overline{p}}{\partial \hat{f}_x} + \frac{\partial \hat{\mathcal{R}}}{\partial \theta_o} \frac{\partial \theta_o}{\partial \hat{f}_x} + \frac{\partial \hat{\mathcal{R}}}{\partial f_s} \frac{\partial f_s}{\partial \hat{f}_x} \quad . \tag{A.38}$$

Entries of the matrix **C** is given by

$$\frac{\partial \hat{\mathcal{R}}}{\partial \theta_z} = \frac{\partial \hat{\mathcal{R}}}{\partial \phi_1} \frac{\partial \phi_1}{\partial \theta_z} + \frac{\partial \hat{\mathcal{R}}}{\partial \phi_2} \frac{\partial \phi_2}{\partial \theta_z} + \frac{\partial \hat{\mathcal{R}}}{\partial \overline{p}} \frac{\partial \overline{p}}{\partial \theta_z} \quad , \tag{A.39}$$

$$\frac{\partial \hat{\mathcal{R}}}{\partial \hat{f}_y} = \frac{\partial \hat{\mathcal{R}}}{\partial \phi_1} \frac{\partial \phi_1}{\partial \hat{f}_y} + \frac{\partial \hat{\mathcal{R}}}{\partial \phi_2} \frac{\partial \phi_2}{\partial \hat{f}_y} + \frac{\partial \hat{\mathcal{R}}}{\partial \overline{p}} \frac{\partial \overline{p}}{\partial \hat{f}_y} + \frac{\partial \hat{\mathcal{R}}}{\partial \theta_o} \frac{\partial \theta_o}{\partial \hat{f}_y} + \frac{\partial \hat{\mathcal{R}}}{\partial f_s} \frac{\partial f_s}{\partial \hat{f}_y} \quad . \tag{A.40}$$

Entries of the matrix **D** is given by

$$\frac{\partial \Gamma_o}{\partial \theta_z} = \frac{\partial \Gamma_o}{\partial \phi_1} \frac{\partial \phi_1}{\partial \theta_z} + \frac{\partial \Gamma_o}{\partial \phi_2} \frac{\partial \phi_2}{\partial \theta_z} + \frac{\partial \Gamma_o}{\partial \overline{p}} \frac{\partial \overline{p}}{\partial \theta_z} \quad , \tag{A.41}$$

$$\frac{\partial \Gamma_v}{\partial \theta_z} = \frac{\partial \Gamma_v}{\partial \phi_1} \frac{\partial \phi_1}{\partial \theta_z} + \frac{\partial \Gamma_v}{\partial \phi_2} \frac{\partial \phi_2}{\partial \theta_z} + \frac{\partial \Gamma_v}{\partial \overline{p}} \frac{\partial \overline{p}}{\partial \theta_z} \quad , \tag{A.42}$$

$$\frac{\partial \Gamma_o}{\partial \hat{f}_y} = \frac{\partial \Gamma_o}{\partial \phi_1} \frac{\partial \phi_1}{\partial \hat{f}_y} + \frac{\partial \Gamma_o}{\partial \phi_2} \frac{\partial \phi_2}{\partial \hat{f}_y} + \frac{\partial \Gamma_o}{\partial \overline{p}} \frac{\partial \overline{p}}{\partial \hat{f}_y} + \frac{\partial \Gamma_o}{\partial f_s} \frac{\partial f_s}{\partial \hat{f}_y} \quad , \tag{A.43}$$

$$\frac{\partial \Gamma_v}{\partial \hat{f}_y} = \frac{\partial \Gamma_v}{\partial \phi_1} \frac{\partial \phi_1}{\partial \hat{f}_y} + \frac{\partial \Gamma_v}{\partial \phi_2} \frac{\partial \phi_2}{\partial \hat{f}_y} + \frac{\partial \Gamma_v}{\partial \overline{p}} \frac{\partial \overline{p}}{\partial \hat{f}_y} + \frac{\partial \Gamma_v}{\partial \theta_o} \frac{\partial \theta_o}{\partial \hat{f}_y} \quad . \tag{A.44}$$

Similarly, entries of the matrix **F** is given by

$$\frac{\partial \Gamma_o}{\partial \theta_1} = \frac{\partial \Gamma_o}{\partial \phi_1} \frac{\partial \phi_1}{\partial \theta_1} , \tag{A.45}$$

$$\frac{\partial \Gamma_o}{\partial \theta_2} = \frac{\partial \Gamma_o}{\partial \phi_2} \frac{\partial \phi_2}{\partial \theta_2} \quad , \tag{A.46}$$

$$\frac{\partial \Gamma_o}{\partial \hat{f}_x} = \frac{\partial \Gamma_o}{\partial \phi_1} \frac{\partial \phi_1}{\partial \hat{f}_x} + \frac{\partial \Gamma_o}{\partial \phi_2} \frac{\partial \phi_2}{\partial \hat{f}_x} + \frac{\partial \Gamma_o}{\partial \overline{p}} \frac{\partial \overline{p}}{\partial \hat{f}_x} + \frac{\partial \Gamma_o}{\partial f_s} \frac{\partial f_s}{\partial \hat{f}_x} \quad , \tag{A.47}$$

$$\frac{\partial \Gamma_v}{\partial \theta_1} = \frac{\partial \Gamma_v}{\partial \phi_1} \frac{\partial \phi_1}{\partial \theta_1} \quad , \tag{A.48}$$

$$\frac{\partial \Gamma_v}{\partial \theta_2} = \frac{\partial \Gamma_v}{\partial \phi_2} \frac{\partial \phi_2}{\partial \theta_2} \quad , \tag{A.49}$$

$$\frac{\partial \Gamma_v}{\partial \hat{f}_x} = \frac{\partial \Gamma_v}{\partial \phi_1} \frac{\partial \phi_1}{\partial \hat{f}_x} + \frac{\partial \Gamma_v}{\partial \phi_2} \frac{\partial \phi_2}{\partial \hat{f}_x} + \frac{\partial \Gamma_v}{\partial \overline{p}} \frac{\partial \overline{p}}{\partial \hat{f}_x} + \frac{\partial \Gamma_v}{\partial \theta_o} \frac{\partial \theta_o}{\partial \hat{f}_x} \quad . \tag{A.50}$$

## APPENDIX B

This section presents explicit results for all entries of matrices $\overline{\mathbf{B}}$, $\overline{\mathbf{C}}$, $\overline{\mathbf{D}}$ and $\overline{\mathbf{F}}$. By recalling that $\sin\phi_1 = \sin(\overline{\theta}_1/2)/\sin(\overline{\theta}_2/2)$ and then differentiating this relation with respect to $\{\overline{\theta}_1, \overline{\theta}_z\}$, we obtain

$$\frac{\partial\phi_1}{\partial\overline{\theta}_1} = \frac{\cos(\overline{\theta}_1/2)}{2\sin(\overline{\theta}_2/2)\cos\phi_1} \quad , \tag{B.1}$$

$$\frac{\partial\phi_1}{\partial\overline{\theta}_2} = \frac{-\tan\phi_1}{2\tan(\overline{\theta}_2/2)} \quad . \tag{B.2}$$

By differentiating $\overline{p} = \sin(\overline{\theta}_2/2)$ with respect to $\overline{\theta}_2$, it yields

$$\frac{\partial\overline{p}}{\partial\overline{\theta}_2} = \frac{1}{2}\cos\frac{\overline{\theta}_2}{2} \quad . \tag{B.3}$$

From the relations $\overline{\theta}_1 = \pi + (\theta_1 - \theta_o)$ and $\overline{\theta}_2 = \pi + (\theta_2 - \theta_o)$, we obtain

$$\frac{\partial\overline{\theta}_1}{\partial\theta_o} = \frac{\partial\overline{\theta}_2}{\partial\theta_o} = -1 \quad , \tag{B.4}$$

$$\frac{\partial\overline{\theta}_1}{\partial\theta_1} = \frac{\partial\overline{\theta}_2}{\partial\theta_2} = 1 \quad . \tag{B.5}$$

By taking derivatives of $\theta_o = \sin^{-1}(-\hat{f}_y/\sqrt{\hat{f}_x^2 + \hat{f}_y^2})$ with respect to $\{\hat{f}_x, \hat{f}_y\}$, it leads to

$$\frac{\partial\theta_o}{\partial\hat{f}_x} = \frac{-\hat{f}_y}{\hat{f}_x^2 + \hat{f}_y^2} \quad , \tag{B.6}$$

$$\frac{\partial\theta_o}{\partial\hat{f}_y} = \frac{-\hat{f}_x}{\hat{f}_x^2 + \hat{f}_y^2} \quad . \tag{B.7}$$

By taking derivatives of $f_s^2 = \sqrt{\hat{f}_x^2 + \hat{f}_y^2}$ with respect to $\{\hat{f}_x, \hat{f}_y\}$, it yields

$$\frac{\partial f_s}{\partial \hat{f}_x} = \frac{\hat{f}_x}{f_s^3} \quad , \tag{B.8}$$

$$\frac{\partial f_s}{\partial \hat{f}_y} = \frac{\hat{f}_y}{f_s^3} \quad . \tag{B.9}$$

By employing (B.1)-(B.2) and (B.4)-(B.9), we obtain

$$\frac{\partial \phi_1}{\partial \theta_1} = \frac{\partial \phi_1}{\partial \bar{\theta}_1}\frac{\partial \bar{\theta}_1}{\partial \theta_1} = \frac{\cos(\bar{\theta}_1/2)}{2\sin(\bar{\theta}_2/2)\cos\phi_1} \quad , \tag{B.10}$$

$$\frac{\partial \phi_1}{\partial \hat{f}_x} = \frac{\partial \phi_1}{\partial \bar{\theta}_1}\frac{\partial \bar{\theta}_1}{\partial \theta_o}\frac{\partial \theta_o}{\partial \hat{f}_x} + \frac{\partial \phi_1}{\partial \bar{\theta}_2}\frac{\partial \bar{\theta}_2}{\partial \theta_o}\frac{\partial \theta_o}{\partial \hat{f}_x} = \left(\frac{\cos(\bar{\theta}_1/2)}{2\sin(\bar{\theta}_2/2)\cos\phi_1} - \frac{\tan\phi_1}{2\tan(\bar{\theta}_2/2)}\right)\frac{\hat{f}_y}{\hat{f}_x^2 + \hat{f}_y^2} \quad , \tag{B.11}$$

$$\frac{\partial \phi_1}{\partial \theta_2} = \frac{\partial \phi_1}{\partial \bar{\theta}_2}\frac{\partial \bar{\theta}_2}{\partial \theta_2} = \frac{-\tan\phi_1}{2\tan(\bar{\theta}_2/2)} \quad , \tag{B.12}$$

$$\frac{\partial \phi_1}{\partial \hat{f}_y} = \frac{\partial \phi_1}{\partial \bar{\theta}_1}\frac{\partial \bar{\theta}_1}{\partial \theta_o}\frac{\partial \theta_o}{\partial \hat{f}_y} + \frac{\partial \phi_1}{\partial \bar{\theta}_2}\frac{\partial \bar{\theta}_2}{\partial \theta_o}\frac{\partial \theta_o}{\partial \hat{f}_y} = \left(\frac{\cos(\bar{\theta}_1/2)}{2\sin(\bar{\theta}_2/2)\cos\phi_1} - \frac{\tan\phi_1}{2\tan(\bar{\theta}_2/2)}\right)\frac{\hat{f}_x}{\hat{f}_x^2 + \hat{f}_y^2} \quad . \tag{B.13}$$

By employing (B.3)-(B.9), we obtain

$$\frac{\partial \bar{p}}{\partial \theta_2} = \frac{\partial \bar{p}}{\partial \bar{\theta}_2}\frac{\partial \bar{\theta}_2}{\partial \theta_2} = \frac{1}{2}\cos\frac{\bar{\theta}_2}{2} \quad , \tag{B.14}$$

$$\frac{\partial \bar{p}}{\partial \hat{f}_x} = \frac{\partial \bar{p}}{\partial \bar{\theta}_2}\frac{\partial \bar{\theta}_2}{\partial \theta_o}\frac{\partial \theta_o}{\partial \hat{f}_x} = \frac{1}{2}\cos\frac{\bar{\theta}_2}{2}\frac{\hat{f}_y}{\hat{f}_x^2 + \hat{f}_y^2} \quad , \tag{B.15}$$

$$\frac{\partial \bar{p}}{\partial \hat{f}_y} = \frac{\partial \bar{p}}{\partial \bar{\theta}_2}\frac{\partial \bar{\theta}_2}{\partial \theta_o}\frac{\partial \theta_o}{\partial \hat{f}_y} = -\frac{1}{2}\cos\frac{\bar{\theta}_2}{2}\frac{\hat{f}_x}{\hat{f}_x^2 + \hat{f}_y^2} \quad , \tag{B.16}$$

By taking derivatives of (3.106) with respect to $\{\phi_1, \theta_o, \hat{f}_s, \overline{p}\}$, we obtain

$$\frac{\partial \hat{\mathscr{R}}}{\partial \phi_1} = \frac{-1}{f_s}(2\cos\theta_o\sqrt{1-\overline{p}^2\sin^2\phi_1} + 2\psi\sin\theta_o\overline{p}\sin\phi_1 + \frac{(1-\cos\theta_o)}{\sqrt{1-\overline{p}^2\sin^2\phi_1}}) \quad , \qquad (B.17)$$

$$\frac{\partial \hat{\mathscr{R}}}{\partial \overline{p}} = \int_{\phi_1}^{\pi/2} \frac{\partial f_u}{\partial \overline{p}} \, d\phi$$
$$= \int_{\phi_1}^{\pi/2} \frac{2\overline{p}\cos\theta_o}{\sqrt{1-\overline{p}^2\sin^2\phi}} + 2\psi\sin\theta_o\sin\phi - \frac{\overline{p}(1-\cos\theta_o)}{\sqrt{1-\overline{p}^2\sin^2\phi}^3} \, d\phi \quad , \qquad (B.18)$$

$$\frac{\partial \hat{\mathscr{R}}}{\partial \theta_o} = \int_{\phi_1}^{\pi/2} \frac{\partial f_u}{\partial \theta_o} \, d\phi$$
$$= \int_{\phi_1}^{\pi/2} -2\sin\theta_o\sqrt{1-\overline{p}^2\sin^2\phi} + 2\psi\cos\theta_o\overline{p}\sin\phi + \frac{\sin\theta_o}{\sqrt{1-\overline{p}^2\sin^2\phi}} \, d\phi \quad , \qquad (B.19)$$

$$\frac{\partial \hat{\mathscr{R}}}{\partial f_s} = \frac{1}{f_s^2}(-\int_{\phi_1}^{\pi/2} f_u \, d\phi)$$
$$= \frac{-1}{f_s^2}(\int_{\phi_1}^{\pi/2} 2\cos\theta_o\sqrt{1-\overline{p}^2\sin^2\phi_1} + 2\psi\sin\theta_o\overline{p}\sin\phi_1 + \frac{(1-\cos\theta_o)}{\sqrt{1-\overline{p}^2\sin^2\phi_1}} \, d\phi) \quad . \qquad (B.20)$$

Similarly, by taking derivatives of (3.107) with respect to $\{\phi_1, \hat{f}_s, \overline{p}\}$ and (3.108) with respect to $\{\phi_1, \theta_o, \overline{p}\}$, it yields

$$\frac{\partial \Gamma_o}{\partial \phi_1} = -\frac{1}{\sqrt{1-\overline{p}^2\sin^2\phi_1}} \quad , \qquad (B.21)$$

$$\frac{\partial \Gamma_o}{\partial \overline{p}} = \int_{\phi_1}^{\pi/2} \frac{\overline{p}}{\sqrt{1-\overline{p}^2\sin^2\phi}^3} \, d\phi \quad , \qquad (B.22)$$

$$\frac{\partial \Gamma_o}{\partial f_s} = -1 \quad , \qquad (B.23)$$

$$\frac{\partial \Gamma_v}{\partial \phi_1} = 2 \sin \theta_o \sqrt{1 - \overline{p}^2 \sin^2 \phi_1} - 2\psi \cos \theta_o \overline{p} \sin \phi_1 - \frac{\sin \theta_o}{\sqrt{1 - \overline{p}^2 \sin^2 \phi_1}} \quad , \tag{B.24}$$

$$\frac{\partial \Gamma_v}{\partial \overline{p}} = \int_{\phi_1}^{\pi/2} \frac{\partial f_v}{\partial \overline{p}} \, d\phi$$
$$= \int_{\phi_1}^{\pi/2} \frac{-2\overline{p} \sin \theta_o}{\sqrt{1 - \overline{p}^2 \sin^2 \phi}} - 2\psi \cos \theta_o \sin \phi - \frac{\overline{p} \sin \theta_o}{\sqrt{1 - \overline{p}^2 \sin^2 \phi}^3} \, d\phi \quad , \tag{B.25}$$

$$\frac{\partial \Gamma_v}{\partial \theta_o} = \int_{\phi_1}^{\pi/2} \frac{\partial f_v}{\partial \theta_o} \, d\phi$$
$$= \int_{\phi_1}^{\pi/2} 2 \cos \theta_o \sqrt{1 - \overline{p}^2 \sin^2 \phi} + 2\psi \sin \theta_o \overline{p} \sin \phi - \frac{\cos \theta_o}{\sqrt{1 - \overline{p}^2 \sin^2 \phi}} \, d\phi \quad . \tag{B.26}$$

By exploiting above information and chain rule for differentiation, entries of the matrix $\overline{\mathbf{B}}$ can readily be obtained as

$$\frac{\partial \hat{\mathcal{R}}}{\partial \theta_1} = \frac{\partial \hat{\mathcal{R}}}{\partial \phi_1} \frac{\partial \phi_1}{\partial \theta_1} \quad , \tag{B.27}$$

$$\frac{\partial \hat{\mathcal{R}}}{\partial \hat{f}_x} = \frac{\partial \hat{\mathcal{R}}}{\partial \phi_1} \frac{\partial \phi_1}{\partial \hat{f}_x} + \frac{\partial \hat{\mathcal{R}}}{\partial \overline{p}} \frac{\partial \overline{p}}{\partial \hat{f}_x} + \frac{\partial \hat{\mathcal{R}}}{\partial \theta_o} \frac{\partial \theta_o}{\partial \hat{f}_x} + \frac{\partial \hat{\mathcal{R}}}{\partial f_s} \frac{\partial f_s}{\partial \hat{f}_x} \quad . \tag{B.28}$$

Entries of the matrix $\overline{\mathbf{C}}$ is given by

$$\frac{\partial \hat{\mathcal{R}}}{\partial \theta_2} = \frac{\partial \hat{\mathcal{R}}}{\partial \phi_1} \frac{\partial \phi_1}{\partial \theta_2} + \frac{\partial \hat{\mathcal{R}}}{\partial \overline{p}} \frac{\partial \overline{p}}{\partial \theta_2} \quad , \tag{B.29}$$

$$\frac{\partial \hat{\mathcal{R}}}{\partial \hat{f}_y} = \frac{\partial \hat{\mathcal{R}}}{\partial \phi_1} \frac{\partial \phi_1}{\partial \hat{f}_y} + \frac{\partial \hat{\mathcal{R}}}{\partial \overline{p}} \frac{\partial \overline{p}}{\partial \hat{f}_y} + \frac{\partial \hat{\mathcal{R}}}{\partial \theta_o} \frac{\partial \theta_o}{\partial \hat{f}_y} + \frac{\partial \hat{\mathcal{R}}}{\partial f_s} \frac{\partial f_s}{\partial \hat{f}_y} \quad . \tag{B.30}$$

Entries of the matrix **D** is given by

$$\frac{\partial \Gamma_o}{\partial \theta_2} = \frac{\partial \Gamma_o}{\partial \phi_1}\frac{\partial \phi_1}{\partial \theta_2} + \frac{\partial \Gamma_o}{\partial \overline{p}}\frac{\partial \overline{p}}{\partial \overline{\theta}_2} \quad , \tag{B.31}$$

$$\frac{\partial \Gamma_v}{\partial \theta_2} = \frac{\partial \Gamma_v}{\partial \phi_1}\frac{\partial \phi_1}{\partial \theta_2} + \frac{\partial \Gamma_v}{\partial \overline{p}}\frac{\partial \overline{p}}{\partial \overline{\theta}_2} \quad , \tag{B.32}$$

$$\frac{\partial \Gamma_o}{\partial \hat{f}_y} = \frac{\partial \Gamma_o}{\partial \phi_1}\frac{\partial \phi_1}{\partial \hat{f}_y} + \frac{\partial \Gamma_o}{\partial \overline{p}}\frac{\partial \overline{p}}{\partial \hat{f}_y} + \frac{\partial \Gamma_o}{\partial \theta_o}\frac{\partial \theta_o}{\partial \hat{f}_y} + \frac{\partial \Gamma_o}{\partial f_s}\frac{\partial f_s}{\partial \hat{f}_y} \quad , \tag{B.33}$$

$$\frac{\partial \Gamma_v}{\partial \hat{f}_y} = \frac{\partial \Gamma_v}{\partial \phi_1}\frac{\partial \phi_1}{\partial \hat{f}_y} + \frac{\partial \Gamma_v}{\partial \overline{p}}\frac{\partial \overline{p}}{\partial \hat{f}_y} + \frac{\partial \Gamma_v}{\partial \theta_o}\frac{\partial \theta_o}{\partial \hat{f}_y} + \frac{\partial \Gamma_v}{\partial f_s}\frac{\partial f_s}{\partial \hat{f}_y} \quad . \tag{B.34}$$

Similarly, entries of the matrix **F** is given by

$$\frac{\partial \Gamma_o}{\partial \theta_1} = \frac{\partial \Gamma_o}{\partial \phi_1}\frac{\partial \phi_1}{\partial \theta_1} \quad , \tag{B.35}$$

$$\frac{\partial \Gamma_o}{\partial \hat{f}_x} = \frac{\partial \Gamma_o}{\partial \phi_1}\frac{\partial \phi_1}{\partial \hat{f}_x} + \frac{\partial \Gamma_o}{\partial \overline{p}}\frac{\partial \overline{p}}{\partial \hat{f}_x} + \frac{\partial \Gamma_o}{\partial \theta_o}\frac{\partial \theta_o}{\partial \hat{f}_x} + \frac{\partial \Gamma_o}{\partial f_s}\frac{\partial f_s}{\partial \hat{f}_x} \quad , \tag{B.36}$$

$$\frac{\partial \Gamma_v}{\partial \theta_1} = \frac{\partial \Gamma_v}{\partial \phi_1}\frac{\partial \phi_1}{\partial \theta_1} \quad , \tag{B.37}$$

$$\frac{\partial \Gamma_v}{\partial \hat{f}_x} = \frac{\partial \Gamma_v}{\partial \phi_1}\frac{\partial \phi_1}{\partial \hat{f}_x} + \frac{\partial \Gamma_v}{\partial \overline{p}}\frac{\partial \overline{p}}{\partial \hat{f}_x} + \frac{\partial \Gamma_v}{\partial \theta_o}\frac{\partial \theta_o}{\partial \hat{f}_x} + \frac{\partial \Gamma_v}{\partial f_s}\frac{\partial f_s}{\partial \hat{f}_x} \quad . \tag{B.38}$$

# BIOGRAPHY

Mr.Peerasak Tangnovarad was born in 1984, at Chulalongkorn Hospital, Bangkok. He graduated from Bangkok Christian College in 2001, and enrolled in B.Eng. and M. Eng. courses at Department of Civil Engineering Faculty, Chulalongkorn University, . The major in his master's degree is structural civil engineering, which includes studies and researches in structural mechanics and with advanced mathematical techniques. This thesis aims to investigate the actual deformed behavior of structures.